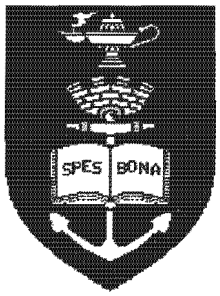

AN INVESTIGATION OF THE FEASIBILITY OF COMPOSITE TURBINE COMPRESSOR BLADES

JOHAN BRANEHÖG

April 2000

Submitted to the Faculty of Engineering and Built Environment of the University of Cape Town in fulfilment of the requirements for the degree of Masters of Science in Materials Engineering.

Centre for Materials Engineering
University of Cape Town
Private Bag, Rondebosch, 7700, South Africa.

ACKNOWLEDGEMENTS

I would like to express my thanks to the following people for their valuable contribution:

Dr. Kashif Marcus, my supervisor, for all his help, advice and constant encouragement during the formulation of this project.

Mrs Samantha Branehög, my wife, for her moral support throughout my years of study.

Mr. Helmut Bowles for his advice and support regarding finite element and programming related problems.

Mr. Victor Balden* for his advice regarding finite element problems.

Dr. Thomas Franz for his advice and enthusiasm regarding fibre composite materials.

Prof. A. Ball, my co-supervisor for his advice.

Mr. Glen Newins for his constant enthusiasm and expert workmanship in preparing test specimens and machining operations for the impact rig.

Ms. Julie Henry for all help regarding administration related problems.

Dr. Torsten Strand and Mikael Nilsson at ABB STAL for their support and assistance with supplying material data for the titanium alloy blade.

Leslie Harris , mattek CSIR*, for support an help during early stages of the project.

Mrs. Mira Topic for her microscopy advice.

Mr. Adrian Loedolff and James Peterson for their photographic assistance.

My family for their support and in particular my brother Sven Branehög at Chalmers University of Technology (CTH), for his advice and enthusiasm regarding fibre composite materials.

Members of the Department of the Materials Engineering for their friendship during the MSc project.

ABB STAL, for their financial support of this project.

Mr. Charles White at Tekochem for supplying polyurethane coatings and Dr. John Bosman for supplying the nickel coated CFRP laminates.

Ms. NEV, for her superior control in the barrel.

Dedicated to the memory of my father, Dr. Ingmar Branehög.

---

* Alias "Jimmy"

* CSIR – Centre for Scientific and Industrial Research

ABSTRACT

A study has been conducted as to the feasibility of using a carbon fibre reinforced polymer (CFRP) composite to replace the titanium alloy (Ti-6Al-4V) for the manufacture of turbine compressor blades. These blades are used in the first compression stage of a gas turbine and suffer from high stresses at the roots and rotor discs induced by the high centrifugal forces during operation and are sensitive to vibrations. The blades are of a transonic type with typical rotational speeds of up to 10 000 rpm. The lighter composite blade will reduce stresses on the rotor disc and on the blade root itself as well as having more controllable vibration frequencies.

This project considers the potential problems of replacing a titanium alloy with a carbon / epoxy composite. A FEA (Finite Element Analysis) investigating the displacements, stresses and vibration frequencies induced in the blade during operation have been made. Comparisons between the titanium blade and the composite blade verify the feasibility of using a composite. The composite material that is modelled is carbon fibre in an epoxy matrix. Different laminates such as plain weave and UD (unidirectional) plies are considered, as well as different orientations of the UD plies. The displacements of the blade during operation are analysed and it is found that the use of different orientations of the layers make it possible to control the twisting behaviour of the fibre / epoxy blade. With an optimum lay-up one can control the twist and achieve a higher efficiency of the turbine unit. It is generally found using FEA, that the composite blades exhibit lower induced stresses compared to corresponding strengths of the titanium blade. The vibration frequencies of the composite are found to be higher and it is possible to control the frequencies using different lay-up configurations in the composite blade.

During operation, there is the possibility of foreign objects such as ice and dust particles entering the turbine. It is therefore important to consider both the erosion and impact properties of the fibre / epoxy. Fibre reinforced polymers exhibit poor erosion resistance and an effort has been made to find a suitable coating to protect the composite blade. It is found that elastomeric polyurethane coatings are the most suitable for this application. The most critical section of the blade is the leading edge and a shield of a metal alloy may be required to prevent erosion by foreign particles. During operation the blade will untwist and bend due to the geometry of the blade and loading conditions. Bending tests performed on carbon-, Kevlar® fibre composites and hybrids of these composite materials show that the carbon fibre composite has a superior bending strength and modulus. A finite element model was used to model the impact behaviour of fibre composites and verified by means of a drop weight impact tester. Various tests were carried out with respect to fibre composite materials. Titanium has a better resistance to impact in comparison with the carbon composite but in this application, the impact event resulting from relatively small foreign particles entering the turbine are not likely to cause severe damage under general operating conditions.

GLOSSARY

ABB	Asea Brown Boveri
CAD	Computer Aided Design
CAE	Computer Aided Engineering
CAM	Computer Aided Manufacturing
CCGT	Combined Cycle Gas Turbine
CFRP	Carbon Fibre Reinforced Polymer
CRISP	Counter Rotating Integrated Shrouded Propfan
CPT	Classical Plate Theory
FAA	Federal Aviation Administration
FE	Finite Element
FEA	Finite Element Analysis
FOD	Foreign Impact Damage
FRP	Fibre Reinforced Polymer
IGV	Inlet Guide Vanes
Kevlar	Aramid (aromatic polyamide) fibre manufactured by Du Pont.
KFRP	Kevlar Fibre Reinforced Polymer
MTU	Motoren- und Turbinen-Union München
MW	Mega Watt, 10^6 W
NASA	National Aeronautics and Space Administration
PAN	Polyacrylonitrile
PEEK	Polyether Etherketone
PMC	Polymer Matrix Composite
PMMA	Polymethylmethacrylate
Pre-Preg	Pre-impregnated fibre laminate
RFI	Resin Film Infusion
RTM	Resin Transfer Moulding
SiC	Silicon Carbide
STAL	Svenska Turbin Aktie Bolaget Ljungström
Transsonic	Subsonic and supersonic velocities experienced at different locations on the same component

TABLE OF CONTENTS

CHAPTER 1

INTRODUCTION

1.1 BACKGROUND TO THE INVESTIGATION

In July 1997, Dr Torsten Strand (the product manager for GT10B gas turbines ABB STAL[i]) approached the author. At the time, Dr T Strand was conducting a preliminary investigation to determine the feasibility of replacing existing titanium compressor blades in one of ABB's gas turbines. The proposed substitute for the titanium blade was a fibre composite blade. The motivation for this research was that the blades in the first compression stages of the gas turbine (GT10B[ii]) were suffering from high centrifugal stresses on the blade roots and the rotor discs where the blades are attached. By using a fibre reinforced polymeric material one could reduce the weight of the blades by more than 50%. Since the centrifugal stresses induced on a component are directly proportional to the mass of that component, it was hoped that this would result in lower stresses and more controllable natural frequencies in the blades.

The concept of using fibre composite materials in compressor blades has been investigated by a number of different companies such as NASA, General Electric[iii] and Rolls Royce[iv]. The only existing commercial gas turbine operating with composite fan blades is the GE 90 turbo-fan aircraft engine. These blades have to be able to resist extreme operating conditions such as bird strikes, moisture and ice particles entering the turbine. The use of composite compressor blades in gas turbines for commercial power generating purposes has thus far, not been explored in great detail. The operating conditions of a stationary industrial power generating gas turbine will be less severe than that of an aircraft engine due to more controllable air inlet conditions. This indicates that using composite blades in the first compressor stages of ABB's gas turbines should be feasible with respect to aerodynamical, mechanical and thermal loads.

The use of fibre reinforced composite materials such as carbon- and Kevlar® fibre reinforced polymers are finding increasing use in a wide range of high technology applications. The main reasons for the use of fibre composite components is the need to improve structural efficiency and thereby reduced structural mass without compromising

[i] STAL – Svenska Turbin Aktiebolaget Ljungström

[ii] See URL at: http://www.abb.se

[iii] Composite fan blades are currently being used in the GE 90, aircraft engine

[iv] Extensive research was done on composite fan blades in Rolls Royce's RB 211, aircraft engine

on structural strength and stiffness. Composites offer a number of distinct advantages compared to more conventional engineering materials such as metals. The advantages that fibre composite materials offer include high specific strength and high specific stiffness. It also suggested that the manufacturing costs for fibre reinforced polymer engineering components can be significantly reduced compared to metals. The use of composite materials gives the designer possibilities to tailor the structural advantages in a specific application. The possibility of using different fibre orientations can be used to control the behaviour of the component under a specific loading condition, which can enhance the overall performance.

Composite materials do, however, suffer from some serious limitations. Perhaps one of the most significant drawbacks is the response to localised impact loading. It appears that severe damage can occur with relatively low impact energies. The ability of fibre composites to undergo plastic deformation is extremely limited with the result that energy is frequently absorbed in creating large areas of fracture, which lead to a reduction in strength and stiffness. Furthermore, the prediction of post-impact performance of a damaged composite structure is more difficult to characterise compared to metals since the damage zone is generally complex. Another disadvantage of fibre reinforced polymers is its inadequacy to resist erosion. The gas turbine will operate in conditions where fly ash, dust, water droplets and ice particles are present and these erosive particles will impinge on the blades causing wear on the blades, especially on the leading edges. This problem can be avoided by using erosion resistant coatings such as metals or ceramics to protect the underlying fibre composite. The overall concept of using fibre reinforced compressor blade in ABB's gas turbine should have a considerable scope of success if adequate modelling and testing is performed.

1.2 PROBLEMS TO BE INVESTIGATED

This investigation is focused on 4 specific areas, listed as follows:

I. To model the displacements, stresses and vibrations on the blade during operation using a *Finite Element Analysis (FEA)* approach.
II. To investigate mechanisms of erosion damage and ways of protecting the fibre composite from erosion damage.
III. To determine the impact resistance of the materials to be used in the compressor blade.
IV. To determine mechanical properties of the material to be used.

1.3 SCOPE AND LIMITATIONS OF THE RESEARCH

The scope of the project entails a consideration of aspects that are important in the replacement of titanium compressor blades with fibre reinforced polymer blades in a gas turbine. The focus of this study was on experimental as well as computational methods

to investigate the feasibility of using such blades. The composite compressor blade will be analysed with the aid of the general-purpose finite element code, ABAQUS®. The aim of this analysis is to compare the displacements, stresses and vibrations of the currently used titanium blade with the fibre reinforced composite blade. Various materials such as carbon fibre reinforced polymer (CFRP) and Kevlar® fibre reinforced polymer (KFRP) is to be investigated, using different lay up configurations. Experimental analysis will be performed to establish the erosion resistance of the composite materials to be considered. Erosion testing on a wide range of coatings, for their use as protective measures, will also be performed. The erosion results for the fibre reinforced polymers and coatings are to be compared to that of the titanium alloy used.

Analysis of the impact response of the FRP materials is to be conducted using the force-time, force-deflection and energy-deflection curves generated by the impact rig. The impacted specimen will be analysed microscopically to study the fracture mode characteristics. These experiments are also to be simulated using a finite element model to investigate the correlation between the experimental and analytical results. An additional aspect of the study is to investigate mechanical properties of composite materials considered, for their use in the compressor blades. Since some of the materials considered have a lack of relevant data, experiments were performed to establish the flexural properties for various fibre composites. The limitation of this thesis was the lack of literature available for the specific application of using fibre composite materials in turbine compressor blades. Although work has been done on similar projects, the companies involved are very reluctant to share any information.

CHAPTER 2

LITERATURE REVIEW

2.1 DEVELOPMENTS OF THE GAS TURBINE

2.1.1 INTRODUCTION

The turbine is, in many ways, the most satisfactory way of producing mechanical power today. The absence of reciprocating and rubbing members in the turbine minimises balancing problems, lubricating oil consumption is relatively low, and its reliability can be high. The advantages of the turbine were first recognised using water as a working medium. Hydroelectric power generation achieve a high efficiency and is still a significant contributor to the world's energy resources. In the beginning of the twentieth century the steam turbine began to emerge and has since become the most important source of electricity generation. Steam turbine plants producing 1000 MW of shaft power with an efficiency of approximately 40% are now being used[1]. In spite of the success of the steam turbine, it has one inherent disadvantage and that is that it involves bulky and expensive *steam generating* equipment for conventional boilers or nuclear reactors. The feature of the steam turbine is that the hot gases produced in the boiler furnace, never reach the turbine but are used to heat water into steam. The gas turbine removes this *intermediate* step to produce steam and utilises the hot gases themselves to drive the turbine. It was not until the late 1930's that considerable development of the gas turbine began. Initially it was developed with power generation in mind but attention was soon directed towards aircraft propulsion. In the 1950's the gas turbine began competing in other fields, and has since made a major impact in a variety of applications.

2.1.2 APPLICATIONS OF GAS TURBINES

A turbine can be defined as a machine that produces power by expanding a continuously flowing fluid to a lower pressure or head, the power output usually being expressed in MW[2]. Gas turbines are typically used for aircraft propulsion, pump and compressor drives as well as for power generation. There is often a distinction made between an 'aircraft gas turbine' and 'industrial gas turbine'. The fundamental theory applies to both types even though the constraints and design of the two differs significantly. The main differences are in the limitation of size and weight for the aircraft gas turbine and overhaul life. Figure 2.1 shows the Volvo RM12 military aircraft engine[3]. The industrial gas turbine has a more sturdy design as the life time required of an industrial plant is of the order 100 000 hours, without the need for major overhaul, which can not be expected by an aircraft engine. Figure 2.2 shows the layout of ABB STAL's GT10B gas turbine which delivers 24.8 MW of power[4]. A major market for these gas turbines is for electricity generation in the offshore market. Most offshore platforms use gas turbines as base-load power.

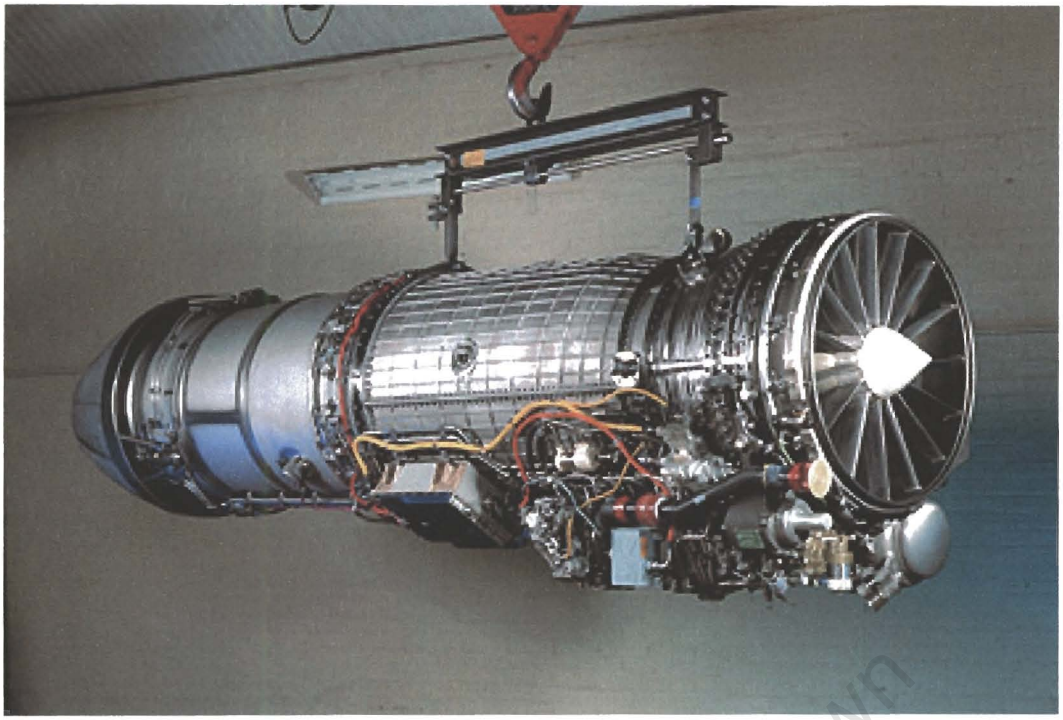

Figure 2.1[3] The Volvo RM12 military aircraft engine powering the single engine Griffin fighter, ordered by the Swedish Air Force and the South African Air Force.

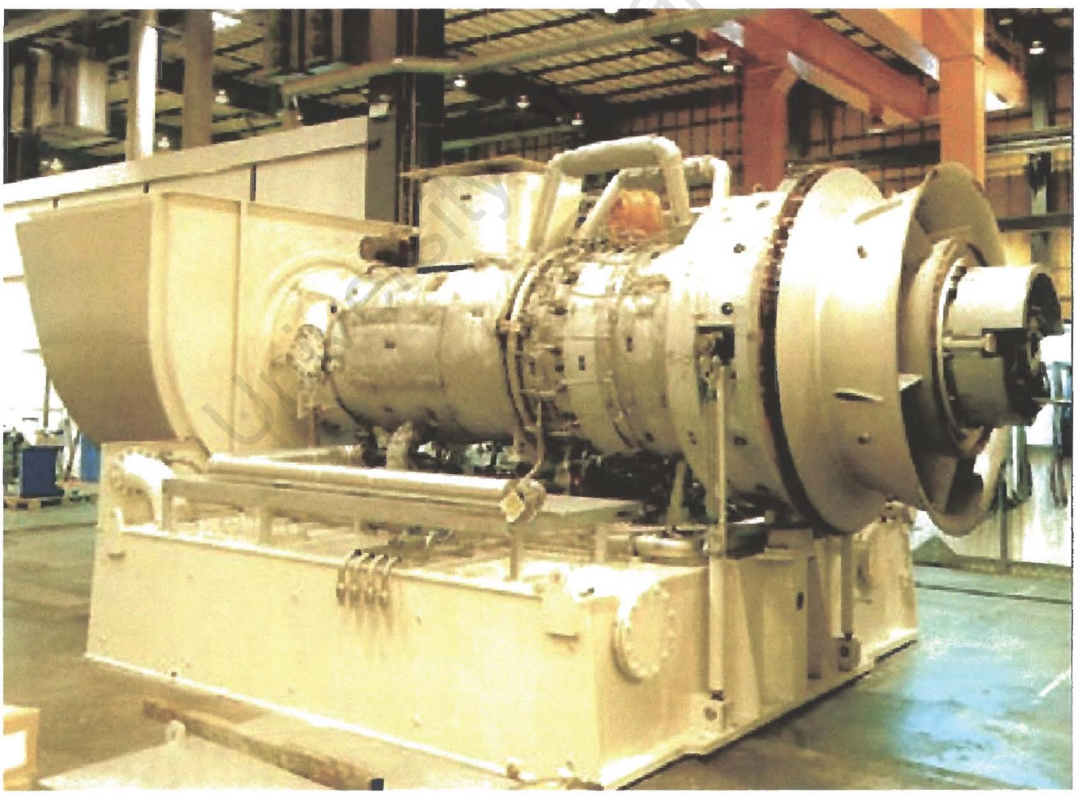

Figure 2.2[4] ABB STAL's gas turbine, the GT10B.

2.1.3 PRINCIPLE OF OPERATION

The three main components in a gas turbine are a compressor, combustion chamber and a turbine connected together. The gas turbine cycle is shown in its simplest form in Figure 2.3[1]. In order to produce an expansion through a turbine a pressure ratio must somehow be provided. The first necessary step in the cycle of a gas turbine plant is to compress the working fluid. The compression stage in this cycle can be performed using different compressors, such as axial or radial compressors (see section 2.1.4). After the working fluid (usually air) has been compressed, fuel is added to the air and the air/fuel mixture is fed into the combustion chamber where combustion is taking place. The hot gases are expanded through the turbine resulting in power output (see Figure 2.4).

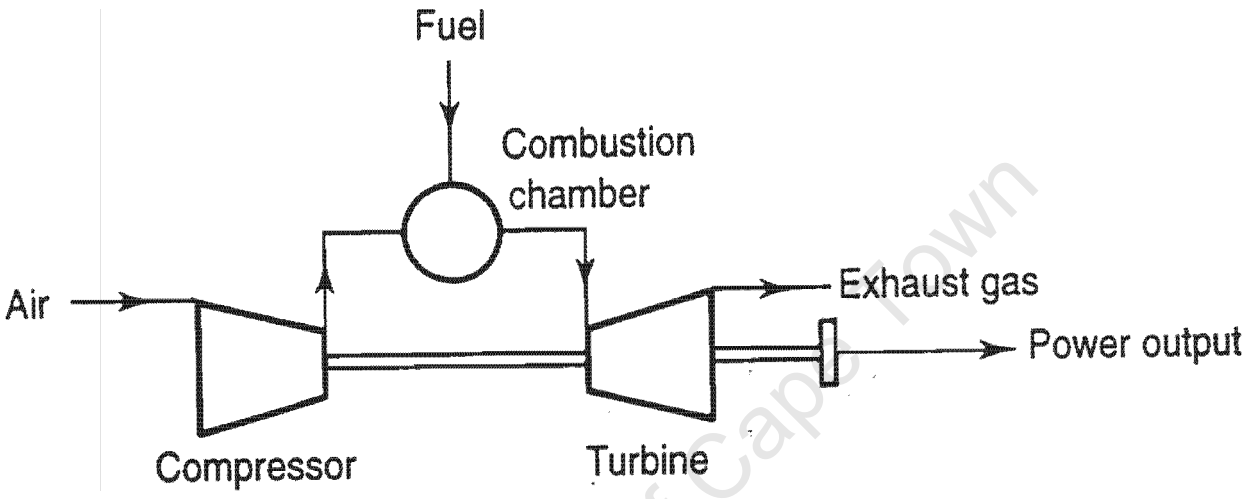

Figure 2.3[1] Schematic of a simple gas turbine system.

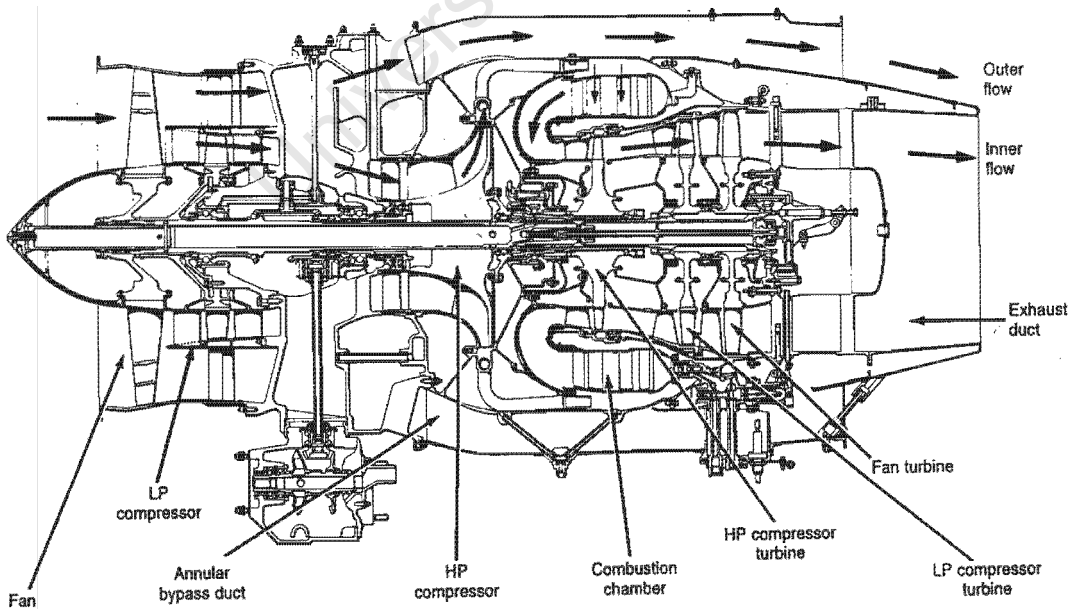

Figure 2.4[1] A small turbofan engine.

The three main factors affecting the performance of gas turbines are the component efficiencies, the turbine working temperature and the pressure ratio of the compressor[1]. The higher these factors can be made the higher the efficiency of the gas turbine unit. The limiting factors are often the turbine and compressor blades, which suffer from high temperatures and rotational speeds, respectively. It is important to realise that the compression, combustion and expansion do not occur in a single process as they do, for example, in a reciprocating engine. These components can be designed, tested and developed individually. Other components can be added to the turbine to achieve a higher efficiency. Often, inter-coolers, re-heaters and heat exchangers are used to improve the efficiency.

In recent years ***combined*** steam and gas cycles have received increased attention due to higher efficiency and lower emission levels of NO_x compared to conventional plants[5,6,7]. Combined gas and steam turbines, the so-called combined cycle gas turbine (**CCGT**) currently offer the most attractive power plant for economic and environmentally friendly electricity generation[7]. Gyarmathy has shown that even at high thermal efficiencies of between 44% and 55%, the CCGT have CO_2 emissions of 30% and 60% lower respectively, than that of a modern steam turbine plant burning natural gas and coal, respectively[8]. Furthermore, its installation costs and build times are relatively low, making the CCGT especially attractive to the privatised electrical supply industry. Combined gas and steam turbines achieve high efficiencies using a Brayton gas turbine cycle combined with a Rankine steam turbine cycle[9].

ABB STAL has recently supplied a combined-cycle co-generation plant to the Finnish utility, Kotkan Energia Oy. The efficiency is above 50% and the plant conforms well to Europe's strict emission regulations[10]. The tightening of European Community (EC) regulations on sulphur emissions from power plants and the availability of natural gas at economic prices, made natural gas ideal fuel for high temperature gas turbines[11]. These recent developments in technology and the stringent regulations have made the gas turbines a feasible source of power generation.

2.1.4 COMPRESSORS

There are presently two distinct types of compressor designs that are being used in gas turbine applications *viz.* the centrifugal (radial) compressor and the axial flow compressor. Although these compressors are used today, there was a compressor design called the *displacement* compressor that was widely used in the 1940's to 1950's. It is essentially a reciprocating combustion engine driving pistons that compresses air. The primary fuel used is diesel. This type of compressor is, however, not widely used today.

2.1.4.1 THE CENTRIFUGAL COMPRESSOR

The centrifugal compressor finds the most widespread use of any type[12]. This type of compressor is suited primary for handling small volume flows. In the late 1950's it became clear that the smaller gas turbines would have to use centrifugal compressors. The advantages of using a centrifugal compared to an axial compressor, include a shorter overall length, better resistance to foreign object damage (FOD) and the ability to operate over a wider range of mass flow at a particular speed[12]. The centrifugal compressor is

largely found in turbochargers, where it is placed on the same shaft as an inward-flow centrifugal gas turbine, which is commonly driven by the exhaust gases. The best efficiencies found for a centrifugal compressor generally lies between 5 and 10% below that of an axial compressor. The principle of operation of the centrifugal compressor involves a stationary casing containing a rotating impeller, which transmit a high velocity to the air, and a number of fixed diverging passages in which the air is decelerated with the result of a rise in static pressure. Figure 2.5 shows a schematic of a centrifugal compressor.

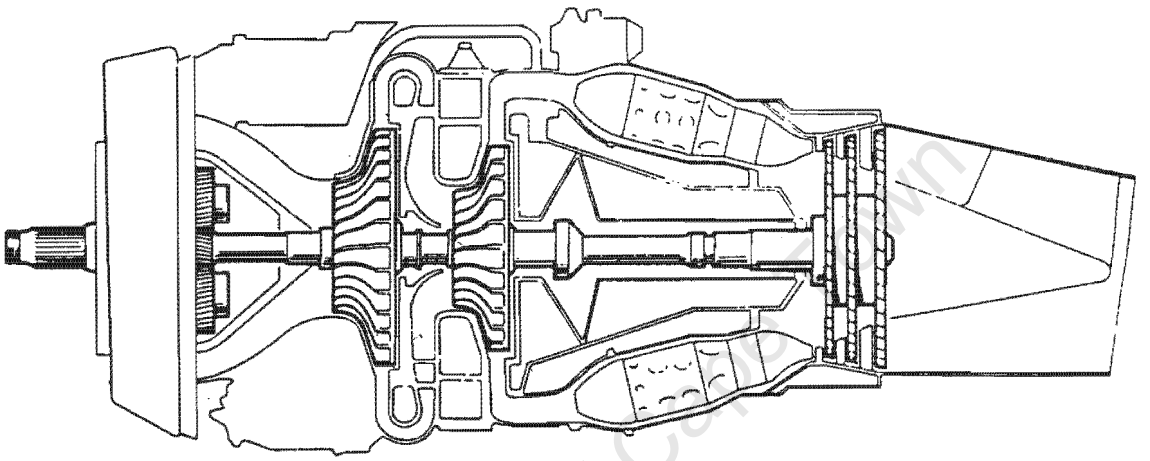

Figure 2.5[1] Schematic of a centrifugal single shaft turboprop engine.

2.1.4.2 THE AXIAL FLOW COMPRESSOR

From an early stage in the history of the gas turbine it was realised that the axial flow compressor had numerous advantages compared to the centrifugal compressor. The three main advantages of the axial compressor compared to the centrifugal compressor are[1]:

- a higher pressure ratio
- a higher efficiency and a
- larger flow rate for a given frontal area

These potential benefits have been fully understood and research into the aerodynamics of axial compressors has resulted in its domination of the field when large power requirements are necessary. The centrifugal compressor is today restricted to the lower end of the power generation where the flow is too small to be managed by axial blading. The axial compressor consists of a rotor of cylindrical or conical form carrying the moving blades. These blades are travelling at high speeds within the *stators* (stationary) blades. Figure 2.6 below shows an axial compressor with 10 stages of compression[4].

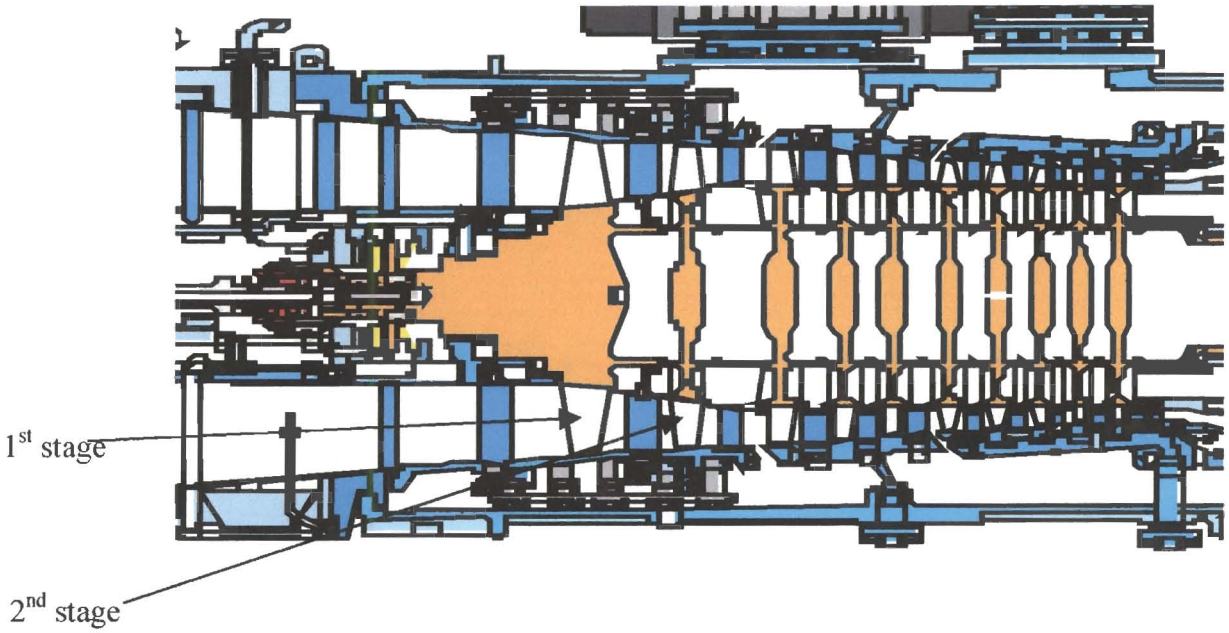

Figure 2.6[4] The layout of ABB STAL's axial compressor, the GT 10B.

Each compression stage consists of rotor blades and stator blades. The working fluid is accelerated by the rotor blades and then decelerated by the stator blades thus converting the kinetic energy to static pressure. The process is repeated to yield the required overall pressure ratio. Figure 2.6[4] show the change in blade size from the front to the rear in a high-pressure ratio compressor. In the axial compressor it is usually desirable to keep the axial velocity fairly constant throughout the compressor. With the compressibility effect of the working fluid, the density of the working fluid will increase as the flow progresses through the compressor. It is therefore necessary to reduce the flow area and hence the blade height. Problems occur when the compressor is running at a lower speed than the design speed. This will result in the density being far from the design value for the last stages, which can cause blade stalling and surging[1]. There are several methods to overcome this problem. One approach is to use inlet guide vanes (IGVs), permitting the flow angle entering the first stage to vary with rotational speed to improve the off-design performance.

2.1.5 RECENT DEVELOPMENTS IN COMPRESSOR BLADES

2.1.5.1 HISTORY

The unsuccessful attempt made by Rolls Royce in 1968 to use polymer matrix composite (PMC) blades for a commercial *aircraft* gas turbine resulted in substantial negative publicity of this potential application[13]. It was not until General Electric (GE) decided to develop a carbon composite fan blade in the early 1990's that revived the concept[14]. The GE 90 turbo fan engine utilises 22 transonic* composite blades. These PMC blades are the

* The blades experience subsonic velocity at the base and supersonic velocities close to the tip of the blade.

first to be used in commercial aircraft gas turbines. The concept of using composite blades in compressors is nothing new. NASA conducted research on using composite compressor blades in the early 1970's and concluded that there were distinctive advantages of using such blades[15]. The mostly common found material used in compressor blades today are titanium alloys. Titanium offers good mechanical properties and offers the "reliable" properties of a metal. Currently Rolls Royce is using a hollow, super-plastically formed and diffusion bonded (SPF/DB) titanium fan blade. Interestingly, this concept was initialised approximately at same time as the PMC blade for Rolls Royce's RB211[13]. The hollow titanium fan blade offers the only viable alternative to PMC fan blades today.

The fate of the original carbon fibre/PMC RB 211 fan blade was mainly due to its "*inability to satisfy the demanding bird ingestion requirement*"[13]. During the take-off phase, the aircraft engines might suffer from bird ingestion, which can cause serious damage or, in the worst case scenario, flight shutdown[16]. The early PAN (polyacrylonitrile) based fibres exhibited a high statistical variability in fibre strength as well as limited quality standards from early production processes. The lack of ductility and toughness characterised by the low strain to failure and interlaminar shear strength of the early carbon fibres proved to be inadequate in soft body impact such as bird ingestion. Additional disadvantages in Rolls Royce's attempt with the PMC fan blade were the lack of design analysis methods and manufacturing options.

2.1.5.2 ENHANCEMENTS IN THE TECHNOLOGY REGARDING FIBRE COMPOSITE FAN BLADES

Since the early attempts of using carbon fibre/epoxy matrix systems in the late 1960's, there have been several significant areas of improvement[17]. The three main areas are:

- enhancements in the mechanical properties of the fibre and matrix,
- more reliable manufacturing methods and
- improved computing facilities and sophisticated design programs that have been developed.

In the past 25 years both the strength and the stiffness of available fibres have increased substantially. Furthermore, it is now possible to obtain fibres with both a high strength and modulus, which was not available previously. The benefits in strength, strain to failure and modulus of carbon and graphite fibres have created considerable improvements in the in-plane properties of laminates in highly loaded composite components[13]. Similar benefits in transverse and interlaminar matrix dominated properties are achieved through gains in polymer matrix ductility, toughness and the improved understanding of the influence of the fibre-matrix interface. Table 2.1[13] illustrates the enhancements in carbon/graphite fibre properties over the years.

Table 2.1 Improvements in the properties for carbon/graphite fibres[13].

Year	Manufacturer	Fibre	Fibre failure strength (MPa)	Modulus (GPa)	Fibre failure strain (%)
1967	Rolls Royce	"HYFIL"	2070	207	0.94
1978	Amoco	T300	3100	234	1.30
1980	Hercules	AS4	3930	234	1.60
1985	Hercules	IM6	5100	276	1.73
1986	Hercules	IM7	5310	276	1.81
1987	Hercules	IM8	5450	303	1.67

The available manufacturing methods currently for high tech applications like composite compressor blades, include using pre-impregnated fibres (pre-preg), resin transfer moulding (RTM) and resin film infusion (RFI). Pre-pregs have been used for the fan blades of the GE-90 and by MTU (Motoren- und Turbinen-Union München) for testing on a counter rotating integrated shrouded propfan (CRISP) with composite blades[18]. While the pre-preg method is widely used for these types of applications, Daimler-Benz Aerospace in Germany developed composite compressor stator vanes and found that the RTM process gave satisfactory results[19]. With the improved properties of fibre/matrix systems all these manufacturing systems will provide a high performance component.

Perhaps the most considerable development that has taken place since the period from 1968 to the present, is the analysis capability available for engineers. Only crude modelling and analysis techniques were available in the late 1960's. Although finite element technology development and application thereof, was rapidly growing in the late 1960's, it was only later (about 1975) before advanced composite anisotropic layered structures could be effectively modelled, recognising the fact that computational capabilities allowed relatively low computational time. The computer applications tools now available can effectively link the computer-aided design (CAD), finite element analysis (FEA) and computer-aided manufacturing (CAM). Numerous special purpose as well as general software developments are being used to analyse complex structures before actual experimental testing is being performed. The finite element (FE) software allows the user to investigate deflections, stress, strains, impact and vibrations for a composite structure. The layered composite component can then be analysed layer by layer to find critical areas that might initiate failure.

2.1.6 THE USE OF COMPOSITE COMPRESSOR BLADES FOR AN INDUSTRIAL GAS TURBINE

Most of the research done on composite compressor blades has been on aircraft applications. Little effort has been made to use PMC blades in industrial gas turbine applications. It is perhaps a bigger advantage using lighter fan blades on an aircraft, since the blades are usually very large. For example, the PMC fan blades of the GE-90, which has a blade, span of 1.2 m weights only 16.3 kg[13]. However, the relatively low impact resistance of carbon fibre composites, which resulted in Rolls Royce terminating their fan

blade project, is a major obstacle. It is important to realise that the bird ingestion requirement is extremely demanding since the blades have to manage a 4-lb soft body ingestion at high velocity. In an industrial gas turbine the impact problems are of far less severity and the compressor blades are much smaller. The potential advantages of using PMC blades in an industrial gas turbine are: less centrifugal stresses on the blade root and rotor discs, more controllable natural frequencies and a manufacturing cost that have been estimated to be almost half that of a titanium alloy. An additional feature is that the deflection of the composite blade during operation can be controlled by the choice of fibre lay-up. This could potentially improve the operating range of the turbine. The problem areas that the PMC compressor blades are likely to encounter are erosion and impact resistance.

The composite blades need to be protected by a suitable coating to avoid erosion when the turbine is operating in environments where dust, ash and sand are likely to enter the turbine and cause damage to the blades. The problem of erosion on gas turbine compressor blades was early recognised by Tilly[20]. When larger particles, such as ice particles, are ingested, there is possibility of damage to the composite blade. Incorporating a more impact resistant material such as Kevlar® will enhance the impact properties of the fibre composite.

2.2 FINITE ELEMENT ANALYSIS FOR COMPOSITE APPLICATIONS

2.2.1 INTRODUCTION

Sophisticated finite element analysis programs and laminated-plate theories help define the properties of a composite structure[21]. An inherent difference between composites and metals is that composite products are constructed in layers or plies of directional material. Interfacial adhesion and the potential for de-lamination under shear or compressive loads must be considered when analysing an advanced composite design. This information is essential when addressing the variable requirements of a composite component. Composites differ from metals in that they do not carry loads equally in all directions, *i.e.* it is anisotropic, but bear loads best in tension. The directional nature of the fibre's load-bearing abilities changes the rules of structural design[22].

When comparing the mechanical properties for different advanced metals to a carbon/epoxy composite, it is obvious that there is a range of advantages using composites. The carbon fibre composite mostly used for advanced applications is less than one quarter the weight of steel, but is about as stiff (which makes it almost four times as stiff on a weight-to-weight basis), and it is roughly four times as strong in tension. Carbon fibre also has a better fatigue life than steel, titanium, or aluminium, and the resins typically used to bond the fibres offer extremely good vibration damping[23].

2.2.2 THE FINITE ELEMENT METHOD (FEM)

The Finite Element Method (FEM) can be stated as follows: "The FEM is a computer-aided mathematical technique for obtaining approximate numerical solutions to the abstract equations of calculus that predict the response of physical systems subjected to external influences"[24]. Problems that can be solved using the FEM include *solid mechanics* (*e.g.* elasticity, plasticity, statics and dynamics), *heat transfer* (*e.g.* conduction, convection and radiation) and *fluid mechanics* (*e.g.* flow field in the vicinity of compressor blades). A finite element is derived by assuming a form of the equation for the internal strains[25]. There will be one equation for each degree of freedom of each node of the element. These equations are most conveniently written in a matrix form for use in computer algorithms. The matrix of the coefficients becomes a "*stiffness matrix*" that relates forces to displacements as stated in equation 1.

$$[F]=[K]*[d] \qquad (2.1)$$

where, F, K and d are the force vector, stiffness matrix and displacement vectors, respectively.

2.2.3 ISOPARAMETRIC ELEMENT FORMULATION

Finite element (FE) methods are implemented in computer code, not algebraically, so numerical integration is the procedure that is used. To implement computer code solving FE problems, isoparametric elements are used for computational advantages[26]. The isoparametric formulation makes it possible to generate elements that are non-rectangular and have curved sides. The isoparametric formulations include elements for solid, plate and shell problems. The features of the isoparametric elements are:

- Isoparametric elements are defined on the ξ, η and ζ axes, not on the x, y and z-axes. (3D)
- Isoparametric elements are defined on the domain: $-1 < \xi, \eta, \zeta < +1$.
- There exists a mapping from the isoparametric domain to the problem domain. The isoparametric mapping of the isoparametric element in the (ξ, η ζ) domain to the (x, y, z) domain (3D), is achieved by the mapping:

  $$x = \sum N_i x_i, \quad y = \sum N_i y_i, \quad z = \sum N_i z_i \qquad (2.2)$$

  where i ranges over the number of nodes in the element. The shape functions N_i (or trial functions) are functions of the isoparametric co-ordinates ξ, η and ζ. The shape functions for a linear solid element (also called eight-noded brick element) are:

  $$N_i = 1/8\ (1\pm\xi)(1\pm\eta)\ (1\pm\zeta), \text{ where } i=1,2,3, \ldots, 8. \qquad (2.3)$$

- The derivative of the mapping, the *Jacobian,* provides a numerical value to the local amount of expansion or contraction of the co-ordinates due to the isoparametric mapping[25]. The Jacobian is a 3×3 matrix for a 3D element and is given by:

$$\mathbf{J}(\xi,\eta,\zeta)=\begin{bmatrix} \frac{\partial x}{\partial \xi} & \frac{\partial y}{\partial \xi} & \frac{\partial z}{\partial \xi} \\ \frac{\partial x}{\partial \eta} & \frac{\partial y}{\partial \eta} & \frac{\partial z}{\partial \eta} \\ \frac{\partial x}{\partial \zeta} & \frac{\partial y}{\partial \zeta} & \frac{\partial z}{\partial \zeta} \end{bmatrix} \tag{2.4}$$

2.2.4 THREE DIMENSIONAL FEM

The linear isoparametric solid element is seen in Figure 2.7.

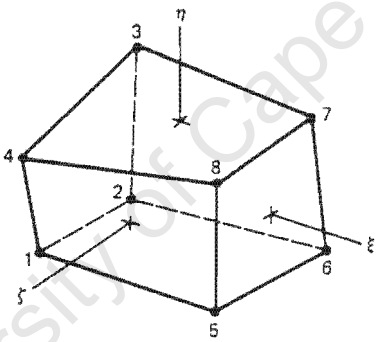

Figure 2.7[27] A three dimensional linear solid element.

The stiffness matrix for a 3 dimensional problem becomes:

$$[\mathbf{K}]=\int_{-1}^{1}\int_{-1}^{1}\int_{-1}^{1}[\mathbf{B}]^{T}\,\mathbf{k}\,[\mathbf{B}]\,\mathbf{J}\,d\xi d\eta d\zeta \tag{2.5}$$

where the *Jacobian determinant*, $|\mathbf{J}|$, expresses the ratio of volume from dx, dy, dz to $d\xi$, $d\eta$, $d\zeta$ and $[\mathbf{B}]$ is a function of ξ, η, and ζ[27].

2.2.5 THE USE OF FEM FOR COMPOSITE STRUCTURES

The finite element method is now the most popular numerical technique for the analysis of composite structures[28]. Today there are a wide range of FE codes available that incorporate composite material analysis. The mechanics behind fibre composite materials make hand

calculations tedious, which is the main reason why FE analysis is used for composite components and structures. One of the critical decisions that have to be decided upon early in the process is to evaluate how detailed and accurate the analysis need to be. If a complex structure needs to be modelled, it is usually necessary to make assumptions in the process of setting up a FE analysis. Assumptions should be made such as to ensure that reasonable results are obtained at an acceptable cost. A FE analysis will generally always contain assumptions that will lead to errors in the predictions of deflections and stresses of a structure [29, 30].

The purpose of FE modelling is to make a model that behaves mathematically like the structure that is modelled, not necessarily one that looks like the real structure[31]. Boundary conditions are required to ensure that the behaviour of the model approximates the behaviour of the real structure. When it is not possible to establish an accurate representation of boundary conditions, it might be advisable to use different sets of conditions that can be examined to investigate the sensitivity of the solution. After the boundary conditions have been determined for the model, the loading conditions are then applied. Most available FE codes have a large number of different loads that can be applied such as: point loads, distributed loads, pressure and centrifugal loads. The loading conditions in a model can sometimes be complex, and again approximations might be necessary. The next step is to define the material data for the composite elements in the model. This is normally straightforward when isotropic systems are concerned, but difficulties are often encountered when composite materials are used.

The analysis of a composite component that involves a through thickness consideration presents problems in determining the material data for the elements. Through thickness properties for Young's modulus and Poisson's ratio of a composite are not readily available and approximations need to be considered when determining these constants. Caution must also be taken when using symmetry in a FE model involving composites; properties will not simplify in all directions. Another important modelling decision to consider is the dimensionality of the problem. The most common situation that arises with advanced composites is the plane stress situation, where out-of-plane stresses are negligible. These problems are best modelled using plate or shell elements, which utilise classical plate theory (CPT) and Mindlin higher order plate theory[32]. The structure is then approximated as an assemblage of plates or shells. If the composite structure is made of a large amount of plies it may be necessary to model the component with 3 dimensional elements. It is also possible to combine shell elements and 3 dimensional elements to form hybrid models, *i.e.* models consisting of combinations of element types.

2.2.6 STEPS IN FE ANALYSIS

Finite element modelling consists of three steps[31]. These are:

1. Pre-processing
2. Solution
3. Post-processing

The pre-processing includes the entire process of constructing the geometry of the FE model, applying physical and materials properties and describing the boundary and loading conditions. This first step involves a decision of the number of elements in the model. Choosing an inadequate finite element mesh can lead to errors in the final model[33]. It is important to have a mesh density that can reveal stress concentration effects. The larger the number of elements in the model the more accurate the solution, but the computational time is always a factor that have to be considered, so the appropriate number of elements in the model is an important consideration for the user to make. The solution part of the analysis involves determining all the local governing stiffness matrices for the elements and assembles all these into a global stiffness matrix, from where all the unknown degrees of freedom can be solved. The analysis of composite structures usually requires more computing capacity than for isotropic models. This is due to the more complex element formulation of the composite elements.

Post-processing involves plotting deflections and stresses. These results can be compared to the failure theories imposed on the material, such as the maximum deflection allowed and the material strength. There are especially two considerations that need to be considered in the post-processing. Is the model accurate, with the assumptions made and is the structure satisfactory? The post-processing should include checking for errors that might not have been detected while building the model, such as performing some kind of hand calculations. Often all the FE steps can be done entirely within a CAE system. Building the FE model is increasingly accomplished by using integrated CAE packages that can create geometry, apply boundary conditions, divide the structure into a grid of elements (meshing), solve and post-process the result all in one.

2.2.7 THE CHOICE OF COMPOSITE ELEMENTS IN FINITE ELEMENT ANALYSIS

The FE modelling done in this thesis has been done exclusively using the general-purpose finite element code ABAQUS/Standard®*. An element's formulation refers to the mathematical theory used to define the element's behaviour. All the stress/displacement elements in ABAQUS are based on the theory that the elements deform with the material. (Lagrangian behaviour) To accommodate for different types of behaviour there are a range of different element families. Each element family is suited for a certain application. Examples of element families in ABAQUS are solid elements, shell elements, beam elements, rigid elements and membrane elements. In ABAQUS there are two element families that can be used to model composites. These two are the solid (brick) and shell elements.

2.2.7.1 PROPERTIES OF COMPOSITE SOLID ELEMENTS

For a solid element there are three translational degrees of freedom at each node compared to six degrees of freedom for shell elements. While laminated composite structures are usually modelled by using shell elements there are cases when 3 dimensional (3-D) brick

* ABAQUS version 5.8

elements should be used. The following cases should be modelled using 3 dimensional (3-D) brick elements[34],

- When transverse shear effects are predominant, it is advisable to use 3-D elements to accurately model this situation.

- Usually composite structures are relatively thin and the assumption of plane stress within this structure is valid. Shell elements are therefore the most suited for thin structures ignoring the out of plane stresses. However, when the out of plane stress cannot be ignored, it is required to use 3-D brick elements to accurately model the composite structure.

- When accurate inter-laminar stresses are required, such as in thick composite structures with complex loading and at localised regions of complex geometry.

2.2.8 FAILURE PREDICTIONS IN COMPOSITE STRUCTURES

There are several theories developed for studying the failure of lamina[35, 36, 37]. The theories are generally based on the normal and shear strengths of a unidirectional lamina. In the case of a unidirectional lamina, there are two material axes, one is parallel to the fibres and one is perpendicular to the fibres. Thus, there are four normal strength parameters to be considered, one for tension and one for compression in each of the material axes. The fifth strength parameter is the shear strength of a unidirectional lamina. These five strength parameters are:

$\left(\sigma_1^{\ T}\right)_{ult}$ = Ultimate longitudinal tensile strength in direction 1.

$\left(\sigma_1^{\ C}\right)_{ult}$ = Ultimate longitudinal compressive strength in direction 1.

$\left(\sigma_2^{\ T}\right)_{ult}$ = Ultimate longitudinal tensile strength in direction 2.

$\left(\sigma_2^{\ C}\right)_{ult}$ = Ultimate longitudinal compressive strength in direction 2.

$\left(\tau_{12}\right)_{ult}$ = Ultimate in-plane shear strength in plane 1-2.

2.2.8.1 MAXIMUMUM STRESS FAILURE THEORY

This theory is related to the maximum normal stress theory by Rankine and the maximum shear stress theory by Tresca[38]. It is similar to theories applied to isotropic materials. The stresses acting on a laminate are resolved into normal and shear stresses and failure is

predicted when the normal or shear stresses equal or exceed the corresponding ultimate strength of the unidirectional lamina[36]. The lamina is considered to fail if any of the following criteria is violated. In these equations all five strength parameters are treated as positive numbers. It is noted that each component of stress compared to its failure criterion has no interaction with the others.

$$-\left(\sigma_1^{C}\right)_{ult} < \sigma_1 < \left(\sigma_1^{T}\right)_{ult} \tag{2.6}$$

$$-\left(\sigma_2^{C}\right)_{ult} < \sigma_2 < \left(\sigma_2^{T}\right)_{ult} \tag{2.7}$$

$$-\left(\tau_{12}\right)_{ult} < \tau_{12} < \left(\tau_{12}\right)_{ult} \tag{2.8}$$

2.2.8.2 TSAI-WU FAILURE THEORY

This theory is based the *total strain energy theory* by Haigh[38]. Tsai and Wu applied this theory to a lamina in plane stress[36]. Failure of the lamina is predicted when:

$$\mathbf{H}_1\sigma_1 + \mathbf{H}_2\sigma_2 + \mathbf{H}_6\tau_{12} + \mathbf{H}_{11}\sigma_1^2 + \mathbf{H}_{22}\sigma_2^2 + \mathbf{H}_{66}\tau_{12}^2 + 2\mathbf{H}_{12}\sigma_1\sigma_2 < 1 \tag{2.9}$$

where, $$\mathbf{H}_1 = \frac{1}{\left(\sigma_1^T\right)_{ult}} - \frac{1}{\left(\sigma_1^C\right)_{ult}}, \quad \mathbf{H}_{11} = \frac{1}{\left(\sigma_1^T\right)_{ult}\left(\sigma_1^C\right)_{ult}} \tag{2.10}$$

$$\mathbf{H}_2 = \frac{1}{\left(\sigma_2^T\right)_{ult}} - \frac{1}{\left(\sigma_2^C\right)_{ult}}, \quad \mathbf{H}_{22} = \frac{1}{\left(\sigma_2^T\right)_{ult}\left(\sigma_2^C\right)_{ult}} \tag{2.11}$$

$$\mathbf{H}_{66} = \frac{1}{\left(\tau_{12}\right)^2_{ult}} \tag{2.12}$$

$$\mathbf{H}_{12} = -\frac{1}{2\left(\sigma_1^T\right)^2_{ult}} \tag{2.13}$$

Figure 2.8 and Figure 2.9 show the comparison of experimental results with the failure theories discussed above.

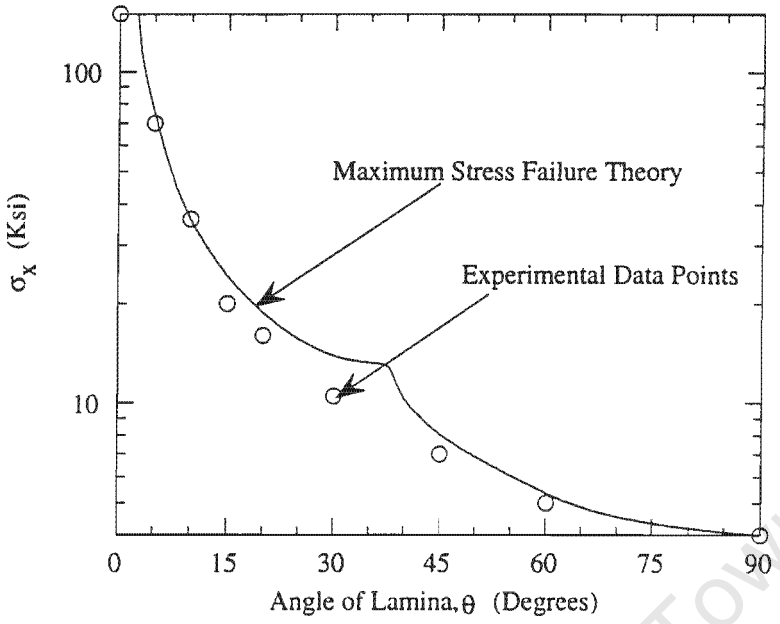

Figure 2.8[36] Maximum normal tensile stress in the x-direction vs. lamina angle using stress failure theory.

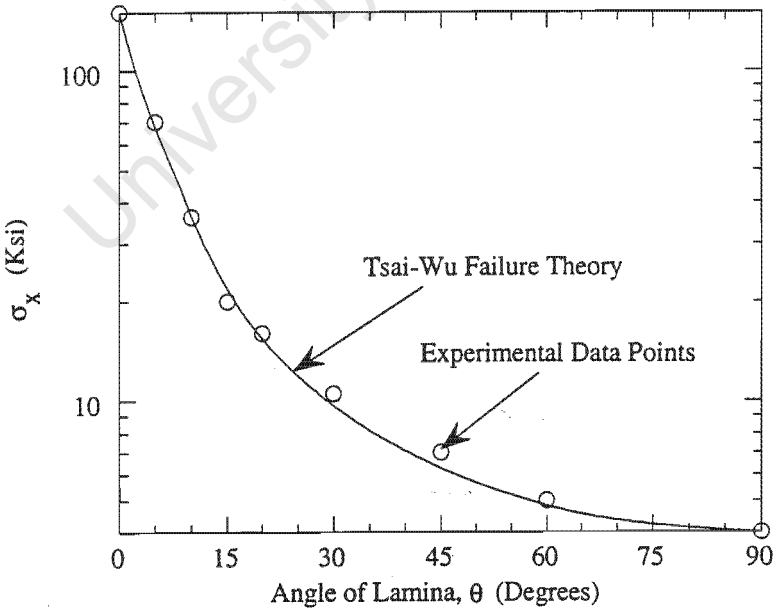

Figure 2.9[36] Maximum normal tensile stress in the x-direction vs. lamina angle using Tsai-Wu failure theory.

2.2.9 VIBRATIONS

If a metal component is to be replaced by using a lighter composite material, the natural frequencies will change due to the stiffness/weight ratio of the composite. Consequently, by using composite materials it is possible to prevent natural frequencies occurring within the operating range for rotating machinery. Considering a rotating turbine shaft with blades on it, there are often problems during start-up due to the fact that the blades have to go through their natural frequencies which coincides with the harmonic excitations of the turbine. If blades were made from a light and stiff fibre composite, the natural frequencies would be higher and resonance frequencies would be less of an obstacle compared to the use of a metallic material.

An additional advantage from resonance point of view is that if fibre composite blades were expected to experience resonance during operation at design speed, it would not be necessary to change the geometry of the blade, which would have been the case with a metal blade. Instead one could change the fibre lay-up to achieve different fundamental blade frequencies. In practice it is important to prevent high cycle fatigue failures due to harmonic excitation. The harmonic excitations ("force functions") must not interact with fundamental blade frequencies at the design speed. In this case the Campbell diagram is the decisive design criterion[18] (see Figure 2.10). The Campbell diagram shows the frequency [Hz] *vs.* rotational speed (rpm) for the entire operating range of a turbine. The operating design speed range has to be free of main resonances.

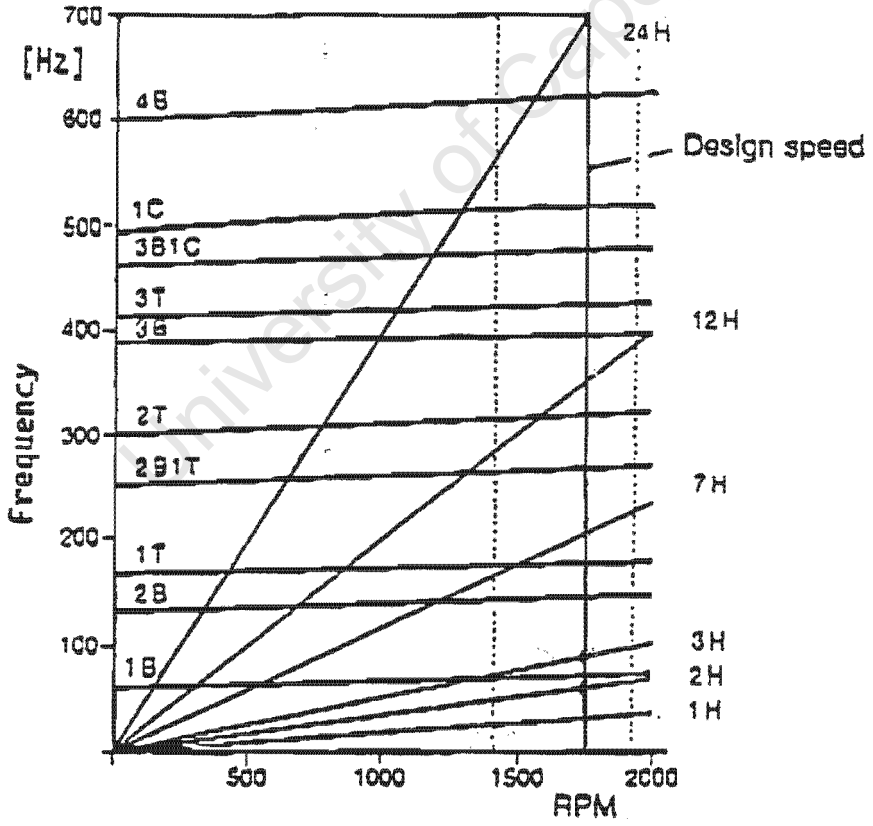

Figure 2.10[18] Campbell diagram for a composite fan blade

2.3 SOLID PARTICLE EROSION

2.3.1 INTRODUCTION

Solid particle erosive wear can be described as the process whereby a solid surface experiences wear as a result of the impingement by solid particles that are carried in a fluid stream[39]. In situations where erosive wear is deleterious to the performance and structural reliability of a component, it is important that a material with high erosion resistance is chosen. Many industrial applications suffer from being exposed to erosive environments, which can reduce the life of a component drastically. Solid particle erosion occurs in pipes carrying slurries, in helicopter engines operating in dusty environments and in the compressor blades of gas turbines, where abrasive particles are ingested and carried in an air stream under high pressure[20, 40].

A particle striking a surface will have several forces acting upon it as shown in Figure 2.11. Inter-particle contact forces are a result of other particles colliding and exerting a force, while a drag force is a consequence of a liquid being present. However, the governing force on the erosive particle is the surface contact force, which is responsible for decelerating the particle from its initial impact velocity[39]. The amount of material removed from the impact event depends on the contact force between the particle and the impact surface. It also depends on the properties of the erodent and the target material. In addition, the amount of wear taking place also depends on the particle flux and the mass of individual particles impinging on the surface.

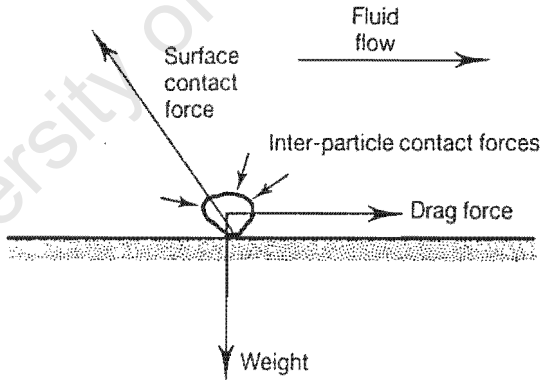

Figure 2.11 Schematic showing the forces acting on an erodent particle in contact with a solid surface. (After Hutchings[40]).

2.3.2 MECHANISMS OF EROSION

The understanding of the erosion phenomenon may be divided into distinct areas, which are discussed in the following sections. The erosion of materials is often divided into plastic deformation (ductile) and brittle fracture in order to understand the mechanism of erosion.

The following sections will identify the various parameters affecting the erosion properties of a material.

2.3.2.1 EROSIVE WEAR BY PLASTIC DEFORMATION

Previous studies have shown that most materials exhibit a combination of ductile and brittle erosion[20, 41]. At low impact angles ductile erosion predominates, whilst the brittle mode becomes more dominant as the angle is increased. Studies of impact sites by single particles at an angle of 30° have revealed three basic types of impact damage as shown in Figure 2.12. Displacement of material to the front and side of the impacting particle results in deformation called *ploughing*. Ploughing is usually due to the erodent particle having a rounded appearance. Further impacts lead to the loss of the heavily strained material from the rim of the crater or the protruding lip that was formed. *Cutting* is the erosion loss as the result of a sharp angular particle removing a chip of material from the target surface[40]. *Type 1 cutting* occurs when angular particles strike the surface and roll forward, indenting the surface and raising material into a large lip. The lip that is formed is likely to be removed by subsequent impacts. *Type 2 cutting* is a result of the impacting particle rolling backwards and producing a machining action. This latter mode of deformation only occurs over a limited range of particle shapes and impact orientations.

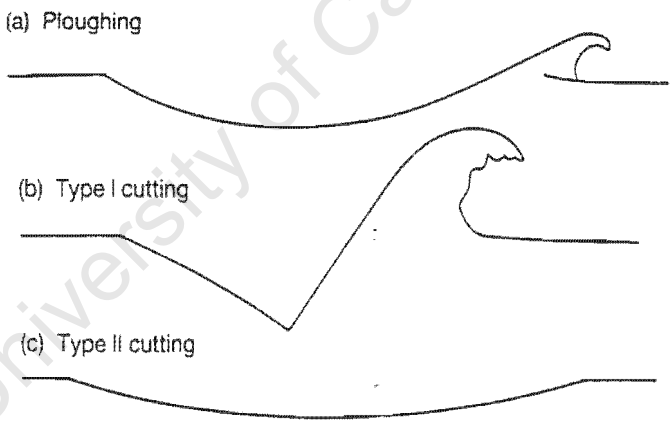

Figure 2.12[40] Shapes of impact sites formed by hard particles striking a ductile material. (a) ploughing deformation by a sphere, (b) type I cutting by an angular particle rolling forward (c) type II cutting by an angular particle rolling backwards.

In each of the deformation modes described above it should be noted that even though each impact displaces material, it will often not become detached as wear debris until it has experienced sufficient cycles of plastic deformation to become severely work-hardened.

The mechanism resulting in the three types of deformation modes, as shown in Figure 2.12, is most deleterious at shallow angles around 30° [40]. At impact angles of normal incidence, cutting does not play any role with this model. At erosion angles of 90° a different mechanism is present. The *platelet* mechanism of erosion of ductile materials was proposed by Levy as the mechanism of material loss by solid particles[42]. The loss of material occurs by a combined extrusion-forging mechanism. The erodent particle impacts the surface and gives rise to *platelets* of material that is extruded from the impact crater. Subsequent erodent impacts induce spreading of the extruded platelets by forging and eventually removal of the platelet occurs. This mechanism of erosion described accounts for the erosion behaviour that the cutting mechanism could not account for.

2.3.2.2 EROSIVE WEAR BY BRITTLE FRACTURE

Material loss by brittle fracture originates from solid particles impacting the surface and result in the formation of cracks. The velocity, shape and mechanical properties of the erodent striking the surface influence the modes of cracking. Conical Hertzian fractures of the form shown in Figure 2.13 are caused by rounded particles[40]. A particle impacting the surface will have a normal load, which initiates a crack outside the contact circle and rapidly propagates to form a Hertzian conical crack.

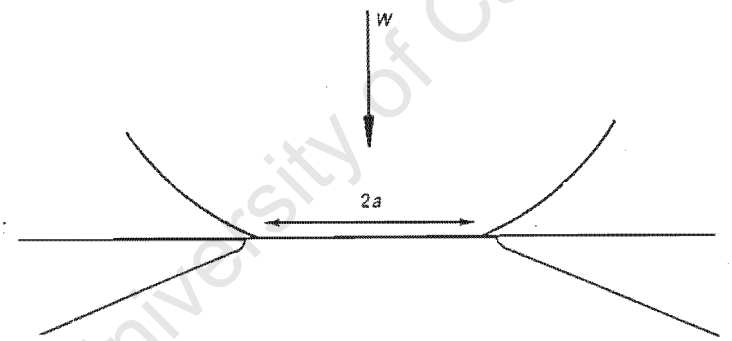

Figure 2.13[40] The geometry of a Hertzian cone crack formed by a spherical particle on a brittle material.

Sharp, angular erodent particles form cracks which are entirely different to Hertzian cracks formed by rounded particles. The sharp angular particles cause median cracks to form directly below the contact point. As the normal force is diminished, lateral cracks develop due to the relaxation of the deformed material around the region of contact. Once the normal load has decreased to zero, the lateral cracks spread upwards until they reached the surface, as illustrated in Figure 2.14[40]. Lateral cracks, in contrast to median cracks can lead to immediate removal of material, *i.e.* wear. The extent of cracking is greatest at angles normal to the surface, and thus erosion is most rapid under these conditions[40].

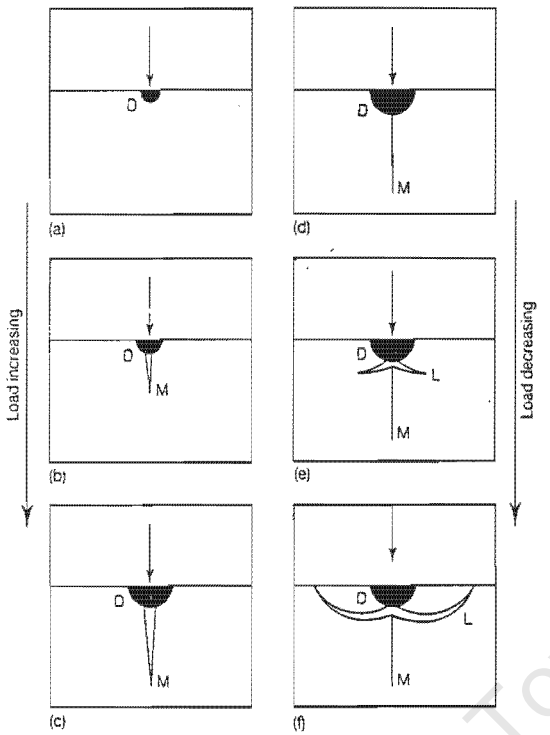

Figure 2.14[40] Crack formation in brittle materials due to sharp particle impacts. Steps a-c show the development of median cracks as the surface is loaded with a sharp particle. Steps d-f show the development of lateral cracks on removal of the applied load. (After Lawn and Swain[43])

2.3.3 MECHANISMS OF EROSION IN COMPOSITE MATERIALS

Over the past few decades the solid particle erosion of composite materials has received considerable attention[44, 45, 46, 47]. Pool *et al.* selected four different fibre composites (see Table 2.2) for erosive wear studies of composites using sand particles of various sizes. The results of the erosion rate as a function of impact angle is shown in Figure 2.15[44].

Table 2.2[44] Polymer composites used by Pool *et al* for erosive wear studies.

Composite	Polymer	Fibre
Unidirectional graphite fibre reinforced polyimide, A	Hexcel's F-173 bismaleimide PI resin	Thornel 300 graphite fibre
Woven (0/90) graphite fibre reinforced epoxy, B	Fiberite's 934 epoxy resin	Thornel 300 graphite fibre
Woven aramid-fibre reinforced epoxy in a quasi –isotropic (0/90/+45) symmetric lay-up, C	Fiberite's 934 epoxy resin	Kevlar fibre
Chopped graphite fibre reinforced thermoplastic, D	LNP corporation's PPS (injection moulded)	40% graphite fibre (chopped)

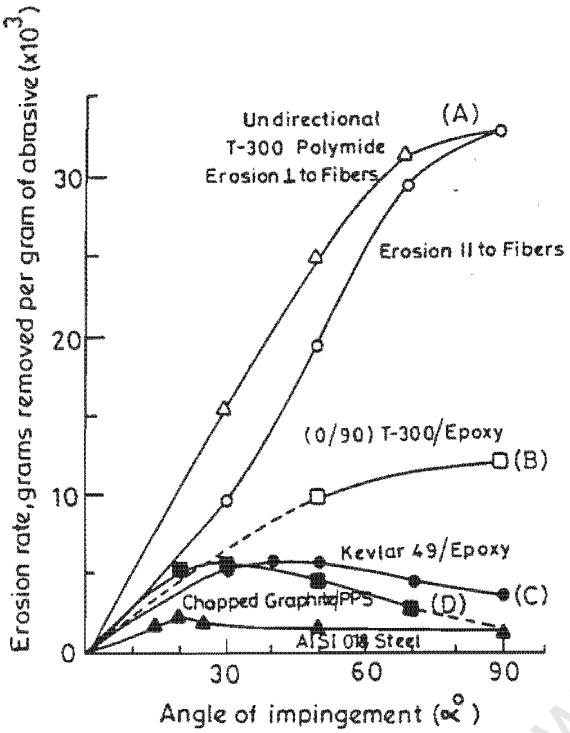

Figure 2.15[44] The erosion rate of various composite materials tested at an impingement velocity of 31 m/s.

The erosion rates for the composite materials tested were at least an order of magnitude greater than for low-carbon steel. The maximum wear rate occurred at an angle of impact of 90° for composites A and B, indicating a brittle-type erosion behaviour, while composite C exhibited wear maxima in the range of angles 34°to 45°, indicating semi-ductile behaviour. Material D showed a maximum at 25°, indicating ductile behaviour. The preliminary investigations on the erosive wear of the selected composites indicated that the brittle nature of the fibre and the interfacial bond strength are the main factors governing the erosion rate of these fibre composites. These authors also found that the erosion rate at impact angles normal to fibres is greater than that parallel to the fibres. The type of polymer (thermoplastic or thermoset) used as matrix material is also an important factor to be considered since it protects the fibres from being exposed and removed. A thermoplastic with well-bonded ductile fibres should ideally exhibit the lowest erosion rate.

Mathias *et al.* studied bismaleimide polymer composites reinforced with unidirectional carbon fibre (65-75%) using angular shaped alumina abrasives of various sizes as the erodent, at different speeds and angles[45]. It was found that for the experimental conditions chosen, the erosive-wear *resistance* of the composite was smaller than that of the parent polymer. The orientation of the fibres showed that composites with fibres perpendicular to the erodent stream exhibited a lower erosion resistance, which is in accordance with the work of Pool *et al.*[44] Zahavi investigated the solid particle erosion properties of uncoated composite materials of quartz-polyimide, glass-epoxy and quartz-polybutadiene using sand as the erodent[46]. He found that the erosion rate increased with increasing impact angle. The mass loss reached a maximum at an angle of about 75°, while the lowest erosion rate was observed at an angle of about 30°. In addition, it was found that the composites, where the fibre reinforcements adhered well to the resin matrix and exhibited a low porosity, provided an erosion resistance of almost an order of magnitude greater than those composites, which did not possess these characteristics.

2.3.4 SOLID PARTICLE EROSION OF POLYMERIC COATINGS

Polymers show a very wide variation in erosion resistance[40]. The mechanism and angular dependence on the erosion properties correspondingly, vary widely. Ductile polymers such as nylon and polypropylene erode by ductile mechanisms of erosion. More brittle thermoplastics and thermosets such as polymethylmethacrylate (PMMA) and epoxy resins erode by brittle fracture and experience maximum erosion rates at higher angles. Polymeric coatings for the protection of components such as radomes, antennas, jet engine fan blades and helicopter rotor blades have been available for protection against erosion by rain. The erosion of *solid particle* impingement on polymer coatings has, however, been less studied.

Zahavi conducted research on the erosion properties of three polymeric coatings with varying impingement angles[48]. The maximum mass loss was found at a 30° impact angle and it was found that for all the coatings investigated, the erosion rates decreased with increasing impact angle. Erosion mechanisms observed in the coatings were associated with formation of micro-cracks and with micro-crack propagation and intersection. This resulted in the formation of fragments of these coatings, which were locally removed from the surface.

Wood[49], studied the performance of polymeric, metallic and ceramic coatings when subjected to a water-sand jet impingement. The study showed that pure epoxy coatings were associated with typical brittle erosion behaviour and the erosion resistance improved with the addition of proprietary mixtures of silicon carbide and other fillers. The most resistant polymeric coating was flexible polyurethane. The study showed that polymeric coatings, in general, exhibit greater erosion rates than ceramic and metallic coatings. The rubbery materials such as polyurethane elastomers have the capacity to resist solid particle erosion due to the high rebound resilience[50].

2.3.5 ERODENT PARTICLE PROPERTIES

The properties of the erodent particles have a fundamental effect on the erosion mechanism and erosion rate on the target material. The effect of erodent variables such as shape, mass, size, impact velocity, feed rate and hardness have been studied by several authors[51, 52, 53, 54, 55, 56, 57, 58, 59, 60, 61, 62]. The following section discusses parameters that govern a material's response to solid particle erosion.

2.3.5.1 PARTICLE SIZE

Tilly found that at high particle velocities of 240 m/s, a decrease in particle size below 100 μm resulted in a decrease in the erosion rate[51]. It was further concluded that there was no effect on erosion for particles of between 100 μm and 200 μm. The reason for the smaller particles giving a lower erosion rate was due to the low impact stresses resulting from particle kinetic energy. Smaller particles will result in a larger amount of impacts in comparison to larger particles. However, the smaller kinetic energy of each particle will cause the erosion to be less severe. Tilly and Sage proposed a two stage mechanism for the erosion of ductile materials[52]. Experiments showed that under certain conditions particles

shatter into smaller fragments upon striking a surface. The fragments move radially outward, their circumferential distribution depending on the impact angle. The effect of particles with different sizes can then be explained by this mechanism, since smaller particles are less likely to shatter on impact. When a material is exposed to erosion there seem to be a threshold size of the erodent and the material, below which no fragmentation occurs. Some materials also exhibit a saturation level, beyond which fragmentation becomes independent of particle size.

Liebhard and Levy performed experiments on 1018 steel using angular and spherical glass beads as a function of particle size[53]. They concluded that the erosivity of spherical particles increased with particle size, to a peak at about 300 μm and then decreased at larger particle sizes. The dominant factor in controlling the mass loss was a decrease in the ability of the spherical particles to penetrate the target surface and cause plastic deformation even though these larger spheres had more kinetic energy. The angular particle erosivity increased with particle size to a level of 200 μm, which became almost constant with size at lower velocities. However, at higher velocities (up to 60 m/s) the erosion rate increased continuously.

2.3.5.2 Impact Angle

Impact angles in erosion are defined as the angle at which the erodent strikes the plane of the surface as shown in Figure 2.16. The erosion of ductile materials such as steel and polyurethane depends strongly on impact angle. As illustrated in Figure 2.16, typically the maximum erosion occurs at angles between 20° and 30° [20, 40, 56, 61]. The erosion at normal angles reduce drastically for ductile materials, falling to a half or a third of the value at glancing angles. It is generally accepted that maximum erosion rates occur at 90° for brittle materials [20, 39, 40, 45, 46, 54, 56, 62]. The difference in behaviour has been attributed to the differences in the underlying mechanisms governing erosion. The shape of the curve however, has been shown not to vary significantly with the changes in particle size or velocity[55]. Mathias *et al.* studied bismaleimide composites reinforced by carbon fibres and found that the composite exhibited a larger wear at 90° impact angle than at 30° for all cases except for low velocity and high particle mass[45]. Thus, when the kinetic energy of the erodent particles are low enough they cannot penetrate the polymer matrix and expose the underlying fibres. The erosion rate will then depend on the polymer matrix alone.

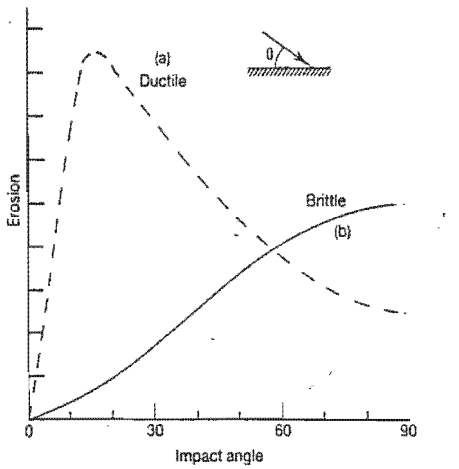

Figure 2.16[40] The dependence of erosion rate on the impact angle.

2.3.5.3 PARTICLE SHAPE AND HARDNESS

Liebhard and Levy concluded that there was a major difference in erosivity between spherical and angular particles[53]. It was found that the erosion rate of the angular particles was generally an order of magnitude more erosive than that for the spherical particles. When the particle size was increased to approximately 600 μm the erosion rate of the angular particles was almost 40 times higher than that for the spherical particles. The hardness of the erodent particle will play an important role in the mechanism of erosion. Particles with lower hardness then the target surface will cause less erosion compared to particles with higher hardness. The energy transfer from the erodent particle to the surface will decrease if the particle deform or fracture on impact. Thus, the erosion rate will increase with particle hardness. The erosion rate will however reach a limit when the particle hardness is considerably greater than the target surface[40].

Bahadur and Badruddin studied the effect of particle shape and hardness on erosion properties[57]. The study compared silicon carbide, aluminium oxide and silica as a function of erosion rate. It was found that the erosion rate increased with decreasing width-to-length ratio for all three types of erodents. Thus, the more elongated and thin particles will produce a larger erosion rate. Feng and Ball found that using 304 steel as target material, the most important factor in governing the erosion rate was the particle shape[59]. The erosion rate was lower using diamonds as erodent than using silica or alumina. The erosion rate is also determined by the kinetic energy of erodents against ductile materials and there is little effect of the hardness of the erodent on erosion rate. However, against *brittle* materials such as glass and alumina, the hardness of the erodent plays an important role on erosion. The higher the hardness of the erodent, the larger the ability for particle penetration into the target causing initiation and propagation of micro-cracks.

2.3.5.4 PARTICLE MASS FLUX

Particle mass flux can be defined as the amount of particles striking the target surface per unit time. This parameter becomes important when the mass flux is large enough to cause inter-particle collisions, which prevent effective erosion from occurring. Liebhard and Levy studied the effect of mass flow rate on 1018 steel using spherical glass beads and angular silicon carbide (SiC)[53]. They found that increasing the feed rate of erodent particles resulted in decreased erosion rates. This indicates that there was inter-particle interference when applying higher mass flux of particles, thus reducing the effectiveness of the particle to erode the target surface. The most likely explanation is particles rebounding from the target surface deflecting the impinging erodent particles. It was also noted that the larger the particles, the more dominate this mechanism became since the bigger particle will interact and decrease the incoming particle's ability to penetrate the target surface. Uuemous and Kleis found the decrease of erosion rate with increased mass flux to be true for most metals and ceramics, but not for rubbers and some plastics[60]. For rubber a "cloud" of rebounding particles is not formed due to the duration of impact and depth of penetrations being much greater.

2.3.5.5 PARTICLE VELOCITY

Particle velocity is considered to be one of the major controlling variables in erosion. Feng found that erosion rate varies as: $E \propto V^n$, where n is the velocity exponent[55]. Values of n are commonly reported to vary between 2.3 to 3. The velocity exponent n is most often found to have a value greater than 2.0 and often lies around 2.4 for ductile metals close to that of maximum erosion rate at shallow impact angles[55, 59]. Furthermore, it is suggested that higher values of n are associated with steeper angles of impact. For brittle type behaviour the value of n can often be found to lie in the range 2.8-3.5. The erosion of glass is governed by a brittle mode of fracture caused by the formation and interaction of lateral cracks. It is suggested that the mode of erosion is the major factor governing the erosion rate and the velocity component is relatively insensitive to microstructure. Tilly and Sage reported that the erosion rate of reinforced nylon and epoxy was related to the impact velocity via a power law[51]. Mathias *et al.* found a power law relationship between wear rate and velocity using a graphite fibre reinforced bismaleimide polymer composite[45].

2.3.5.6 TARGET HARDNESS

Hardness is a measure of a material's resistance to plastic flow. There are many different theories on its influence on the erosion rate. For brittle materials, Srinivasan and Scattergood found that the relative hardness between target and particle (H_t/H_p) emerged as an important factor that determines the mechanism of material removal[58]. When harder particles were used a large increase in erosion rate was obtained. When the hardness of the sample is considerably greater than the striking particles, the particles experience crushing and damage accumulation is needed to nucleate and produce a crack. This lead to more impacts needed for the softer erodents and the efficiency of erosion is lower as a consequence.

Earlier thinking supported the belief that harder materials, such as hard alloys, ceramics and coatings of these materials, provided the best erosion resistance. An alternative approach, however, is to use rubbery materials which resist erosion through their high deformation capacity and high rebound resilience. Li and Hutchings[50] investigated the erosion resistance of cast polyurethane and found a trend of increasing erosion rate with increasing hardness. The highest resistance to erosion was found in the softest material. The mechanism of removal was suggested to be the incremental growth from the surface into the bulk, under cyclic impact loading, of fine cracks.

Wilson and Ball [63] studied the solid particle erosion of aluminium matrix composites and found that the addition of hard ceramic reinforcements resulted in a deterioration of the erosion resistance. This indicates that the mass losses were not dependent on the erosion resistance to indentation, but rather on each material's ability to absorb strain, followed by shear failure of the matrix.

2.4 PROPERTIES OF FIBRE REINFORCED COMPOSITES

2.4.1 INTRODUCTION

The mechanisms operating in composites during loading, the damage progression, failure modes and ultimately the strength are all affected by the nature and micro-geometry of the composite components *viz.* the fibres, the matrix and the interface[64]. The most pronounced advantage of polymer matrix composites (PMC) is that the material can be tailored to a given application leading to efficient material utilisation. However, the material is simultaneously processed at the manufacturing stage. It is therefore important that the component is designed for the process. This often proves to be an obstacle for an engineer unfamiliar to these materials. In addition to the considerations usually made when designing with conventional constraints, the engineer using PMC also has to bear in mind the selection of constituents, types, distribution and orientation depending on the properties required and the choice of processes.

2.4.2 MATRIX PROPERTIES

Polymer matrices are classified either as thermoplastics or thermosets, the thermosets being the most commonly used. Thermosets are polymers, which undergo a chemical cross-linking reaction (curing), where a resin of relatively low molecular weight is transformed into a material of high molecular weight. The liquid resin is converted into a hard brittle solid leading to the formation of a tightly bound three-dimensional network of polymer chains. The curing process is irreversible, so that the material cannot be re-used. Curing can be performed at room temperature but is usually done at a specific temperature for a specific cure time to achieve optimum cross-linking[35]. Thermosetting resins are isotropic and their most characteristic feature is their response to heat, as they do not melt at elevated temperatures but decompose instead. The most commonly used thermoset for advanced applications is epoxy. Epoxy resins cover a wide class of chemicals and therefore a range of mechanical and chemical properties can be obtained. The significant functions of the matrix can be summarised by the following points [65, 66, 67]:

- The matrix must maintain the structural integrity by bonding the reinforcement together.
- The matrix should transfer the load applied to the structure into the reinforcing fibres.
- It is important that fibres can behave as "separate entities", consequently the matrix must separate the fibres from each other to achieve beneficial load carrying abilities.
- The matrix should provide protection in order for the fibres not to suffer mechanical, environmental and chemical damage.
- A ductile matrix will provide a means of slowing down or prevent crack propagation that might have originated from broken fibres.
- The interface between fibre and matrix often provide an increased toughness for the composite.

2.4.3 FIBRE PROPERTIES

There are a variety of reinforcing agents available for fibre reinforced polymers, *viz.* fibres, particles, flakes and whiskers. Fibres are the most common method of reinforcing polymers. The introduction of fibres into the matrix results in directionality or anisotropy in the material. The properties of the fibre composite are therefore highly dependent on the alignment of the fibres. Other parameters that affect the properties of the composite are fibre *type*, volume fraction, distribution of the fibres, the fibre/matrix interface, size and shape of the fibres and the loading direction. The two different fibres that are being investigated in this work are carbon and Kevlar®.

2.4.3.1 CARBON FIBRES

Carbon fibre is manufactured by the use of a precursor. The most commonly used precursors are pitch, rayon and polyacrylonitrile (PAN). The different properties of carbon fibres mainly depend on the heat treatment used. There are three different grades (*i.e.* three different heat treatments) of carbon fibres available; these are classified as high modulus (type I), high strength (type II) and general purpose (type III). High strength carbon fibres are about 7 to 8 μm in diameter and consist of small crystallites of graphite, one of the allotropic forms of carbon (See Figure 2.17(a)). In a graphite single crystal the carbon atoms are arranged in a hexagonal array, stacked on top of each other in a regular ABAB...sequence. The atoms in the basal planes are held together by strong covalent bonds and by weak Van der Waal forces between the layers. Therefore the basic crystal units are highly anisotropic with a Young's modulus in the layer plane approximately equating to 1000 GPa while that between the basal planes being equal to about 35 GPa, as shown in Table 2.3[35,68].

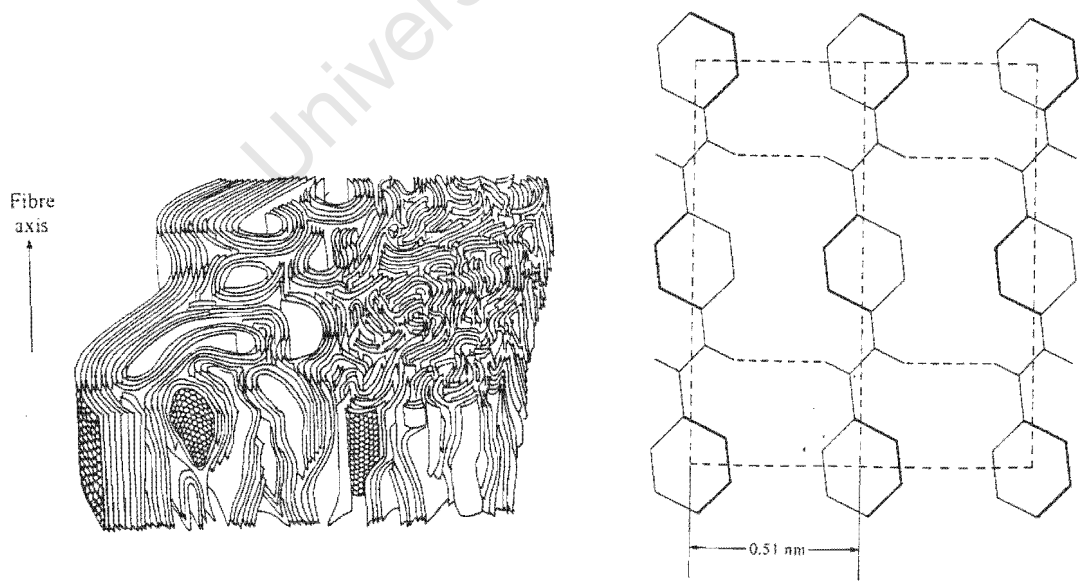

Figure 2.17[35] (a) Carbon fibre structure. (b) *Kevlar®* structure showing inter-chain bonding.

Table 2.3 [35,68] Tensile properties of carbon- and Kevlar® fibres.

Property	High modulus carbon	High modulus Kevlar ®49
Axial tensile modulus (GPa)	380	131
Axial tensile strength (GPa)	1.7	3.6-4.1
Transverse tensile modulus (GPa)	21	5.4

2.4.3.2 ARAMID FIBRES

This is the generic name for aromatic polyamide* fibres, a class of synthetic organic fibres. A high modulus aromatic fibre is produced commercially by Du Pont under the trade name *Kevlar®*. Kevlar® is produced from poly-para-terepthalamide by a spinning and extrusion process followed by stretching and drawing treatments. The chemical formula of Kevlar® is shown in Figure 2.17(b)[35]. The aromatic rings result in the polymer having the properties of a rigid chain. Kevlar® has a crystalline structure with strong covalent bonding in the fibre direction and relatively weaker hydrogen bonding in the fibre transverse direction. The anisotropic nature of the fibre causes Kevlar® to have poor compressive properties. Under compressive loads the fibre develops structural defects known as kink bands, which eventually leads to ductile failure[35, 68]. Typical properties of Kevlar® 49 (high modulus) fibres are tabulated in Table 2.3 [35,68]

2.4.4 FIBRE / MATRIX INTERFACE

The structure and the properties of the fibre / matrix interface play an important role in the mechanical and physical properties of composite materials. The large differences between the elastic properties of the fibres and the matrix have to be communicated through the interface when loaded[35, 68]. Generally, the surface of the fibres is treated in order to improve the level of adhesion between the fibres and the resin. It has also been found that by varying the level of surface treatment of the fibres, the failure mode as well as the mechanical properties of the composite materials can be changed[35, 65, 68, 69]. In order to analyse the stress transfer between fibre and matrix, the following assumptions are usually made[35]:

- The matrix and the fibre behave as elastic materials.
- The interface is infinitesimally thin.
- The bond between the fibre and the matrix is perfect *i.e.* there are no strain discontinuities across the interface.
- The material close to the fibre has the same properties as the material in the bulk form.
- The fibres are arranged in a regular and repeating array.

* Poly paraphenylene terephthalamide

The interface is a dominant factor in the fracture toughness properties of composite materials. Composite materials with a weak interface have relatively low strength and stiffness but high resistance to fracture, whereas materials with strong interfaces exhibit high strength and stiffness but are brittle. This effect is related to the capability of de-bonding and fibre pull-out from the matrix during crack propagation[35]. Since the bond is dependent on the atomic arrangement and chemical properties of the matrix material and the fibre, it follows that the interface is specific to each fibre-matrix system[35].

2.4.5 PROPERTIES OF FIBRE REINFORCED POLYMERS

Fibre reinforced polymers consist of high modulus reinforcing fibres in a low modulus polymeric matrix. The combination of the two distinct phases allows the load to be transferred between fibres due to the elasticity of the matrix. The stiffness and strength of a polymer matrix composite (PMC) depends on [65]:

- the proportions of fibre and resin,
- the distribution and orientation of fibres,
- the type of fibres used
- the length of the fibres and
- the void content

The mechanical properties of a PMC depend particularly on the orientation of the fibres. The fibre orientation ranges from random (*e.g.* in chopped fibres), through to bi-directional (*e.g.* in a woven cloth), to unidirectional. For random orientation of fibres, a PMC has equal properties in all directions *i.e.* it is quasi isotropic; for a bi-directional orientation, a PMC has equal properties in two directions and for unidirectional orientation, the PMC has the greatest properties parallel to the fibre. If the same volume fraction fibre-matrix combination were used in each case, the unidirectional PMC would exhibit the highest mechanical properties and the random PMC the lowest. However, the unidirectional PMC is only superior in the direction parallel to the fibres. Small angle deviations away from the fibre axis decrease the mechanical properties significantly. The directional nature of unidirectional PMC's is illustrated in Figure 2.18, where Young's modulus, Poisson's ratio and the shear modulus is determined as a function of fibre orientation[70].

The tensile properties of carbon and Kevlar® are very high compared to most conventional metals[68]. However, if the compressive properties are considered, different results are obtained. The compressive, bending and shear strength of Kevlar® is poor[35, 65, 70]. The major contributors to this are the inclination for the fibre to buckle easily and the poor bonding between the fibre and resin. This behaviour is however, favourable in impact situations where the visco-elastic behaviour of the aramid fibres lead to a higher work of fracture and the high ductility leads to better damping characteristics. The properties of some common fibre-epoxy composites, with 60% volume fraction unidirectional fibres, and for comparative purposes, metals are given in Table 2.4[65].

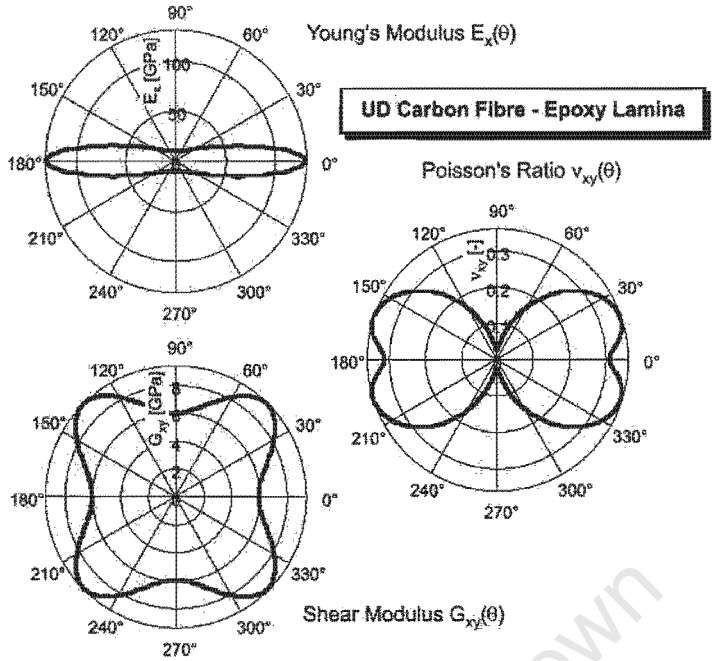

Figure 2.18[70] Global elasticity properties of unidirectional carbon/epoxy composite.

Table 2.4[65] A comparison of the mechanical properties of popular composites with metals.

Material	Density (g/cm^3)	Tensile strength (GPa)	Tensile modulus (GPa)	Specific strength	Specific stiffness
Composites					
Kevlar	1.4	1.4	75	1	90
Type 1 carbon	1.5	1.1	220	0.7	130
Type 2 carbon	2	1.5	140	1	90
Metals					
Steel	7.8	1.3	200	0.2	26
Aluminium	2.8	0.3	73	0.1	26
Titanium	4	0.4	100	0.1	25

The properties of the composite can be predicted using the constituent properties by "*the rule of mixtures*". This mathematical expression can predict Poisson's ratio, density and tensile modulus by knowing the fibre volume fraction. The model is, however, a poor predictor of *tensile* strength but does provide a maximum value. The reason for this is that that the matrix behaves in a non-linear way and fails at a different level of stress to the fibre. Assuming there is a perfect bond between the fibre and the matrix, the rule of mixtures (ROM) can for example predict the tensile modulus as:

$$E_c = E_f V_f + E_m (1 - V_f) \qquad \textbf{(2.14)}$$

where, E_c = *composite modulus* E_f = *fibre modulus* E_m = *matrix modulus*
V_f = *fibre volume fraction*

2.5 IMPACT CHARACTERISTICS OF COMPOSITES

2.5.1 INTRODUCTION

The use of composite materials in high-speed compressor blades entails high velocity impact of foreign particles that will impinge on the blades. The toughness evaluation of the composite is an important criteria in the design of ply sequence and orientation through the composite component. The low velocity impact resistance has received considerable attention through the use of instrumented impact testers[66]. These tests generate load and energy data during the impact event and this have provided valuable information of the mechanisms and variables affecting the impact resistance of PMC's. The relevant material and structural properties that determine a material's respond to impact loading and the predicted mode of failures are reviewed.

2.5.2 IMPACT TECHNIQUES FOR COMPOSITE MATERIALS

The impact problem can be divided into two separate domains, *viz*. low velocity impact by a large mass and high velocity impact by a small mass[66]. The former is generally simulated using a drop weight tester and the latter using a gas gun or a ballistic launcher of some kind.

2.5.2.1 LOW VELOCITY IMPACT

There are a variety of methods used for simulating low level impact. The most widely used are the:

- Charpy pendulum
- Izod
- Hydraulic and
- Drop weight test

The Charpy pendulum was originally developed for the testing of metals but since it is simple to use and can be instrumented it can be used to study the process of energy absorption and dissipation in composite materials. The test specimen geometry is generally a thick beam specimen, which often incorporate a notch at the midpoint. The impact event can be analysed further by attaching strain gauges to the specimen. One drawback of this method is the use of a short, thick beam specimen that seldom is typical of an engineering component. The Charpy test is useful for determining dynamic toughness as a first step in the ranking of composite materials[66]. The Izod test method experiences the problems mentioned for the Charpy method and is also a suitable device for ranking the impact resistance for composite materials.

Hydraulic test machines have been widely used and have the advantage of it being able to determine material properties such as tensile strength, modulus, and inter-laminar fracture toughness[66]. The specimens are usually of a double cantilever beam (DCB) type. Attaching strain gauges to the specimens allow the strain history to be determined. The drop weight impact apparatus has the advantage in that a wider range of specimen geometries can be tested and thereby simulating more accurately the use of composite materials in engineering applications. This method involves a weight being allowed to fall from a pre-determined height to impact the specimen. The specimen is supported in the horizontal plane. The incident velocity can be determined by the use of optical sensors above the target. It is common for the impact apparatus to be instrumented, enabling force/time characteristics to be determined. Another advantage is that different shape impactors can be used to simulate different impact conditions. (see section 3.4).

2.5.2.2 HIGH STRAIN RATE IMPACT

The two most widely used methods for determining high strain rate impact events are the Hopkinson-bar technique and the gas gun. The Hopkinson-bar technique has the advantage of being able to determine material properties as a function of strain rate. The specimen is bonded into slots in an inertia bar and input bar. The specimen is then fitted in a weigh-bar which is accelerated, using for example gas driven projectiles, and this loads the input bar. The inertia of the inertia bar enables the specimen to be loaded dynamically. Strain gauges are fitted on the inertia and input bar to allow stress waves to be analysed and to determine a stress strain relationship for the material.

The use of a gas gun can be used to test a wide variety of specimens. Large engineering structures can be accounted for at high velocity. The schematic layout of the gas gun is shown in Figure 2.19. The gas gun is normally operated with pressurised gas. The gas accelerates a projectile down the barrel to strike the specimen, which is supported vertically, and the resulting damage can be analysed. The speed of the projectile can be measured prior to the impact by using optical sensors. The specimen can then be analysed and the damaged area quantified by using x-ray or scanning methods. Recent developments on this technique have been to instrument the gas gun, enabling force / displacement diagram histories to be analysed. The test is generally not completely destructive but often result in large damage of the specimen.

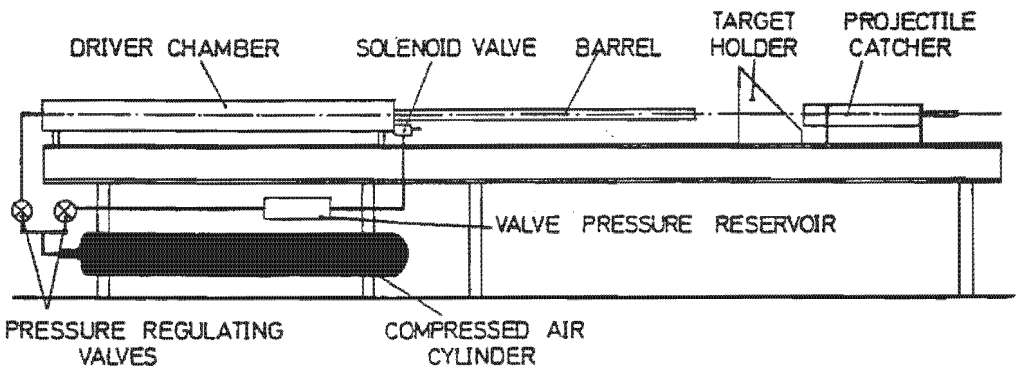

Figure 2.19 Gas gun apparatus for high velocity impact testing. (After Cartmel [71])

2.5.3 INFLUENCE OF MATERIAL PROPERTIES ON IMPACT DAMAGE

The impact response of PMC's depends on the mechanical and chemical properties of its constituents and on the interface region between the fibre and the matrix. Analyses of different failure mechanisms reveal that there are several ways in which a fibre composite can fail. These mechanisms include delaminations, intra-laminar matrix cracking, longitudinal matrix cracking, fibre matrix debonding, fibre pull-out and fibre fracture[66]. The following sections will investigate the role of these three constituents and how they affect the impact response of a fibre composite exposed to an impact event.

The fibres are responsible for carrying the main part of the load in a composite structure; hence the fibres are extremely important in consideration of the impact resistance of a composite material. It is well known that Kevlar®is used for applications which require good impact properties[66], whereas carbon fibres which are more brittle than Kevlar tend to failure in a more catastrophical manner. Kevlar® fibre materials fail in a more progressive way and absorb energy through delamination and "fibre necking". The difference in damage is mainly due to the lower strain to failure of the carbon fibres compared to the Kevlar® fibres[70, 72]. The difference in failure mechanisms between carbon and Kevlar® fibre show that Kevlar® exhibit a far superior impact resistance compared to carbon fibres.

Foreman investigated the use of hollow fibres and found that the hollow fibres had an additional mechanism for energy absorption during impact, *viz.* fibre crushing[73]. The study showed great improvement in the residual load capability of glass/carbon hybrids. Another way of improving the impact resistance of, for example carbon fibres is to reduce the diameter of the fibres leading to higher strains to failure and thereby increasing the capability to absorb energy[73]. It is further found that fibres such as Kevlar®, which have large areas under their stress-strain graph curves, offer good impact resistance.

The damage initiation, *i.e.* the appearance of the first matrix crack, has been proposed to be matrix-dominated[66]. It has further been shown that the *threshold* kinetic energy is strongly influenced by the matrix properties and essentially independent of fibre properties, lay-up and form of reinforcement, *i.e.* woven or unwoven fibre material. The damage to the matrix can reduce the load bearing capability of the composite significantly and a large amount of research has been done on trying to improve the matrix properties. The resin toughness plays a vital part in the fibre composites' ability to resist impact damage. Figure 2.20 shows how the damaged area (internal delaminations) varies with impact energy. It is clear that the tougher graphite-PEEK (thermoplastic) has a smaller damaged area than the less tough graphite-epoxy (thermoset) for various impact energies[68].

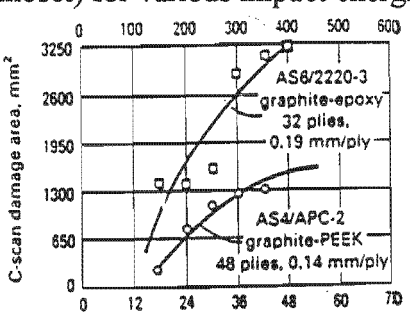

Figure 2.20[68] Influence of material on impact damage size.

The interface of the fibre/matrix is well known to play an important role on impact properties as well as mechanical properties for fibre composite materials. In general, the surface of the fibres is treated by an oxidative process in order to improve the level of adhesion between fibre and matrix. Other processes involve introducing a rubbery interface between fibres and matrix. Sun and Rechak studied the effect of adding adhesive layers along interfaces of graphite/epoxy laminates[72]. The experimental results showed that the adhesive layer can effectively suppress delaminations up to relatively high impact velocities. In addition, matrix cracking in the lamina can be greatly reduced.

2.5.4 PROJECTILE CHARACTERISTICS

The geometry of the striking object has been shown to have strong influence on the target response. Siow and Shim compared the impact response of woven carbon/epoxy laminates as a function of impactor tip radius[74]. Two different radii of 6.3 mm and 21 mm for the steel strikers were used. Figure 2.21 shows the delamination area as determined by a C-scan as a function of impact energy. The study involved two different masses and impact heights for the sharp and blunt tip. It was observed that the sharp impactor introduce larger delamination areas than the blunt impactor for each particular impact energy considered. Furthermore, it was found that the energy threshold for initiation of delamination is lower for the sharp impactor.

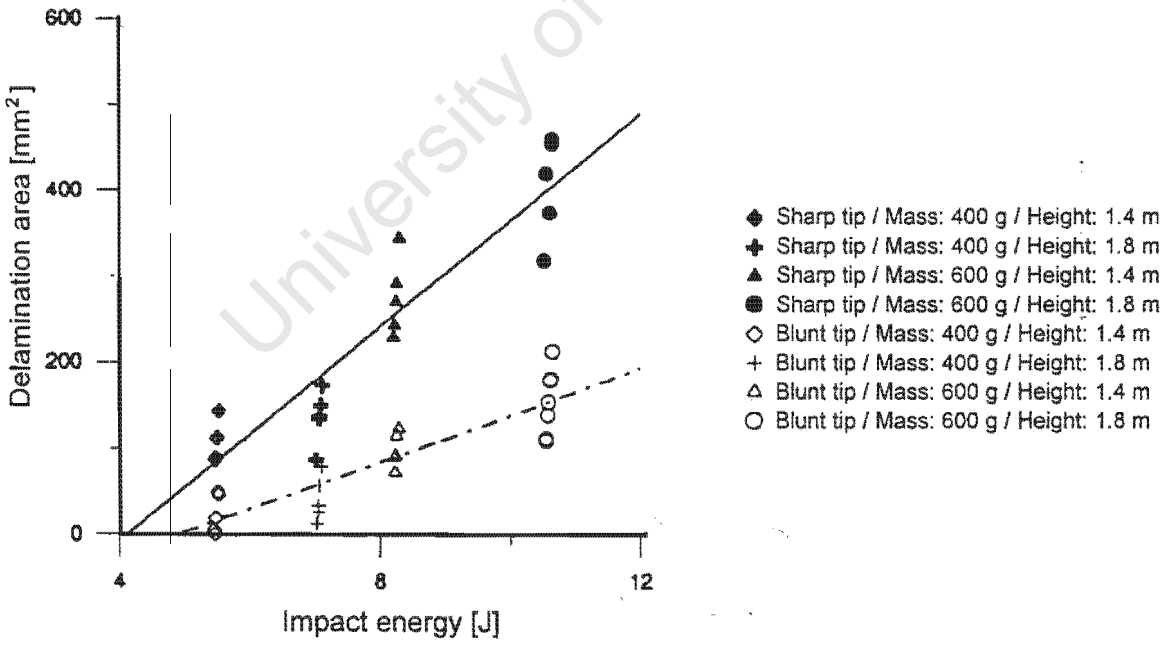

Figure 2.21[74] The variation of delamination area with impact energy for strikers of different nose radii.

2.5.5 TARGET PROPERTIES

The stacking sequence of laminates has proven to have a profound effect on delamination damage[66, 73]. It is found that a large difference in angle between adjacent layers causes a mismatch in mechanical properties and as a result delamination occurs. In addition, it is suggested that for adjacent plies with the same orientation, there cannot be any delaminations developing[75]. Geometrical effects are significant under conditions of low velocity impact loading[66]. Varying the geometry changes the target's ability to store energy and therefore its impact resistance. Large targets are not necessarily better energy absorbers than small targets[66]. Thus, care needs to be taken when using small test specimens to describe the impact response of the real target. High velocity impact by a light projectile induces a more localised mode of target deformation resulting in energy being dissipated over a small region immediate to the point of impact[66]. It appears that under certain conditions, small test specimens can be used to characterise high velocity impact on a larger structure.

2.5.6 FAILURE OF PMC FAN BLADES IN AN AERO ENGINE

There are two situations where the fan blade in aero-engines could cause serious damage if failing catastrophically, *viz.* bird strike and the blade becoming detached[16, 76]. A standard bird strike condition specified by the Federal Aviation Administration (FAA) is the ingestion of several 2.5 lb (1.1kg) birds under take-off operating conditions. The engine has to withstand the test without a significant thrust loss. Frischbier *et al.*[16] performed both analytical and experimental procedures on a bird strike situation for a carbon composite fan blade. The study showed that the analytical as well as experimental results were successful for the proposed blade. The experimental procedure was carried out on a scaled 0.5 m fan blade, experiencing impact from a bird substitute mass (gelatine) at 167 m/s. The tests showed no obvious blade damage. When an aero-engine is running at full speed, it is obvious that the fan blades have large kinetic energy and the possibility of a blade becoming detached cannot be ignored. Modern aero-engines have to contain the fragments that may arise from failure of the fan blades. Kevlar® are being used extensively to contain the fragments of fan blades[76].

2.5.7 FINITE ELEMENT SIMULATION OF IMPACT

A finite element simulation can be considered to be successful if a good correlation is obtained with the computed results and results from experimental procedures. It is then possible to assess complex geometry and large deformations in a parametric study. For advanced or large composite structures, the cost of full size experimental impact testing can be extremely expensive since it often results in large damage of the component. The use of FE could be much more cost effective and provide valuable insight of the impact behaviour of composites. A finite element code to be useful, should be capable of handling geometric as well as non-linear material behaviour in addition to modelling layered anisotropic materials. There are a number of general-purpose FE codes available which such capabilities.

Lakshminarayana *et al.* used ABAQUS to model impact on graphite/PEEK composite plates[77]. The study conducted found that the FE analysis correlated well with measured data and complicating effects such as plate shape, thickness, ply-orientations and the duration of impact on deformation could also be predicted. Furthermore, the study suggested the indispensable importance of combining FE analysis with experimental studies due to limitations of available test facilities, instrumentation and data acquisition systems. Al-Bastaki conducted a study on KFRP tubes subjected to a dynamic internal pressure pulse using ABAQUS[78]. He investigated the correlation between experimental and FE analysis of hoop stress *vs.* hoop strain experienced in the tubes and found good agreement between the two. The FE analysis could not however, predict final failure of the tubes, which was a drawback in the analysis.

CHAPTER 3

EXPERIMENTAL TECHNIQUES

3.1 EROSION ANALYSIS PROCEDURES

3.1.1 THE EROSION APPARATUS

The erosion experiments were carried out at room temperature with a test rig that allows erosion parameters, such as particle velocity and impact angle, to be varied according to the conditions that are required. Figure 3.1 shows a schematic of the solid particle erosion apparatus, while Figure 3.2 is a photograph of the rig used.

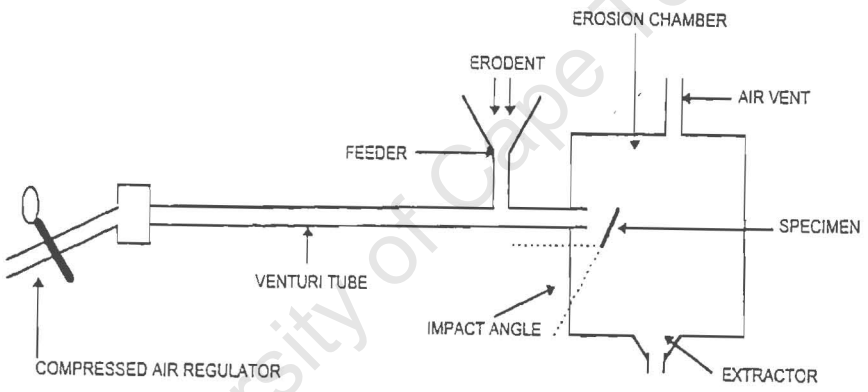

Figure 3.1 Schematic of the solid particle erosion apparatus.

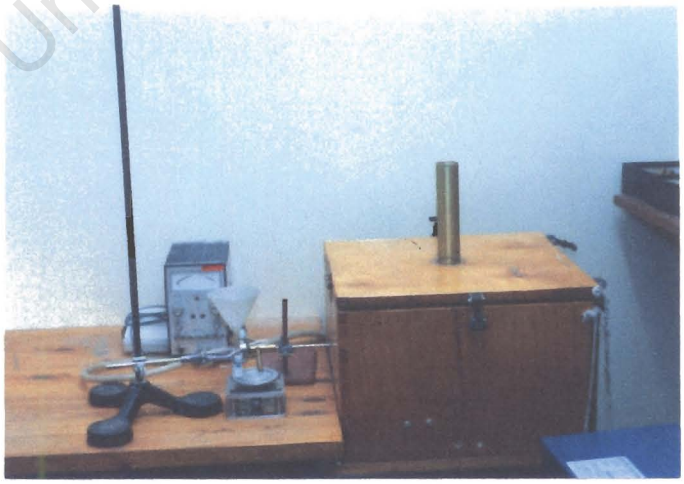

Figure 3.2 Photograph of the solid particle erosion apparatus.

A predetermined mass of erosion particles is placed into the feeder mechanism, which is designed to allow a particular amount of erodent to be fed onto the rotating turntable (Figure 3.3). The erodent particles are then ingested into the venturi tube and accelerated using compressed air from the laboratory air supply. By varying the air pressure, different particle velocities can be obtained.

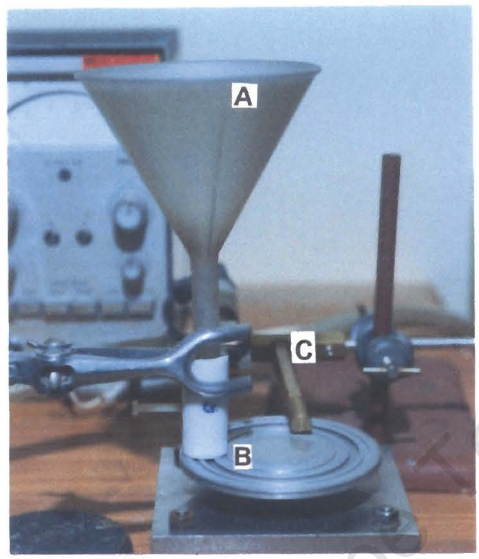

Figure 3.3 Erosion-feeder mechanism. A-funnel, B-turntable, C-Venturi.

The erodent particles exit the stainless steel tube inside the erosion chamber to be blasted onto the specimen. The specimen is located at a certain distance and angle in front of the erosion nozzle. After impacting the specimen, the erodent particles are removed from the erosion chamber using an extractor fan.

3.1.2 MASS FLOW CALIBRATION

Mass flow rate can be defined as the amount of erodent, in grams, exiting the nozzle per second. The mass flow rate is regulated by the hole at the bottom of the feeder and the speed of the turntable. The size of the hole determines the amount of erodent onto the turntable and the turntable speed controls the rate at which the particles are introduced to the air stream. The mass flow rate decided upon was approximately 0.17 $g.s^{-1}$. The required flow rate was obtained by recording the time for a measured mass of erodent to pass through the erosion tube. The time for each erosion test could be monitored to ensure that the mass flow rate was constant.

3.1.3 PARTICLE VELOCITY CALIBRATION

The velocity of the particles depends on the air pressure used in the erosion apparatus and the type of particle being used. As one particle size was used for this project it was only necessary to calibrate the apparatus once. The velocity of the particles was measured using the double rotating disk method of Ruff and Ives[80]. The double disk configuration can be seen in Figure 3.4. The two disks are a certain distance apart and connected by a common shaft. One of the disks has slots machined on its circumference where the erodent particles are allowed through. The second disk is coated with a permanent marker before the calibration.

During calibration the double disk is attached to a rotating shaft that is adjusted using a speed controller. The speed controller has an electronic speed counter, which gives the rotational velocity of the shaft in revolutions per second. The double disk is positioned in front of the particle stream in the erosion chamber. The erodent particles pass through the slot in the front disk and leave an erosion mark on the rear disk, which has been coated with the permanent marker. As can be seen in Figure 3.4, there are two marks on the rear disk. To achieve more accurate results the direction of rotation of the shaft is reversed thus causing a wider separation of the erosion marks. The two erosion marks give a larger value of the linear distance denoted as **s** in Figure 3.4. The linear separation is determined by using vernier calipers.

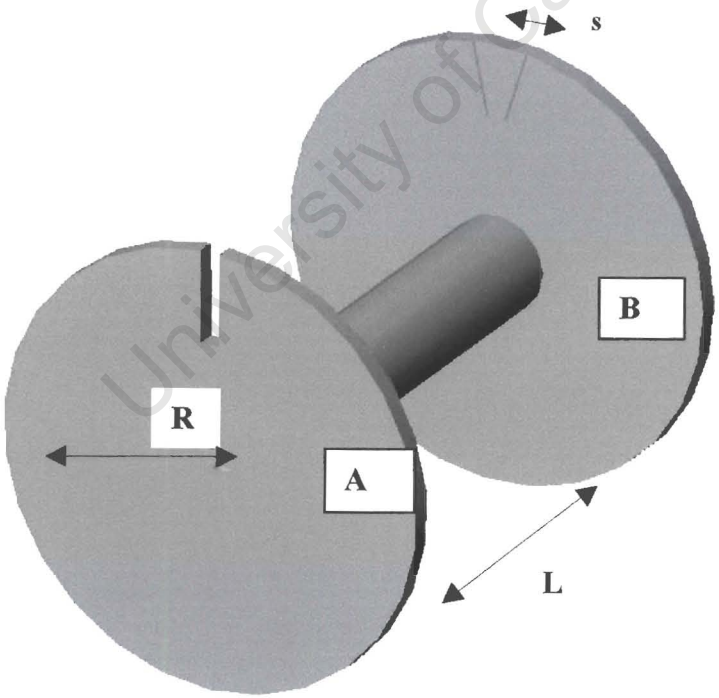

Figure 3.4 Schematic diagram of the double disk used for velocity calibration.

Once the value of **s** is determined, the velocity of the particles can be determined using equation 3.1 below.

$$V = \frac{4\pi RUL}{s} \qquad \textbf{(Eq 3.1)}$$

where:

V = particle velocity (m. s^{-1})
R = radius of the disks
U = angular velocity (radian. s^{-1})
L = distance between the two disks
s = linear separation of the two erosion marks on disk B

3.1.4 ERODENT AND TARGET SAMPLES

The erodent used in this project was silica sand, SiO_2. The silica sand was obtained from Consol glass Minerals. The erodent particles selected for the experimentation were between 180μm and 200μm in size and irregular in shape as shown in Figure 3.5. The required erodent size was obtained using a *Fritsch* vibrating sieving apparatus and the *Endecott* teat sieve shaker. There are four different sample types used in this project *viz.* polymer coatings, metal coatings, fibre composite materials and metal (titanium) specimens.

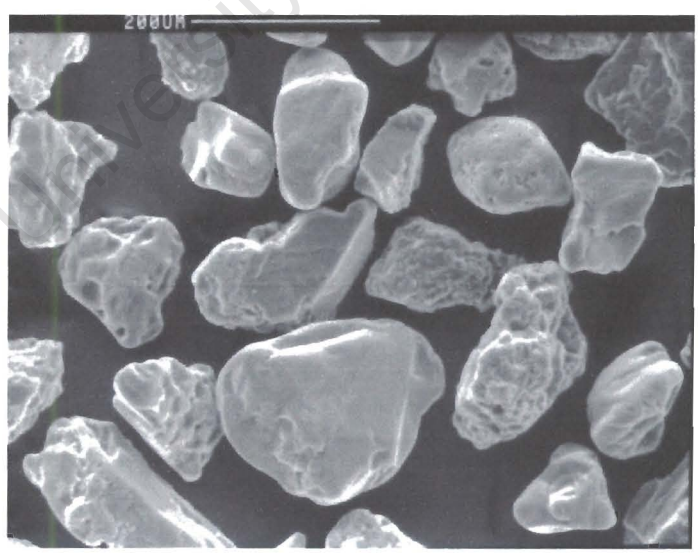

Figure 3.5 Silica sand particles used for the erosion studies.

3.1.5 EXPERIMENTAL PARAMETERS

Table 3.1 shows the experimental parameters that were used during the course of the erosion tests.

Table 3.1. The particle erosion experimental parameters

Experimental Parameter	Value
Mass flow rate	0.17 $g.s^{-1}$
Supply pressure	6 bar
Particle velocity	110 $m.s^{-1}$
Erodent size	180-200 μm
Angle of specimen	30°, 45°, 60° and 90°
Temperature	Room temperature

3.1.6 STEADY STATE EROSION TESTING

Before testing commences the specimen is cleaned and weighed using a *Sartorius* digital balance to obtain the original mass. The individual specimen was positioned in the specimen holder at a particular angle and distance from the erosion nozzle. The supply air pressure valve is then opened and the weighed mass of erodent is inserted into the feeder mechanism. After completion of the erosion test, the specimen is removed from the rig and is cleaned and re-weighed. The mass loss can then be calculated for that particular erosion test. This procedure is repeated until satisfactory steady state erosion is reached. The erosion rate can thus be calculated from the slope of the graph obtained. The erosion results can be presented as either the erosion rate or erosion resistance. The erosion resistance is the inverse of the erosion rate. In Figure 3.6 the cumulative mass of erodent used is plotted as a function of the cumulative volume loss of the target specimen. In this example, the target specimen was a nickel coated composite at 45° impact angle.

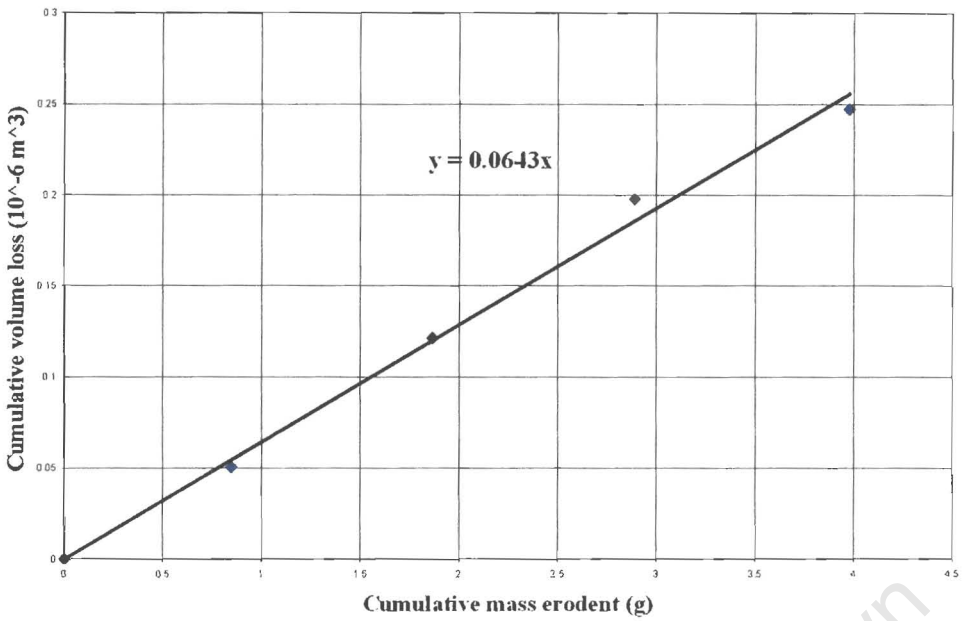

Figure 3.6 Cumulative mass of erodent (g) *vs.* cumulative volume loss (10^{-6} m^3) on the target specimen (Ni coating)

3.1.7 MICROSCOPY

The scanning electron microscope (SEM) was used to view the eroded surfaces and identify erosion mechanisms taking place during erosion of the specimens. The particular microscope used was a Cambridge S200 operating at 15 kV for both the metal and polymer composite specimens. The specimens were fixed on aluminium stubs and sputter coated with gold/palladium to ensure electrical conductivity.

3.2 LAMINATE SPECIMENS

The composite laminate specimens used for the flexural bend tests, impact tests and erosion tests (see following two sections) were manufactured in the laboratory. The laminates were made from carbon, Kevlar® and carbon/Kevlar® hybrid fabric. Each laminate was made up of twelve layers and the different fabric materials used had approximately the same mass/area (195 g/m^2) of cloth. The volume fractions for the laminates were measured to be approximately 50% using optical microscopy.

3.2.1 FIBRES INVESTIGATED

The fibres investigated were produced by Hexcel and the specific fibre production codes are shown below. All the fabrics investigated were of plain weave construction, each warp fibre passes alternately under and over each weft fibre.

Carbon	HXL 43193P
Kevlar®	HXL 281
Carbon/Kevlar® hybrid	HXL G882
Carbon UD	GA090

3.2.2 EPOXY RESIN INVESTIGATED

The specific epoxy resin used was chosen by the recommendation of Advanced Materials Technologies (AMT Pty Ltd) for its excellent mechanical and chemical properties. The epoxy and hardener used are produced by SP systems, the production codes are:

Epoxy resin	Ampreg-20
Hardener	Ampreg-20 Standard hardener

3.2.3 MANUFACTURE OF THE LAMINATES AND TEST SPECIMENS

The laminates were made by a wet lay up process. In the wet lay up process the low viscosity resin is impregnated into the dry fibres. The wet lay up process involves a vacuum procedure to increase the volume fraction of fibres in the laminate and to decrease void content. The vacuum procedure was approximately 6 hours, which would allow the resin to cure to a point where it was unable to be drawn out of the laminate due to the increase in viscosity of the curing reaction. Figure 3.7 shows a typical vacuum stack indicating the components that are used in the vacuum process.

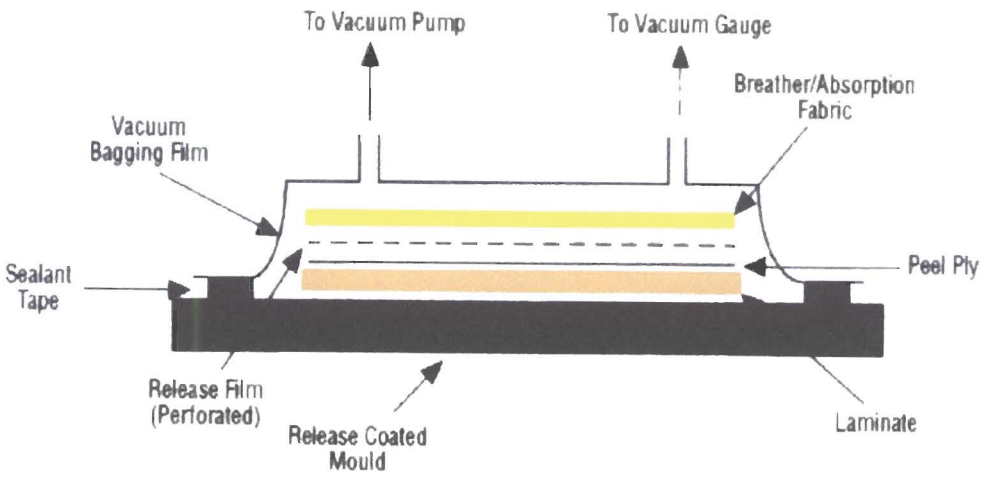

Figure 3.7 Vacuum procedure lay-out.

Once the vacuum procedure was complete, the laminates were cured in an oven at 80°C for a period of 5 hours. The curing temperature increases the curing reaction and the time period was chosen for optimum cross-linking within the resin.

3.3 FLEXURAL BEND TESTING

Flexural bending tests offer the possibility of determining the modulus of elasticity in bending and the flexural strength of flat specimens. The bending test used was a three three-point bend test. In the three-point bend test, the test specimen is supported near each end and is loaded at one point equi-distant from each support. The modulus of elasticity in bending is obtained from measurements of the load / deflection curve at stresses below the proportional limit. The three-point bend apparatus consists of two adjustable supports and a means of measuring deflection and applied load. The three-point bend test cage was used in combination with the *Zwick* 1484 to apply the load to the specimens as shown in Figure 3.8.

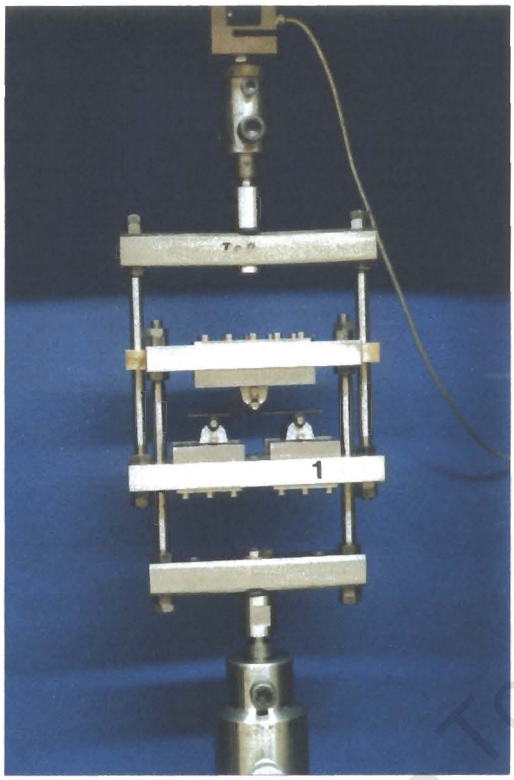

Figure 3.8 The three-point bend test rig.

From the data obtained in the test, the modulus of elasticity in bending E_b, and the bending strength, σ_b can be calculated using equations 3.2 and 3.3.

$$E_b = \frac{L^3}{4bh^3\left(\frac{\Delta p}{\Delta \delta}\right)} \qquad \textbf{(Eq. 3.2)}$$

where:

L = span length (mm)
h = specimen thickness (mm)
b = specimen width (mm)
Δp = load increment as measured from pre-load (N)
$\Delta \delta$ = deflection at midspan (mm)

The bending strength, σ_b can be determined by:

$$\sigma_b = \frac{3P_bL}{2bh^2} \qquad \textbf{(Eq. 2.3)}$$

where P_b, is the load at failure of the specimen.

The specimens were machined to a specific geometry with reference to ASTM[81] standards. The thickness of the specimens ranged from 2.5-3.1 mm, therefore the specimen were machined to a width of 20 mm and a length of 100 mm. The specimens were machined so that the 0° fibre orientation direction runs longitudinally in the specimen. Four specimens were tested from each laminate. The specimens were loaded and data assessed to a drop in load of 20% of the maximum applied load. The displacement velocity of the test was 4.5 mm/min.

3.4 LOW VELOCITY IMPACT TESTING

The low velocity impact test consists of dropping a known mass from a predetermined height onto a test specimen. From the impact test apparatus (Figure 3.9), the force-time, force-displacement and energy-displacement data can be obtained. The impact apparatus relies on gravitational acceleration to supply a known energy and velocity to a free falling impacting crosshead. Optical sensors record the velocity of the hemispherical impactor. The load and deflection information is obtained from strain gauges in the crosshead. Square test specimens with sides of 95 mm were cut from the laminates. The specimens were cut to specific dimensions to minimise vibrations and movements within the grip plates during the impact event. Impact tests were carried out from various heights and the crosshead used had a mass of 1.095 kg. The impact tup used was of hemispherical shape and measured 6 mm in diameter.

Figure 3.9 The impact test rig.

CHAPTER 4

RESULTS

4.1 FINITE ELEMENT ANALYSIS

The approach in this section is to determine deflections, stresses and vibrations for the currently used titanium blades and the composite compressor blades and make comparisons between the two materials. The carbon fibre reinforced polymer (CFRP) blade is modelled using two different lay-ups. The one model has 70 % of the unidirectional (UD) fibres in the radial direction ("0° direction") of the blade and the rest of the fibres alternating in the +/- 45° direction. The second lay-up consists of a cross-ply configuration with alternating $(0°/90°)_s$ plies. These two lay-up configurations will be referred to as *lay-up 1 and lay-up 2,* respectively.

4.1.1 CALCULATIONS OF THE NUMBER OF LAYERS NEEDED

The composite blade will consist of approximately 50 layers[f] of unidirectional cloth at the base of the compressor blade. The blade then tapers so that approximately 2 layers are needed at the tip of the blade. It is therefore necessary to determine the number of layers at any position along the blade outline. The Finite Element code used has no function to deal with this problem, thus a separate Fortran code was written to solve this problem. (See Appendix A, for parts of the program). The program reads in all the nodes and elements of the blade. It then calculates the heights of the four corner nodes with respect to the base of the element. The approximate height of the element is found by adding the heights of the individual nodes and dividing by four. Figure 4.1 shows the vectors used for calculating the height of each element.

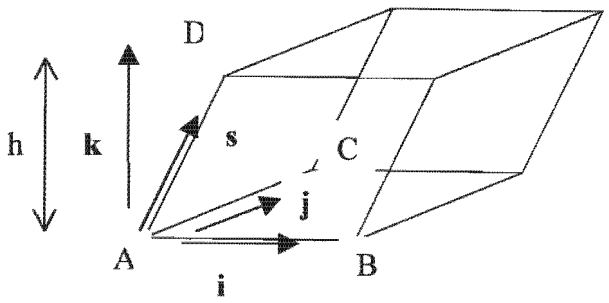

Figure 4.1 The vectors used for calculating the height of an element.

[f] For unidirectional pre-preg carbon fibre/epoxy

The height of the left top corner, D, is calculated by using the following procedure.

Find the three vectors **i** , **j** and **s**,

Calculate **k** by using the *cross product*,

$$\mathbf{k} = \mathbf{i} \times \mathbf{j}$$

Normalise the vector **k**,

$$\mathbf{K} = \frac{1}{\sqrt{k_1^2 + k_2^2 + k_3^2}}(k_1,\ k_2,\ k_3),$$

The height, h is found by using the *dot product*,

$$h = \mathbf{K} \cdot \mathbf{s} = |\mathbf{K}|\,|\mathbf{s}| \cos\theta = |\mathbf{s}| \cos\theta \qquad (|\mathbf{K}| = 1),$$

The height is then found to be:

$$h = \mathbf{K} \cdot \mathbf{s} = \left(\frac{1}{\sqrt{k_1^2 + k_2^2 + k_3^2}}(k_1,\ k_2,\ k_3)\right).(s_1,\ s_2,\ s_3)$$

where:

$$\mathbf{i} = (i_1,\ i_2,\ i_3)$$
$$\mathbf{j} = (j_1,\ j_2,\ j_3)$$
$$\mathbf{k} = (k_1,\ k_2,\ k_3)$$
$$\mathbf{s} = (s_1,\ s_2,\ s_3)$$

This procedure is repeated for all the corner (nodes) heights. The final height is then calculated by taking the average of these four heights. This procedure is repeated for all elements and the element heights are divided by the thickness of an individual layer to yield the number of layers needed at that element. Elements are then grouped to form element sets with the same number of layers. The element sets can be seen in Figure 4.2. Each colour represents a different element set containing a certain number of plies. (Note that in the leading edge, the red colour is used although there is only one ply present. This is the same as the base section colour, due to the restriction of colours available.) At the leading edge and the trailing edge, few layers are needed due to the thin profile of the blade. As the blade-section gets thicker towards the base of the blade the number of layers increase to 50 layers.

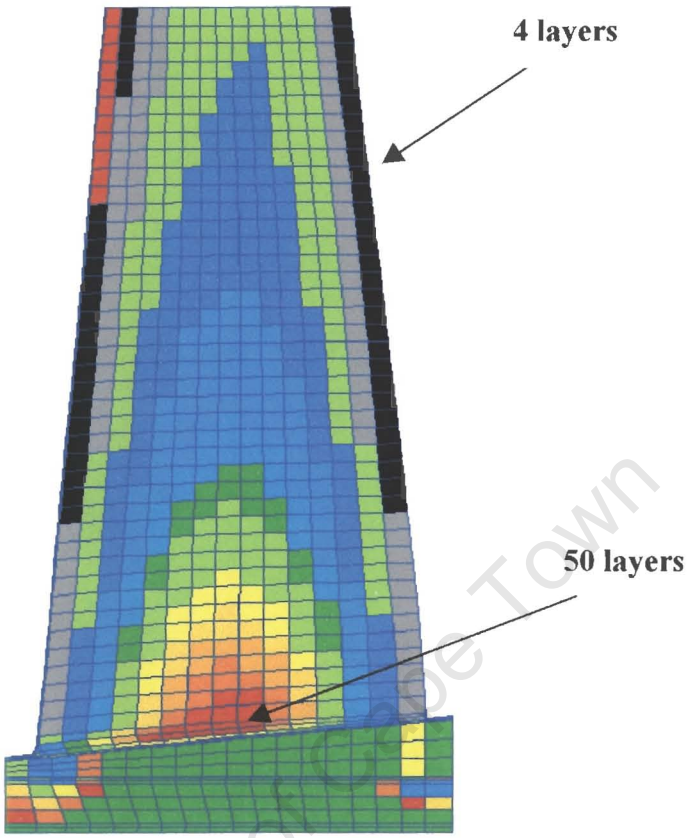

Figure 4.2 A representation of the number of layers needed at any location in the CFRP composite compressor blade.

4.1.2 BOUNDARY CONDITIONS OF THE FE MODEL

The compressor blades are restrained in the rotor disc from moving upwards and forwards. These boundary conditions have been set perpendicular to the contact surface of the blade. The blade experiences a centrifugal force that arises from the rotation. The design speed of the compressor is 10 000 rpm, which is implemented on the FE model. The two additional loads that arise are the drag and pressure difference loads. These loads have been measured by ABB STAL and are approximated by two point loads. In reality these two loads are distributed over the entire surface of the blade and varying with position. However, these loads are small in comparison to the centrifugal loads so the approximation is acceptable.

Another simplification that has been made is a compromise in the geometry of the model. The fillet at the root section of the blade model has been slightly modified compared to

the actual geometry to avoid distorted elements. The elements used in the model are continuum composite 8 noded brick elements. The model is solved using ABAQUS® version 5.8 implicit FE code. The non-linear geometry option is used for large deflections. The *orientation* specified in the ABAQUS® input deck is used to specify a local co-ordinate system for each element *for the composite blade*. All the fibre layers in the model are given an orientation with respect to a local axis of rotation, which allow the user to orientate individual layers in the model. Since stresses are plotted with respect to the local co-ordinate system, the global axis shown in the stress plots (lower left corner) for the PMC blade will ***not*** correspond to the stress direction specified in the legend. (See Appendix B for the ABAQUS® input deck of the FE model.)

4.1.3 ENGINEERING CONSTANTS OF THE FE MODEL

The engineering constants for the titanium alloy used in the compressor blades were provided by ABB's specifications and are shown in Table 4.1. The engineering constants are taken from a 60 % volume fraction CFRP unidirectional pre-preg system, manufactured by Ciba-Geigy (HTA/6376)[34] and are shown in Table 4.2.

Table 4.1 Engineering constants for the titanium alloy (Ti-6Al-4V)

Property	Value
Tensile modulus	103 GPa
Poisson's ratio	0.29
Tensile strength	931 MPa (minimum)
Proof stress (0.2 %)	862 MPa (minimum)
Density	4.420 g/cm^3

Table 4.2 Engineering constants for the unidirectional CFRP composite.

Property	Value
Tensile modulus, longitudinal, E_{11}	141 GPa
Tensile modulus, transverse, E_{22}	10 GPa
Tensile modulus, through thickness, E_{33}	11 GPa
Shear modulus, in plane, G_{12}	5.2 GPa
Shear modulus, out of plane, G_{13}	5.2 GPa
Shear modulus, in plane, G_{23}	3.9 GPa
Poisson's ratio, in plane, ν_{12}	0.3
Poisson's ratio, out of plane, ν_{13}	0.5
Poisson's ratio, out of plane, ν_{23}	0.5
Tensile strength, longitudinal	1300 MPa
Tensile strength, transverse	45 MPa
Compressive strength, longitudinal	830 MPa
Compressive strength, transverse	140 MPa
Shear strength	62 MPa
Density	1.500 g/cm^3

4.1.4 COMPARISONS OF DEFLECTIONS

The **deflection directions** will be referred to as directions **1**, **2** and **3**, corresponding to the *Cartesian* co-ordinate system x, y and z. The axes are shown in the bottom left corners of the following figures and the deflection contour unit is in *meters*.

4.1.4.1 DEFLECTION OF THE TITANIUM BLADE

Figure 4.3(a) shows one of the compressor blades located on the rotor disc. The deflection of the titanium blade during operation is shown in Figure 4.3(b). The significant deflection that occurs during operation for the compressor blade is the untwisting of the blade. Figures 4.4 to 4.6 show the deflections for the titanium blades in the 1, 2 and 3 directions, respectively. The direction of rotation for all the deflection plots is out of the page.

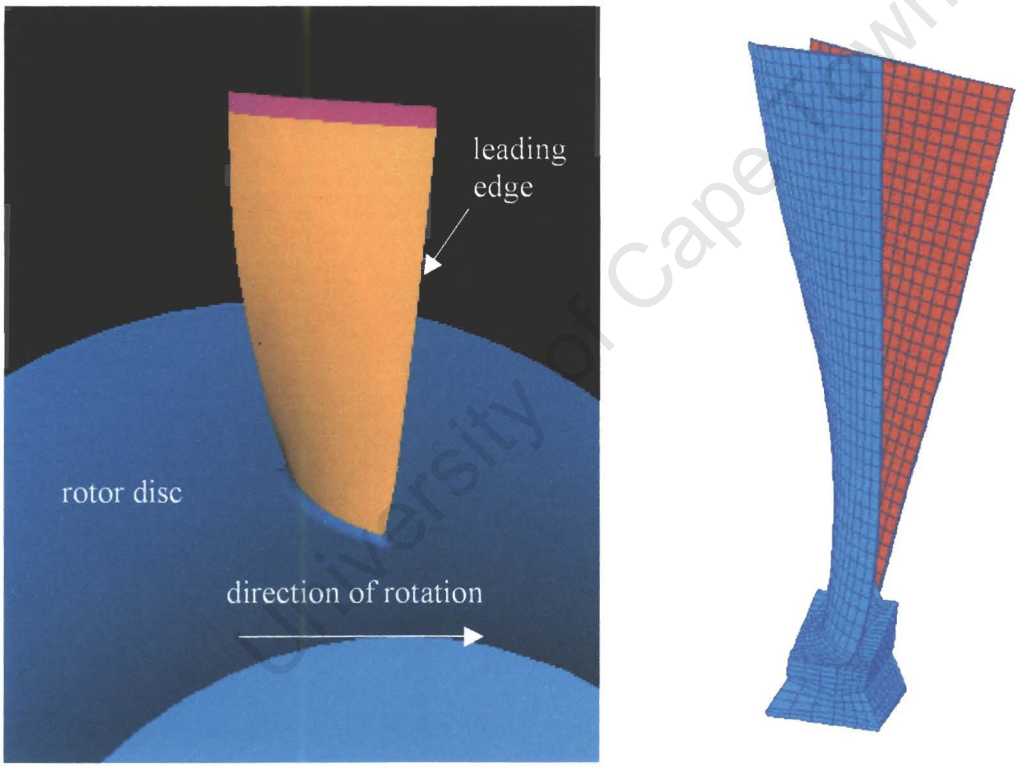

Figure 4.3(a) Compressor blade located on the rotor disc of the turbine. Figure 4.3(b) Deflection of the titanium compressor blade during operation. (The red image is showing a stationary blade).

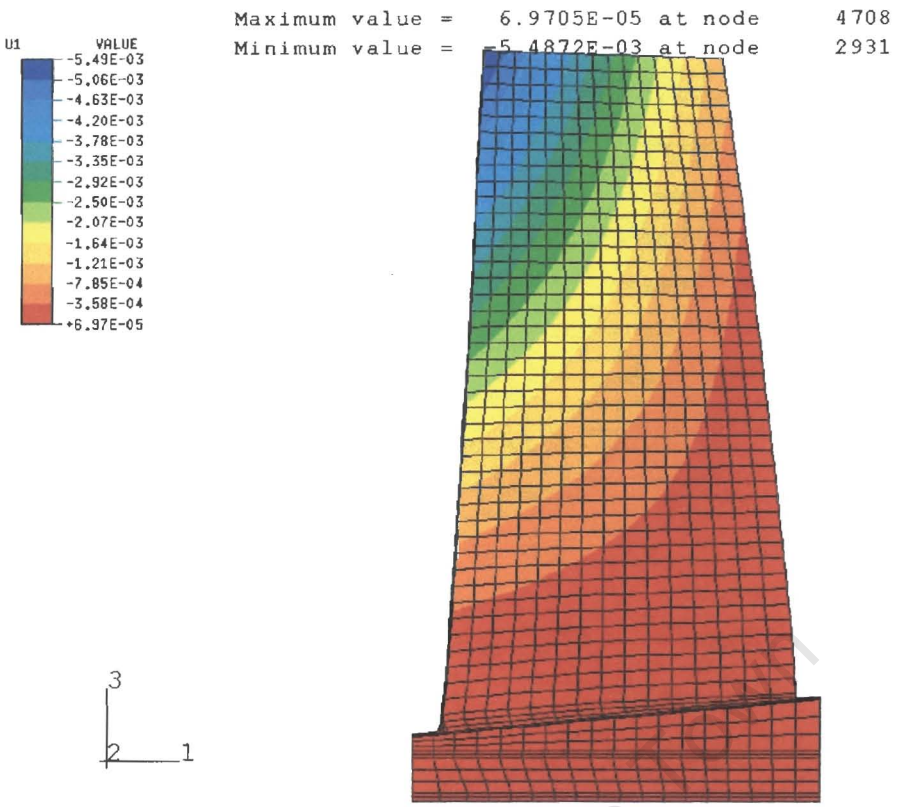

Figure 4.4 Deflection of the titanium blade in the 1 direction during operation.

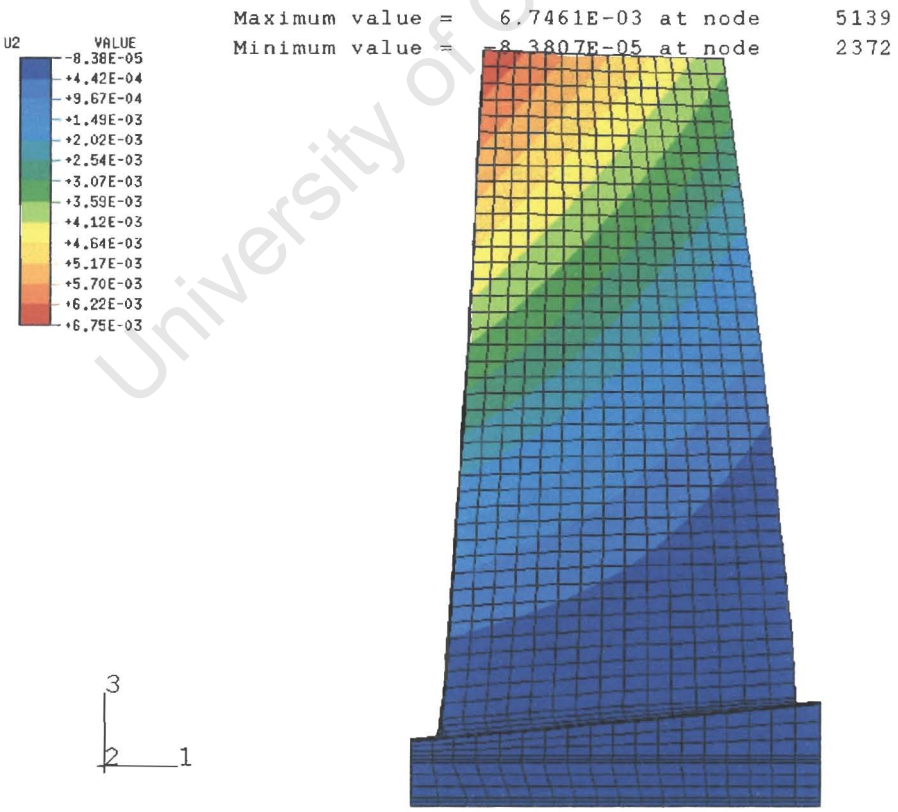

Figure 4.5 Deflection of the titanium blade in the 2 direction during operation.

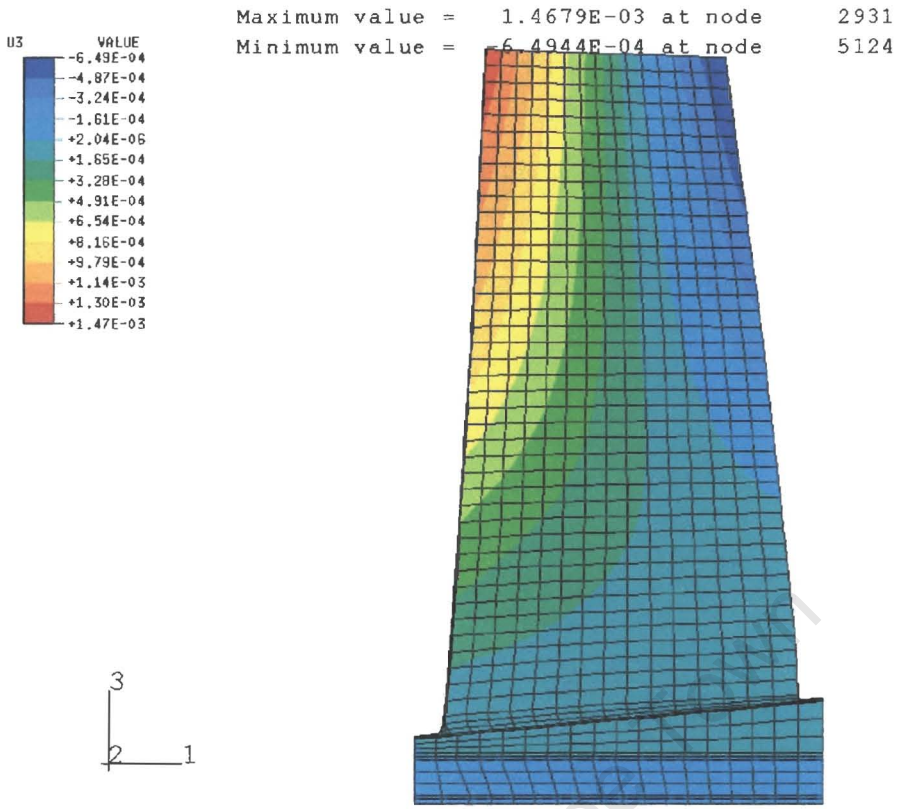

Figure 4.6 Deflection of the titanium blade in the 3 direction during operation.

As can be seen from Figures 4.4 to 4.6, the greatest deflection occurs towards the tip of the leading edge, resulting from the untwisting behaviour. The tip deflection of the blade in the 2 direction (into the page) reaches a value close to 6.7 mm during design speed, *i.e.* a rotational speed of 10 000 rpm. The deflection of the blade in the 3-direction ("radial direction") of 1.5 mm is considerably less in comparison to the other directions due to the geometry of the blade.

4.1.4.2 DEFLECTION OF THE COMPOSITE BLADE, LAY-UP 1

The deflection of the CFRP blade of lay-up 1, during operation, is shown in Figure 4.7. The deflection of the composite compressor blade is similar to that of the titanium blade *i.e.* the untwisting of the blade is the dominant behaviour. Figures 4.8 to 4.10 show the deflections for the CFRP blade in the 1, 2 and 3 directions, respectively. As can be seen from Figures 4.8 to 4.10, the greatest deflection occurs towards the tip of the leading edge, resulting from the untwisting behaviour similar to that of the titanium blade. The tip deflection of the blade in the positive 2 direction (into the page) reaches close to 6.59 mm during design speed. The deflection of the composite blade is less in all directions compared to that of the titanium blade. See Table 4.3.

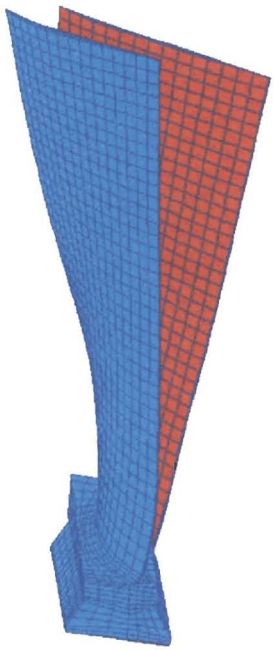

Figure 4.7 Untwisting of the composite compressor blade during operation.

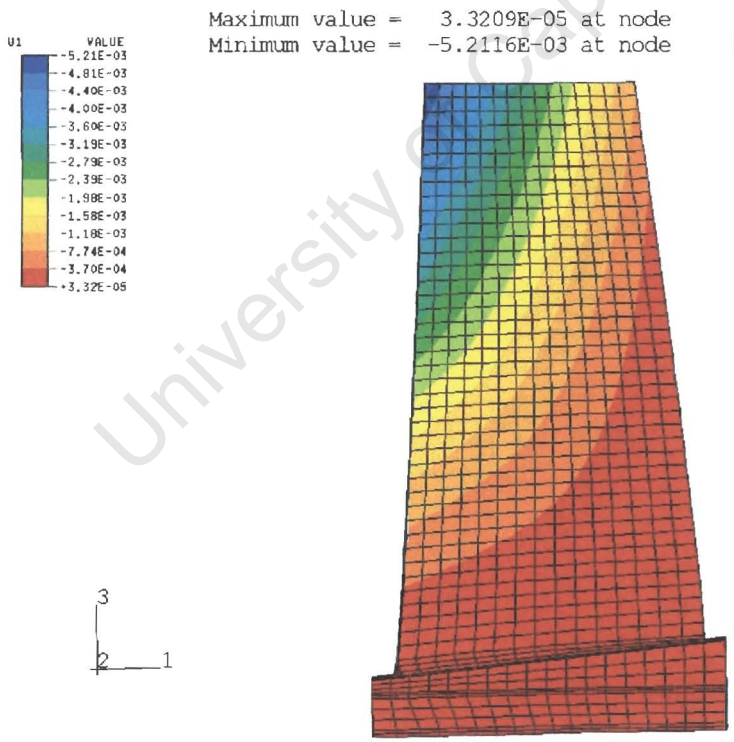

Figure 4.8 Deflection of the CFRP blade (lay-up 1) in the 1 direction during operation.

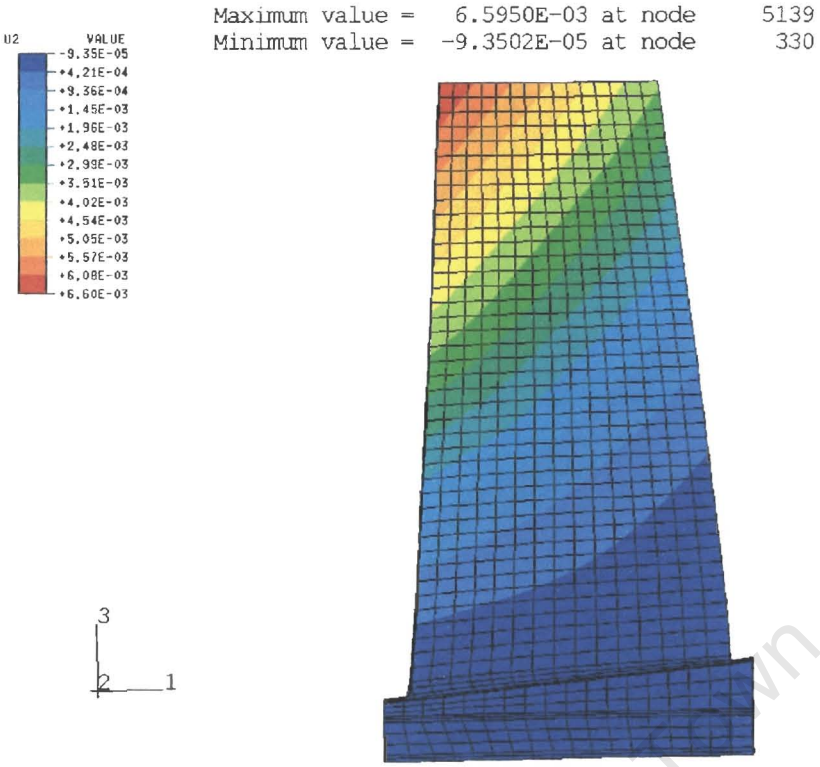

Figure 4.9 Deflection of the CFRP blade (lay-up 1) in the 2 direction during operation.

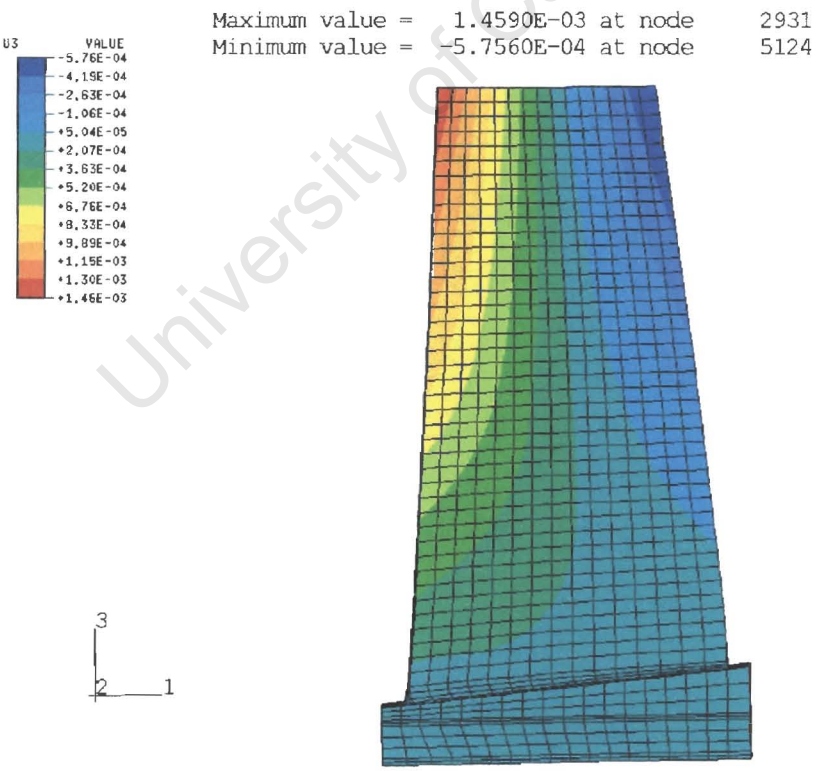

Figure 4.10 Deflection of the CFRP blade (lay-up 1) in the 3 direction during operation.

4.1.4.3 DEFLECTION OF THE COMPOSITE BLADE, LAY-UP 2

This CFRP FE model has a cross ply configuration, *i.e.* 50 % of the fibres are in the 0° direction alternating with the remaining 50 % in the 90° direction. The untwisting of the CFRP blade lay-up 2 is similar to that of lay-up 1 shown in Figure 4.7. The deflections in the three Cartesian directions of lay-up 2 are shown in Figures 4.11 to 4.13. The untwisting of the CFRP blade lay-up 2 are higher than those found in the composite blade lay-up 1. This is due to the lack of fibres in the +/- 45° direction which contributes to the torsional rigidity of the blade. Table 4.3 gives a summary of all the maximum deflections of the blades investigated.

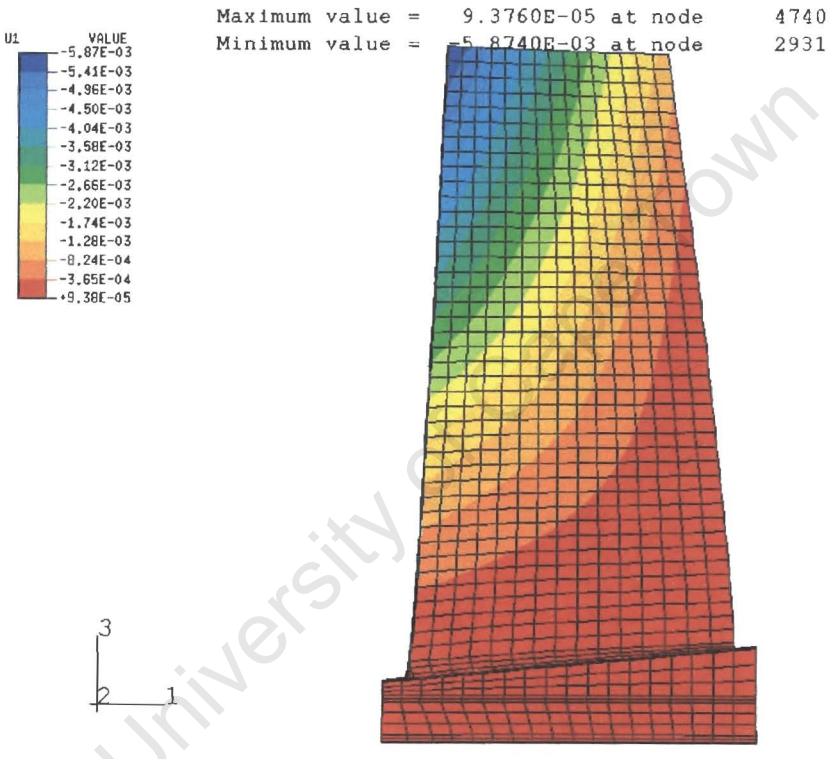

Figure 4.11 Deflection of the composite blade (lay-up 2) in the 1 direction during operation.

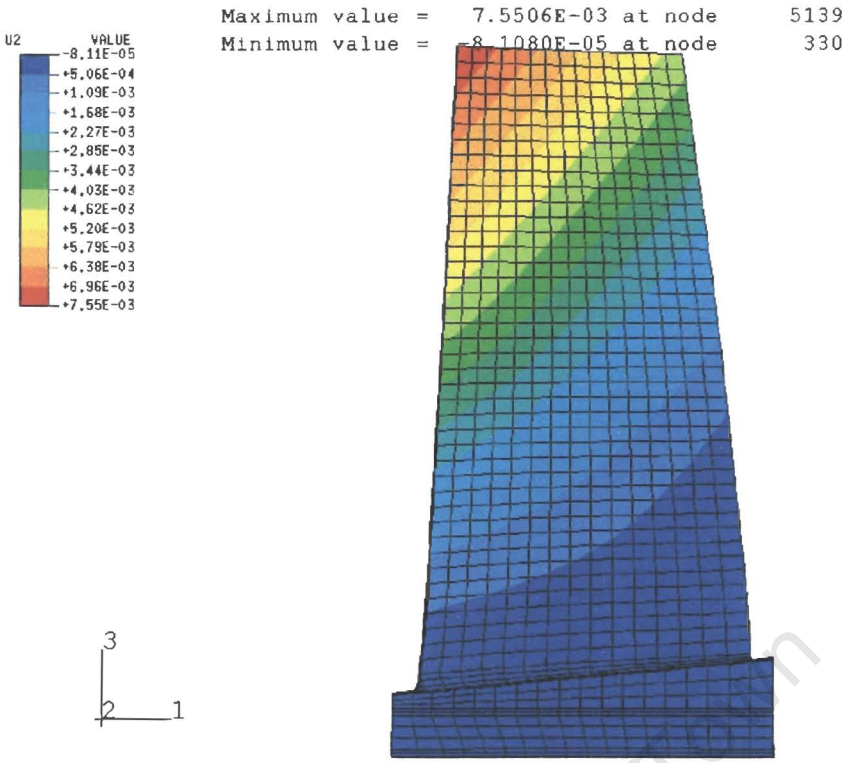

Figure 4.12 Deflection of the composite blade (lay-up 2) in the 2 direction during operation.

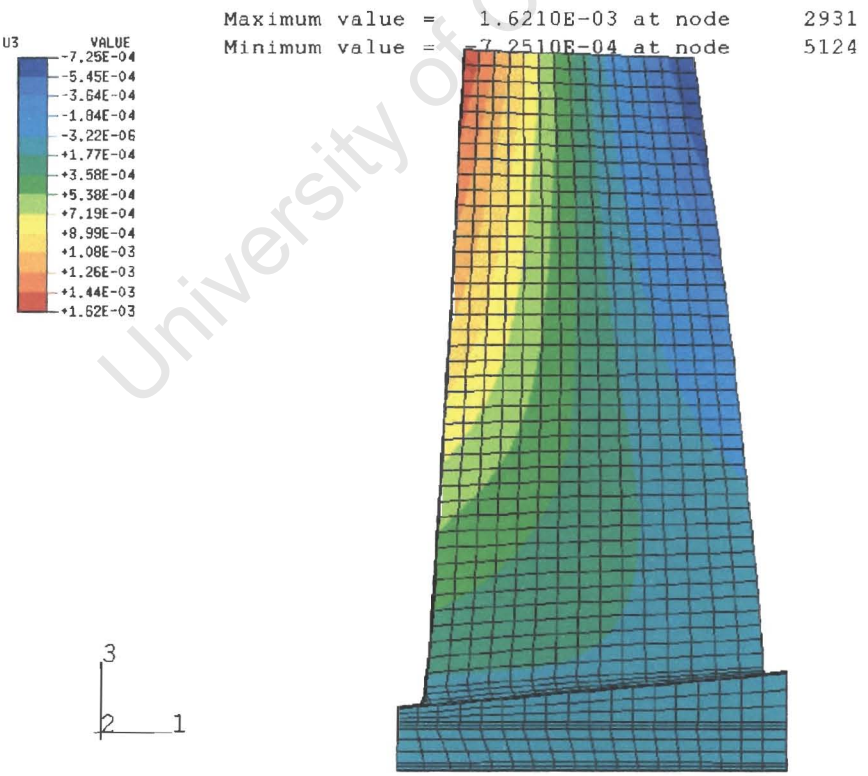

Figure 4.13 Deflection of the composite blade (lay-up 2) in the 3 direction during operation.

Table 4.3 Summary of deflection for the compressor blades.

Material	Tip Deflection (mm)		
	1 direction (x)	2 direction (y)	3 direction (z)
Titanium	-5.49	6.75	1.47
CFRP lay-up 1	-5.21	6.60	1.46
CFRP lay-up 1	-5.87	7.55	1.62

4.1.5 INDUCED STRESSES IN THE COMPRESSOR BLADES

The purpose of this section is to determine the stresses occurring in the compressor blades during operation. In addition, comparisons of stresses with respect to strength properties will be carried out. The stresses given in the stress plots are all in Pascals (Pa).

4.1.5.1 STRESSES IN THE TITANIUM BLADE

The stresses experienced in the blades during operation are predominantly caused by the centrifugal forces arising from the high rotational speed. The currently used titanium blades are suffering from high stresses at the root of the blades as shown in Figure 4.14.

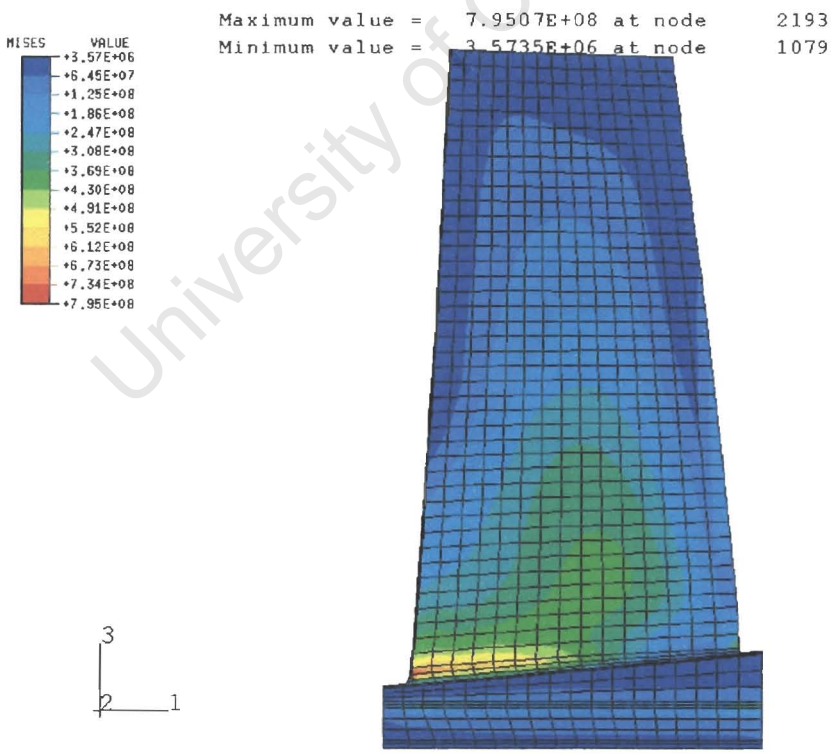

Figure 4.14 Von Mises stresses in the titanium blade.

Due to the untwisting and bending of the blade during the design speed, the stress pattern for the titanium blade shows high stresses at the bottom leading edge of the blade. The maximum principal stress pattern for the titanium blade in Figure 4.15 also shows that the blade suffers from high tensile stresses at the lower leading edge of the blade. In Table 4.1 the proof stress and tensile strengths were shown as 862 and 931 MPa, respectively. The von Mises and principal stresses of 795, 783 MPa, respectively are close the proof and tensile strengths, respectively. This indicates that the titanium blades are operating close to their design limit criteria, with respect to material properties.

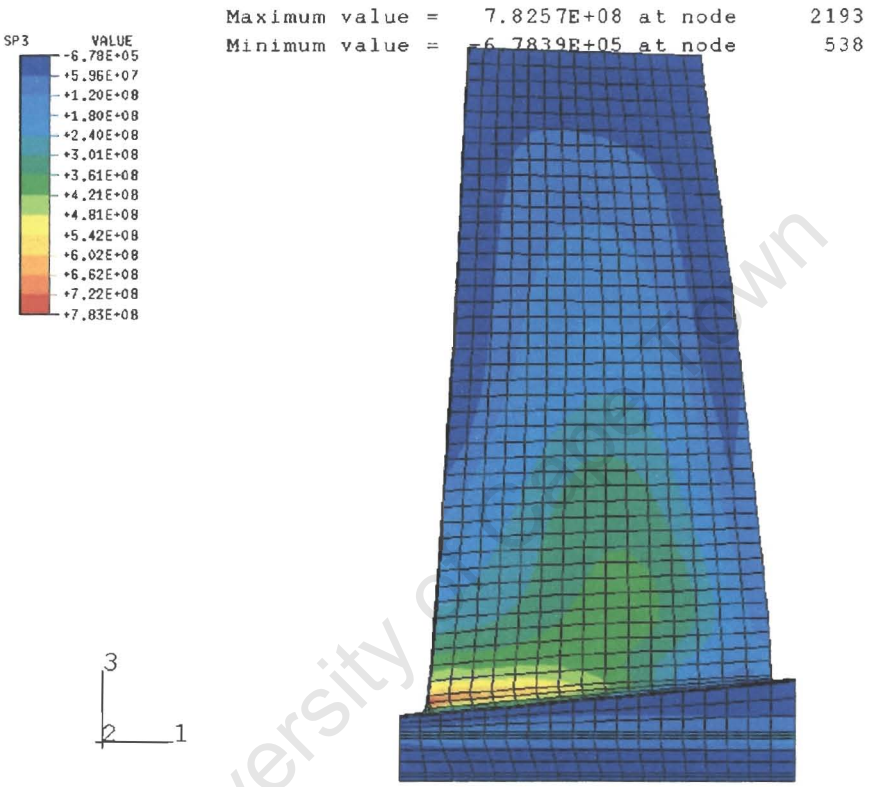

Figure 4.15 Maximum principal stress of the titanium blade.

4.1.6 STRESSES IN THE COMPOSITE BLADE

The purpose of this section is to consider the stresses parallel and perpendicular to the fibre direction, as well as the shear stresses acting on individual plies in the blades. These values are then compared with the corresponding strengths of the laminate to assess if the plies can withstand the induced stresses during operation. The stress values given in the top left corner of the contour plots are in Pa. Each colour represents a given stress state.

4.1.6.1 STRESSES ACTING ON THE FIRST LAYER IN THE CFRP BLADE, LAY-UP 1

Figures 4.16 to 4.18 show the various stresses acting on the outermost ply of the CFRP blade. The fibre direction for the outermost layer is in the radial direction. It is found from these stress plots that there is a stress concentration appearing in the base section of the blade close to the lower leading edge for the transverse and shear stress plots (circled in Figures 4.17 and 4.18). The maximum tensile stress occurring in the parallel fibre direction is approximately 408 MPa, which is well below the corresponding tensile strength for a unidirectional CFRP laminate of 1300 MPa (see Table 4.2). In the case of the transverse stress to the fibre direction, the stress value of 73 MPa exceeds the corresponding strength value of 45 MPa in Table 4.2. The maximum shear stress (47 MPa) in the blade is found in the base section of the blade, which is lower than the allowed shear strength value of 62 MPa. The geometry of the blade at this location incorporates a small fillet, which may act as a stress raiser.

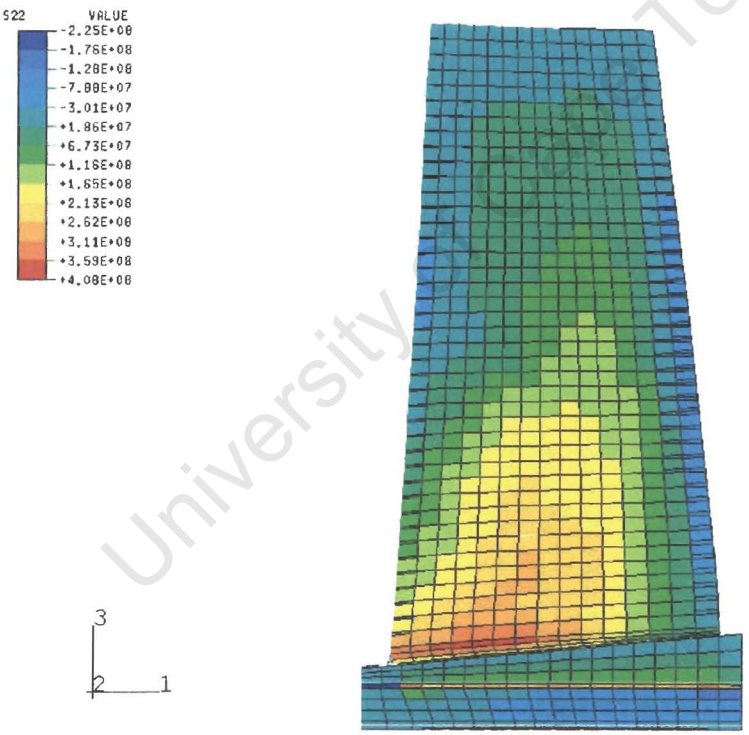

Figure 4.16 Stresses in the fibre direction of the outermost ply, lay-up 1.

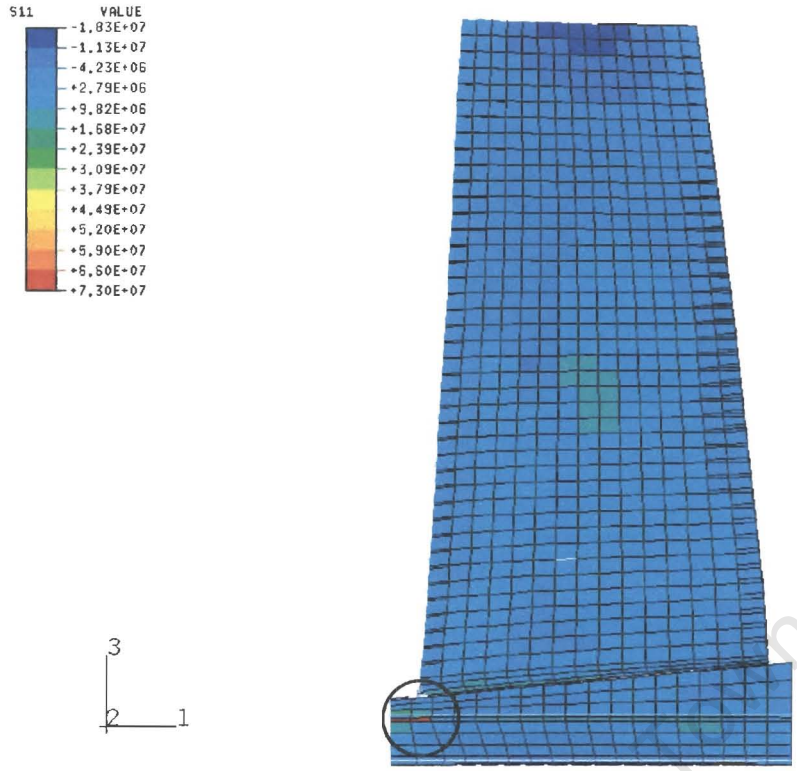

Figure 4.17 Stresses in the transverse fibre direction of the outermost ply, lay-up 1.

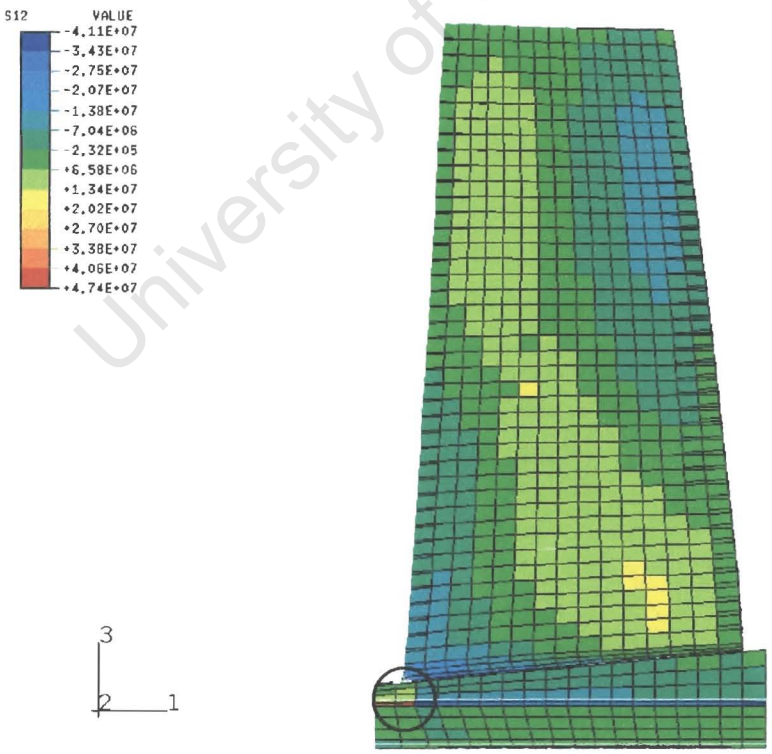

Figure 4.18 Shear stresses in the outermost ply, lay-up 1.

4.1.6.2 STRESSES ACTING ON THE SECOND LAYER IN THE CFRP BLADE, LAY-UP 1

Figures 4.19 to 4.21 show the various stresses acting on the 2nd ply of the CFRP blade, lay-up 1. These figures show that there is no second ply on the top leading edge. It is observed for the CFRP blade that the stresses occurring are lower than that of the outermost layer. This trend proves to be true for the remaining layers as summarised in Table 4.4 below. The plies further toward the centre of the blade experience less stress. This is suggested to originate from the untwisting / bending behaviour of the blade which result in the highest stresses on the outside plies. This section is investigated more in Appendix C to verify this behaviour. The stresses in the transverse fibre direction in the second layer still shows that failure will occur in the base section of the blade, as found from Figure 4.20.

Table 4.4 Maximum stress values in the five plies closest to the pressure side of the blade, lay-up 1.

Layer	Max. stress parallel to fibre, σ_L (MPa)	Max. stress transverse to fibre, σ_T (MPa)	Max. shear stress, τ_{LT} (MPa)
1	408	73	48
2	391	70	44
3	374	63	39
4	356	54	35
5	331	48	24

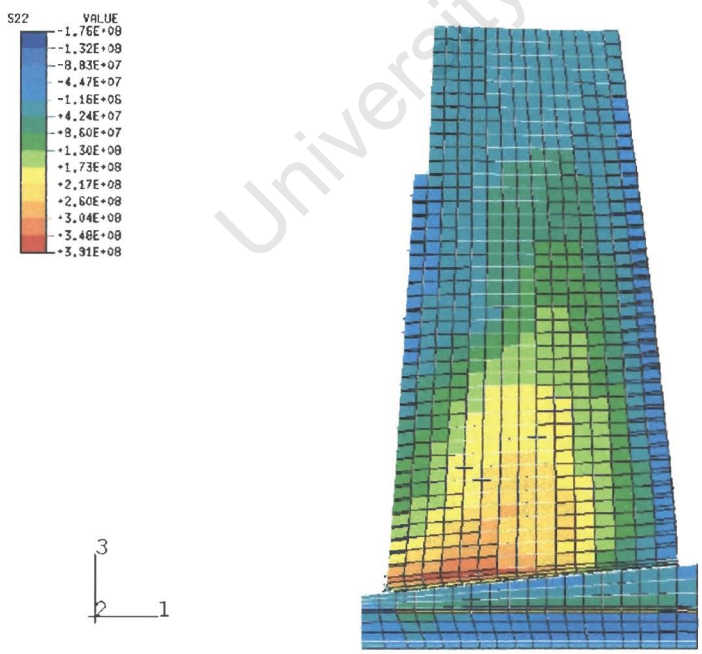

Figure 4.19. Stresses in the fibre direction of the 2nd outermost ply, lay-up 1.

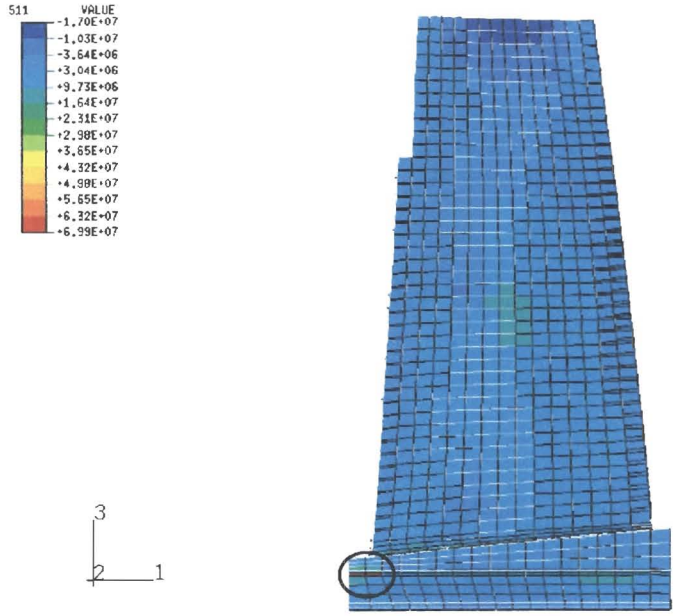

Figure 4.20 Stresses in the transverse fibre direction of the 2nd outermost ply, lay-up 1.

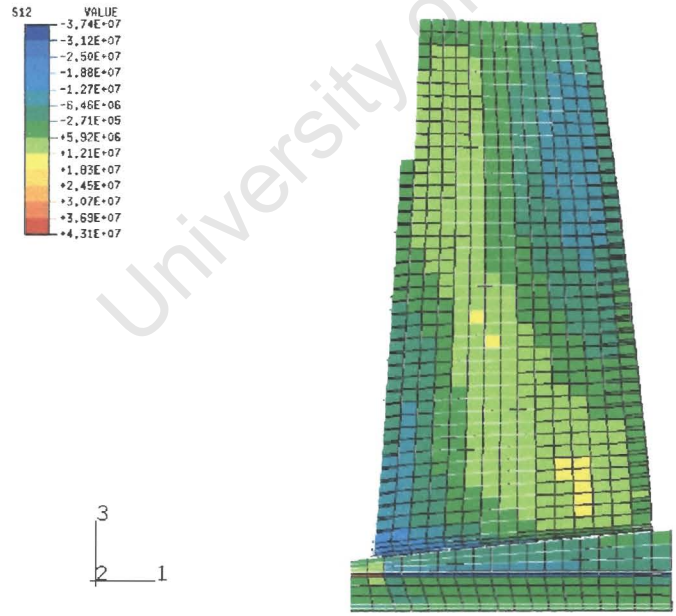

Figure 4.21 Shear stresses in the 2nd outermost ply, lay-up 1.

4.1.6.3 STRESSES ACTING ON THE FIRST LAYER IN THE CFRP BLADE, LAY-UP 2

Figures 4.22 to 4.24 show the various stresses acting on the outermost ply of the CFRP blade, lay-up 2. The same trend found for that of lay-up 1 is present in lay-up 2, which suggests that the stresses further towards the centre of the blade profile, experience lower stresses. The maximum stresses for the cross ply model never exceed the corresponding strength values. This is due to fact that the lay-up 2 has more fibres in the 90° direction, which can accommodate the transverse stresses. The maximum tensile stress occurring in the parallel fibre direction is approximately 569 MPa, which is still well below the corresponding tensile strength for a unidirectional CFRP laminate of 1300 MPa (see Table 4.2). This value is approximately 30 % higher than that for lay-up 1 and is higher due the lower amount of fibres in the radial direction. It is found that the maximum transverse stress to the fibre direction, is approximately 41 MPa, which is found in the base section of the blade. This value is close to the corresponding strength but does not exceed 45 MPa in Table 4.2. The maximum shear stress (47 MPa) in the blade is found in the base section of the blade, which is lower than the allowed shear strength value of 62 MPa.

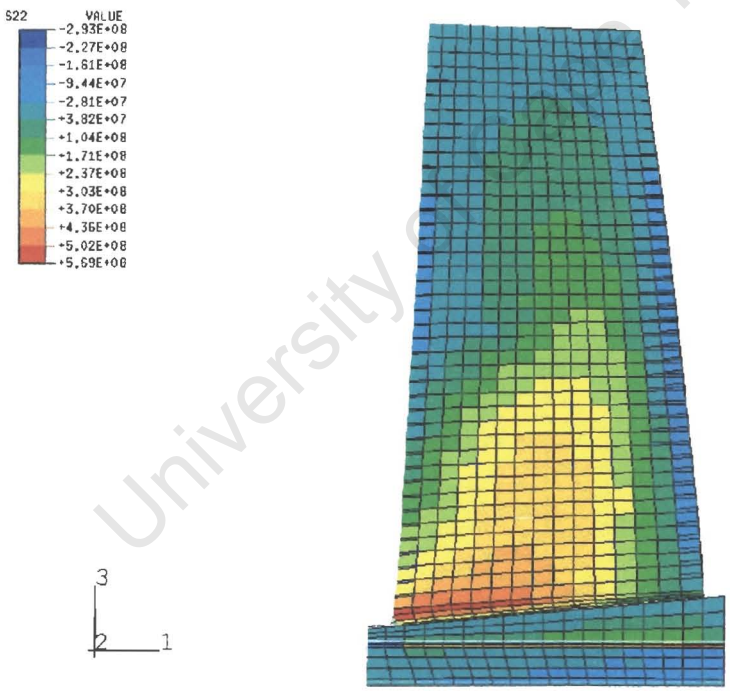

Figure 4.22 Stresses in the fibre direction of the outermost ply, lay-up 2.

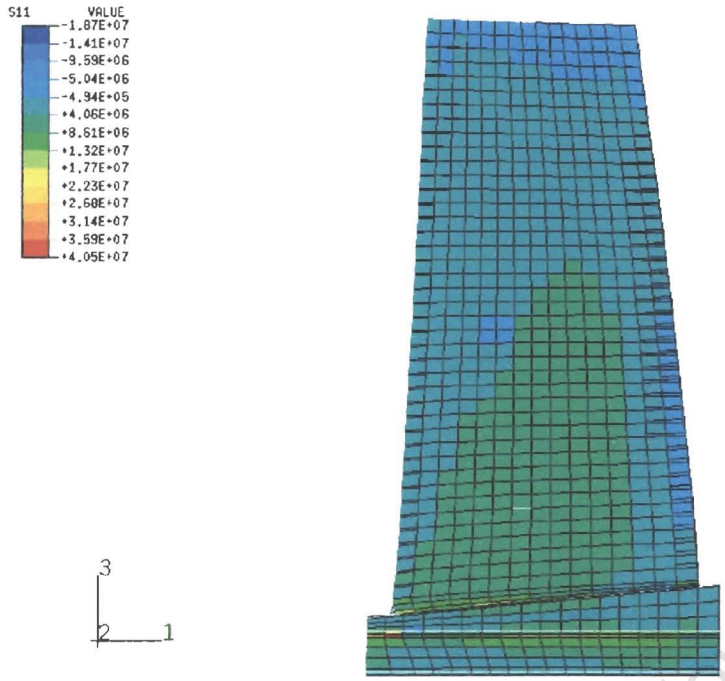

Figure 4.23 Stresses in the transverse fibre direction of the outermost ply, lay-up 2.

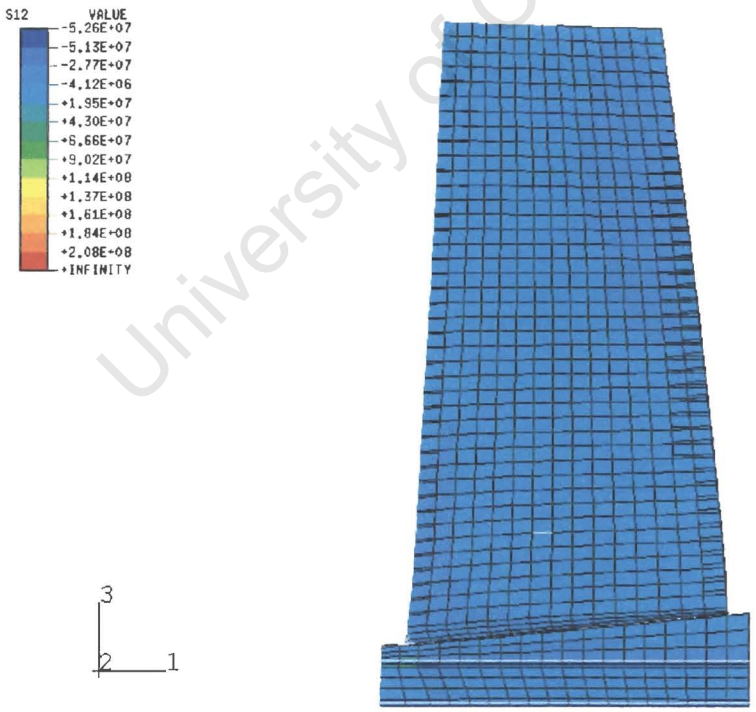

Figure 4.24 Shear stresses in the outermost ply, lay-up 2.

4.1.7 VIBRATION ANALYSIS FOR THE TITANIUM BLADE

In practice it is important to prevent high cycle fatigue failures due to harmonic excitations. The harmonic excitations ('force functions') must not interact with the fundamental blade frequencies at the design speed from the engine. The compressor blades exhibit a particular shape at each fundamental frequency. The shape of the first mode of the titanium blade at the design speed can be seen in Figure 4.25. This first mode shape is found to be a pure bending mode. The mode shapes for all the FE models are found in Appendix D. The engine harmonics are supplied from ABB STAL (see Table 4.5).

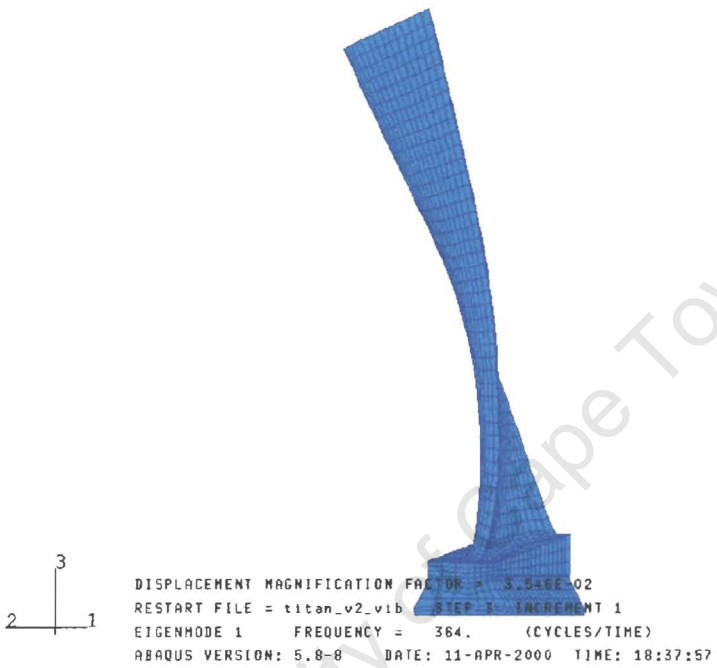

Figure 4.25 The first mode shape for the titanium blade at 10 000 rpm.

Table 4.5 The engine harmonic frequencies at design speed.

Engine speed	0 rpm	10 000 rpm
Harmonic order	**Frequency, Hz**	**Frequency, Hz**
H1	0	167
H2	0	333
H3	0	500
H4	0	667
H5	0	833
H6	0	1000
H7	0	1167
H8	0	1333
H9	0	1500
H10	0	1667

The fundamental frequencies predicted by the FE model are shown in Table 4.6. During operation, the fundamental blade frequencies must not be too close to the harmonics of the engine. ABB STAL specifications state that the frequencies must not lie within 10 Hz from each other. During start up, excitations will occur for the blades, which can be visualised in the Campbell diagram when the engine 'harmonic lines' crosses the 'mode lines' of the blades. Since this occurs only during a brief time during start up, there is not a major problem with this behaviour. However, at the design speed shown in the far right of the Campbell diagram, there must be no excitation from the engine, *i.e.* the 'mode lines' must not lie within 10 Hz of the engine 'harmonic lines' (H1-H10) in the diagram. The Campbell diagram, Figure 4.26, can be constructed from the data given in Tables 4.5 and 4.6[18]. The closest interaction with the engine harmonics for the titanium blades is approximately 16 Hz for the 6th engine harmonic at design speed.

Table 4.6 Fundamental blade frequencies at 0 and 10 000 rpm for the titanium blade.

Engine speed	0 rpm	10 000 rpm
Mode	Frequency, Hz	Frequency, Hz
1	223	364
2	796	896
3	943	1016
4	1892	1903
5	2123	2231

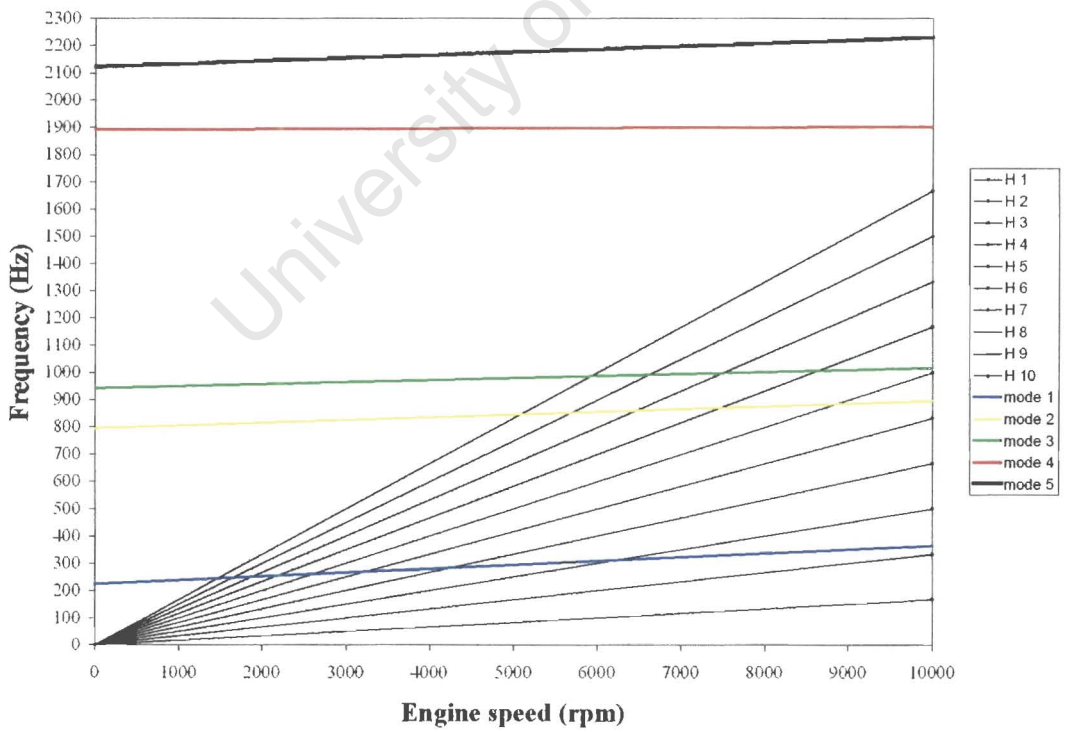

Figure 4.26 Campbell diagram for the for titanium blade.

4.1.8 VIBRATION ANALYSIS FOR THE CFRP BLADE, LAY-UP 1

Figure 4.27 shows the Campbell diagram for the CFRP blade lay-up 1. The blade frequencies of the CFRP blade are found to be higher to that of the titanium blade. Table 4.7 shows the fundamental blade frequencies for the CFRP blade as predicted by the FE analysis. The closest interaction with the engine harmonics for the CFRP blades, lay-up 1 is approximately 38 Hz for the 3rd engine harmonic at the operating speed.

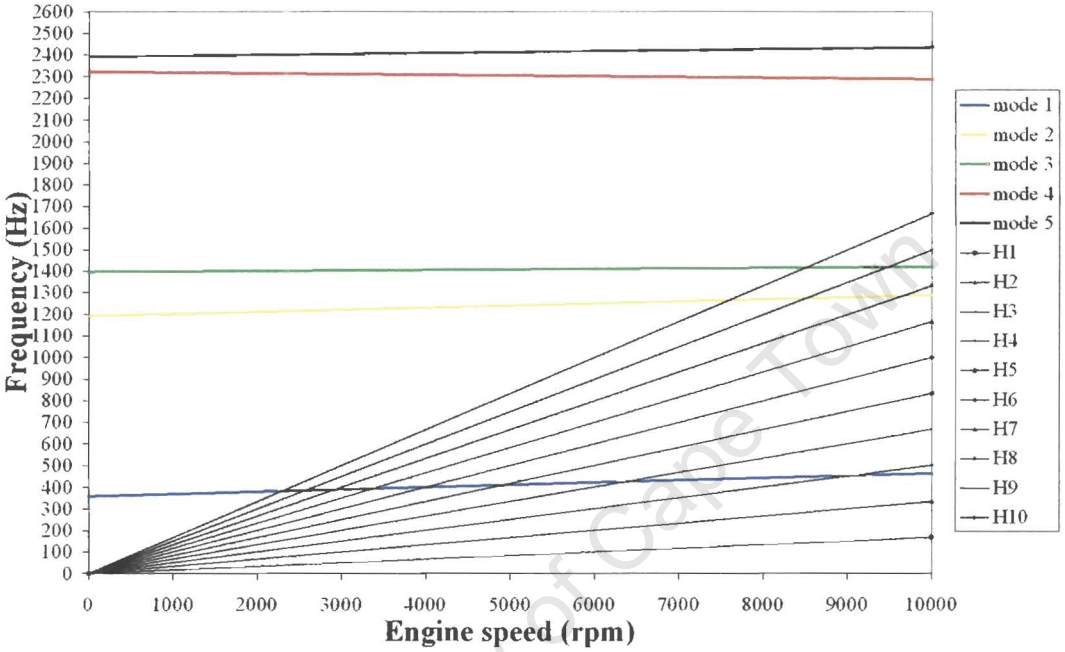

Figure 4.27 Campbell diagram for carbon composite blade, lay-up 1.

Table 4.7 Fundamental blade frequencies at 0 and 10 000 rpm for CFRP blade, lay-up 1.

Engine speed	0 rpm	10 000 rpm
Mode	Frequency, Hz	Frequency, Hz
1	358	462
2	1192	1289
3	1397	1420
4	2322	2289
5	2392	2437

4.1.9 VIBRATION ANALYSIS FOR THE CFRP BLADE, LAY-UP 2

Figure 4.28 shows the Campbell diagram for the CFRP blade lay-up 2. The blade frequencies of the CFRP blade are found to be lower than that of the CFRP blade lay-up 1. This is because the lay-up 2 blade has fewer fibres in the radial direction, which will make it less rigid and therefore lowering the blade frequencies. Table 4.8 shows the fundamental blade frequencies for the CFRP blade as predicted by the FE analysis. The closest interaction with the engine harmonics for the titanium blades is approximately 20 Hz for the 6th engine harmonic at the operating speed.

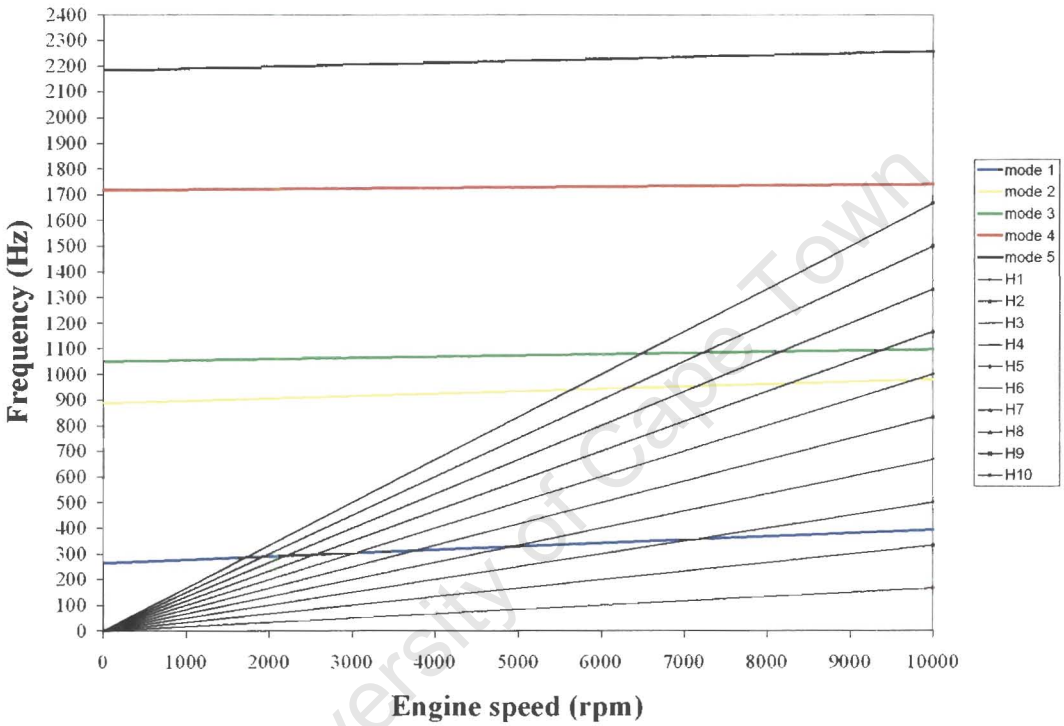

Figure 4.28 Campbell diagram for carbon composite blade, lay-up 2.

Table 4.8 Fundamental blade frequencies at 0 and 10 000 rpm for the CFRP, lay-up 2.

Engine speed	0 rpm	10 000 rpm
Mode	Frequency, Hz	Frequency, Hz
1	264	391
2	887	980
3	1050	1097
4	1717	1740
5	2182	2259

4.2 EROSION RESULTS

4.2.1 EROSION OF THE TITANIUM ALLOY

This section presents the erosion tests performed on the titanium alloy, Ti-6Al-4V, that is currently used in the compressor blades of ABB's GT10 gas turbine. The tests were carried out at four different angles to investigate how the erosion rate varies with impact angle. For each angle a graph of cumulative volume loss of the target material *vs.* cumulative mass of erodent is plotted. The reason for plotting volume loss *vs.* mass of erodent is that a comparison between *different materials* can be made. Using cumulative mass loss *vs.* cumulative mass erodent will not be a valid comparison for different materials having different densities. These graphs can then be utilised to find the steady state erosion rate, which is the slope of the graph, for each angle obtained.

4.2.1.1 STEADY STATE EROSION TESTING

The erosion tests for the different angles can be summarised as seen in Figure 4.29. These graphs show that there is no incubation taking place and that a steady state erosion is immediately obtained. The correlation coefficients R^2 for each test was greater than 0.99.

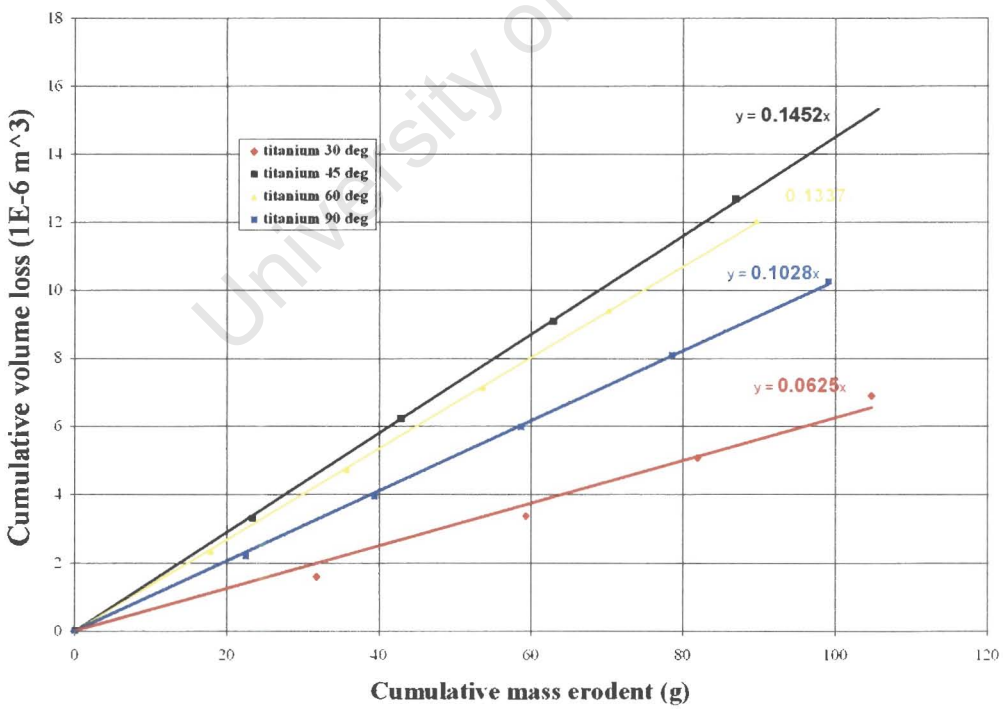

Figure 4.29 The cumulative volume loss *vs.* cumulative mass loss of titanium (Ti-6Al-4V) at four different impact angles.

4.2.1.2 EFFECT OF IMPACT ANGLE ON THE EROSION RATE OF TITANIUM

The steady state erosion tests on the titanium targets are plotted for each angle in Figure 4.30. From Figure 4.30 it can be seen that the titanium alloy experiences a maximum erosion rate at 45° and a minimum erosion rate at 30° for the impact angles tested. This behaviour is typical of ductile behaviour[40].

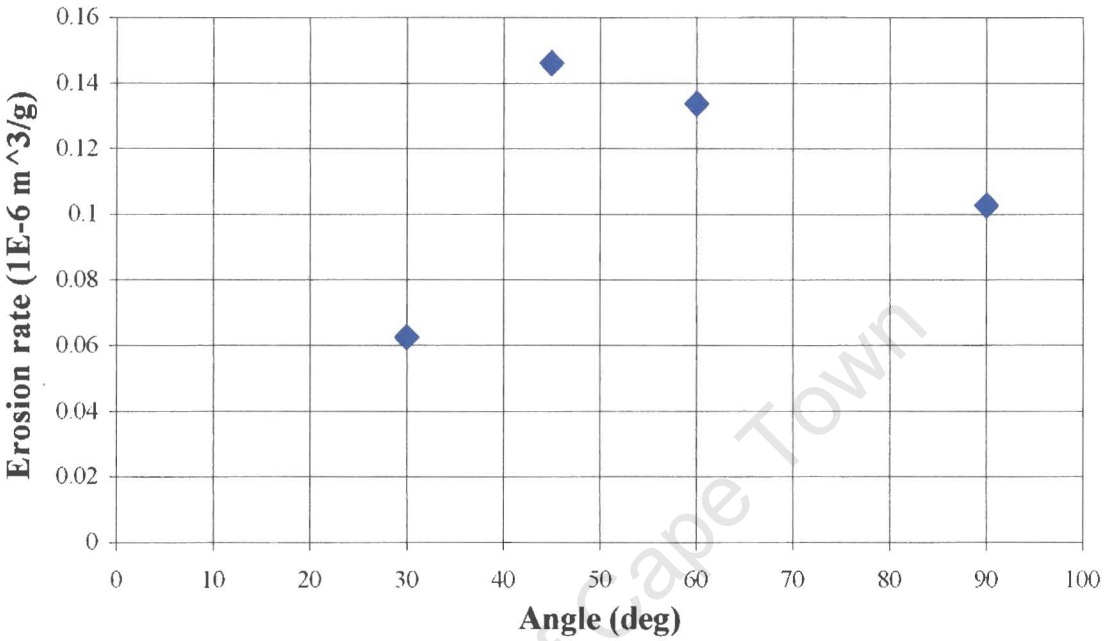

Figure 4.30 The erosion rate *vs.* impact angle for the titanium alloy.

4.2.2 EROSION OF THE FIBRE COMPOSITE MATERIALS

Steady state erosion tests were performed on carbon fibre/epoxy (CFRP) and Kevlar®/epoxy (KFRP) with approximately 50 % volume fraction fibre. The materials used to manufacture the laminates are shown in Table 4.9.

Table 4.9 Fibre composites selected for erosion studies.

Fibre Material	Matrix Resin
Hexcel's Plain weave carbon HXL 43193P	SP Epoxy Ampreg-20
Hexcel's unidirectional carbon GA 090	SP Epoxy Ampreg-20
Hexcel's Plain weave Kevlar® HXL 281	SP Epoxy Ampreg-20

4.2.2.1 EROSION OF THE CARBON FIBRE/EPOXY COMPOSITE

The steady state erosion results for both the woven and the unidirectional carbon fibre composites as a function of impact angle are shown in Figures 4.31 and 4.32. The unidirectional specimens were orientated so that the erosive particles struck perpendicular to the fibres. It was found that when the erodents struck the fibres orientated parallel to the particle stream, the wear rates were lower. Both figures indicate a typical brittle behaviour.

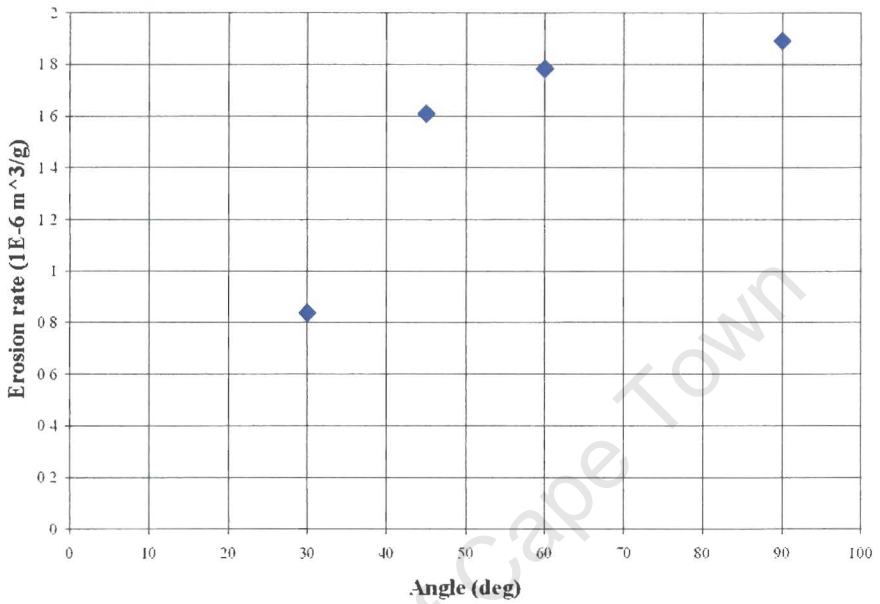

Figure 4.31 The erosion rate *vs.* angle of impingement of plain weave carbon/epoxy.

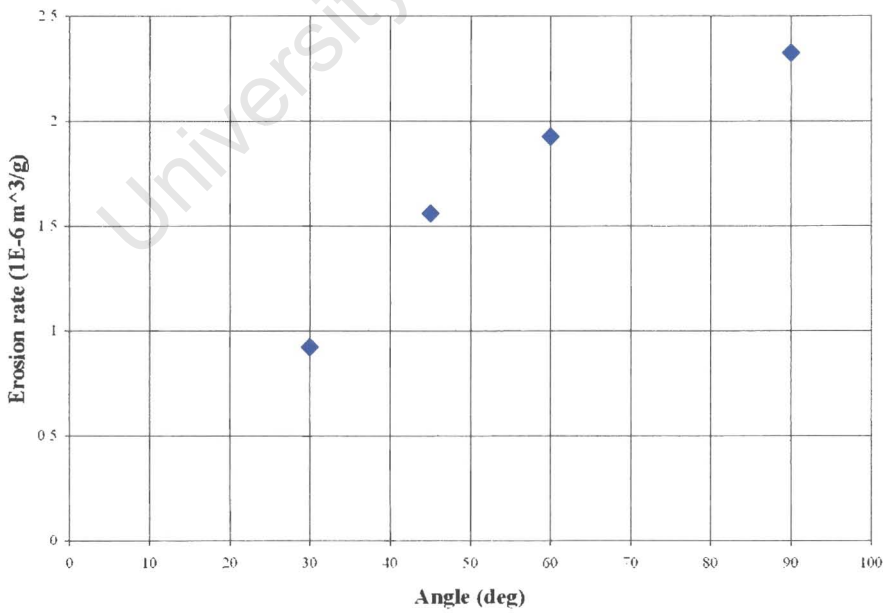

Figure 4.32 The erosion rate *vs.* angle of impingement of unidirectional carbon/epoxy.

The maximum erosion rate for the plain weave and unidirectional carbon composites occurs at 90°. The lowest erosion rate occurs at low angles for both materials. This behaviour can be identified as brittle behaviour[40, 44, 46]. The results are found to be similar to that found of Pool *et al*[44]. The erosion rate of these two materials is high in comparison to the titanium, which exhibit at least an order of magnitude lower erosion rate than the composites. Inspection of the CFRP specimens shows that the fibres break in a brittle manner and are removed easily by the silica particles. Figure 4.33 shows an eroded area in a woven CFRP composite that was eroded by approximately 30 grams of silica particles. From this figure it can be observed that the damaged area forms ridges and valleys due the nature of the woven carbon fibre plies. It is observed that where more matrix rich areas are encountered in the plain weave composite, the damage to the fibres is less severe.

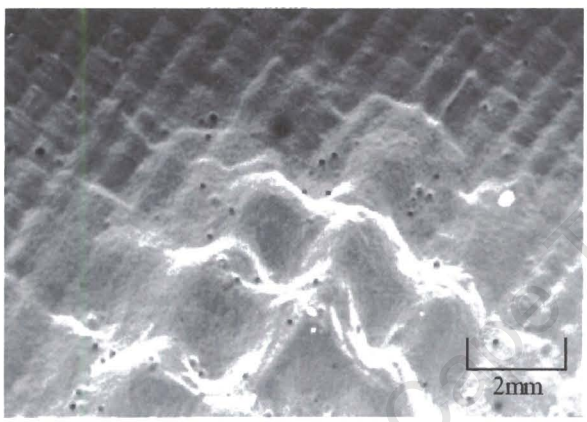

Figure 4.33 SEM micrograph showing a typical eroded area in a woven CFRP.

The extremely high resolution of the near field scanning optical microscope (SNOM) allowed the determination of the depth profile of the damaged areas. The SNOM image in Figure 4.34 also gave the profile of the broken carbon fibres that protrude from the epoxy matrix. The SNOM image verified the brittle nature of the carbon fibres in the damaged zone.

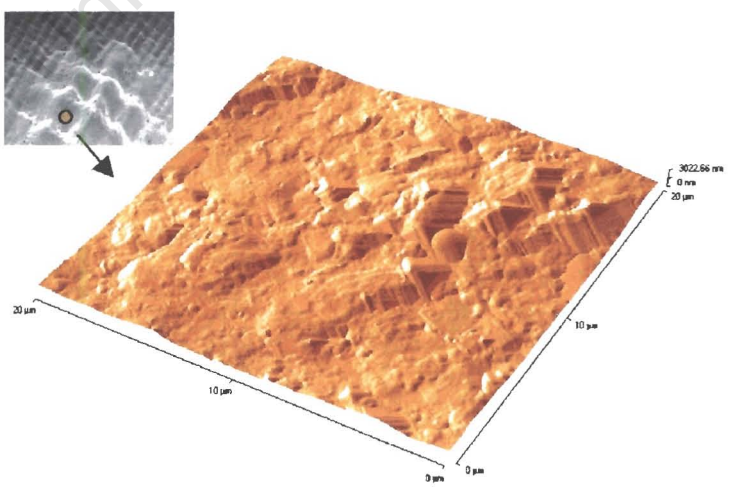

Figure 4.34 SNOM image of the CFRP eroded area and damage mode.

Figure 4.35 shows a SEM micrograph of the eroded area of a CFRP unidirectional with the fibres orientated perpendicular to the erodent stream. This image shows the fibre breakage and subsequent removal after the resin has been eroded.

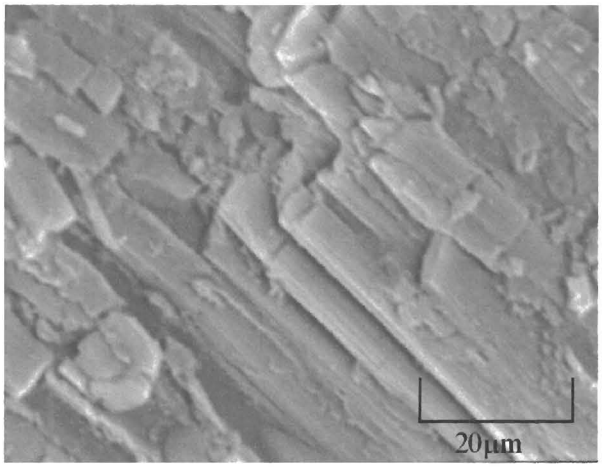

Figure 4.35 SEM micrograph showing a typical eroded area in a unidirectional CFRP.

4.2.2.2 EROSION OF THE KEVLAR® FIBRE/EPOXY COMPOSITE

The Kevlar® composite was exposed to the same erosion conditions as the carbon composites and the erosion rate for the various impact angles can be seen in Figure 4.36.

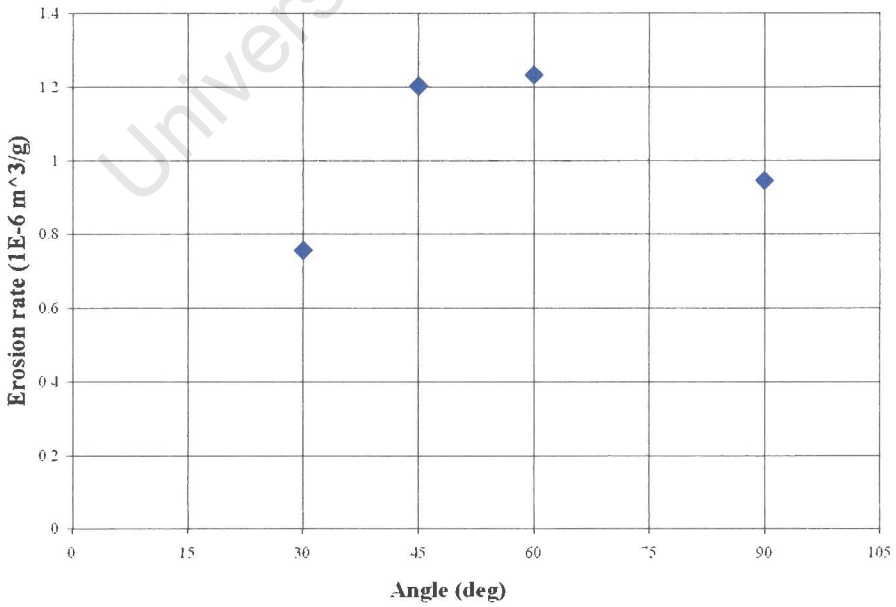

Figure 4.36 The erosion rate *vs.* angle of impingement of Kevlar® plain weave.

The maximum erosion rate for the KFRP composite occurs at a 60° impingement for the angles tested. This indicates a more ductile behaviour than the carbon fibre composites investigated [44]. The erosion results of the fibre composites studied show that the KFRP composite exhibits a superior erosion resistance than the CFRP composites. This conforms to previous studies done by Pool *et al.* on fibre composites[44]. It is suggested that CFRP and KFRP have different mechanisms of erosion. Inspection of the eroded Kevlar® specimen in Figure 4.37 shows that the fibres break in a ductile manner with fibres undergoing large deformations before the subsequent removal of the composite material.

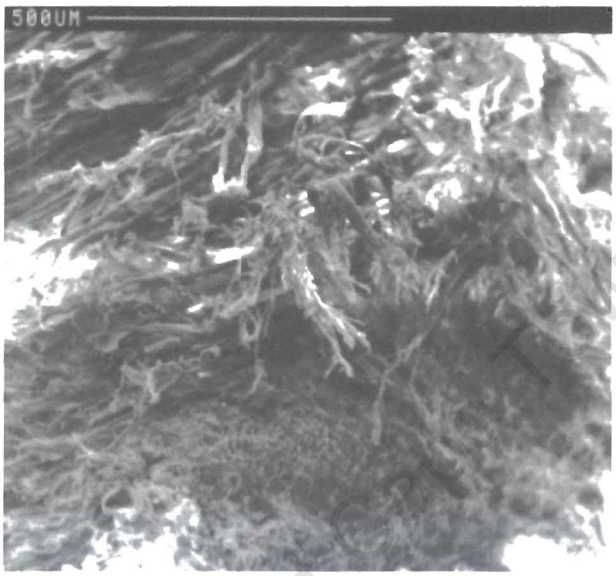

Figure 4.37 SEM micrograph of the eroded surface of woven KFRP eroded at a 60° impingement angle.

4.2.3 EROSION OF THE POLYMER COATINGS

Steady state erosion tests were performed on epoxy and polyurethane coatings. The materials used for these tests are shown in Table 4.10.

Table 4.10 Polymer coatings investigated.

Manufacturer / Supplier	Production code	Coating description
AXSON	EPO 1021	Epoxy gelcoat
AXSON	UR 3144	Urethane gelcoat
AXSON	Epolam 2022	High performance epoxy
3M	3M tape	Polyurethane tape for the protection of helicopter rotor blades
Tekochem	T1	Polyurethane coating, (with primer)
Tekochem	T2	Polyurethane coating, (without primer)

Figures 4.38 to 4.43 show the erosion rates as a function of impingement angles for all the coating materials investigated. All the coatings were applied onto CFRP specimens to investigate the erosion properties of the coatings as well as the bonding between the coating and the composite. The general trend for the polymer coatings tested is lower erosion rate at shallow impact angles, which indicates ductile behaviour[40]. The five different polymer coatings show wide variation in erosion resistance. The erosion rate is found to be the lowest at perpendicular impact angles for all the coatings, where the erosion rates are comparable to that of the titanium alloy (Ti-6Al-4V). The bonding between the fibre composite and the polymer coatings was found to be satisfactory. The erosion tests were carried out until the coating was worn through at some location on the specimens and inspection revealed there were no signs of the coating "flaking off" due to poor bonding.

From these figures it can be observed that the erosion resistance of the polyurethane coatings are superior by an order of magnitude compared to that of the epoxy and the epoxy gelcoat. The best polymer coating tested was the Tekochem, T1 followed by the 3M tape. The Tekochem T2 sample performed poor under erosion and this is believed to be due to the poor bonding between the coating and substrate. The relatively good erosion resistance of the polyurethanes is believed to be due to low cross-linking density leading to better rebound resilience.

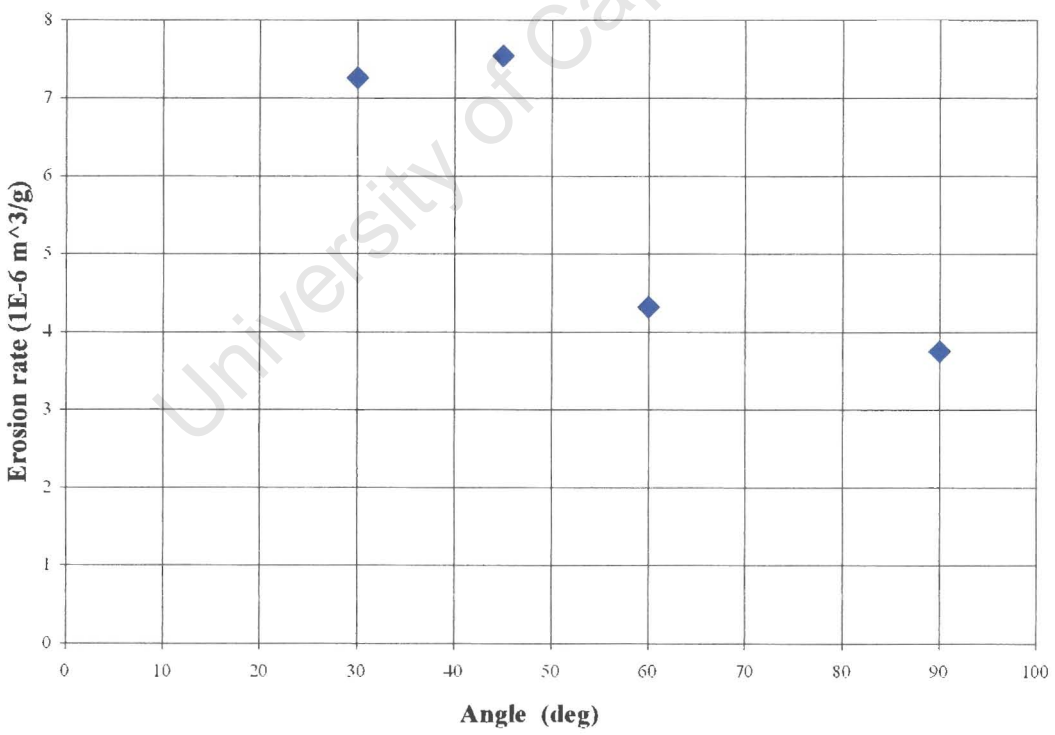

Figure 4.38 The erosion rate *vs.* angle of impingement for epoxy gelcoat.

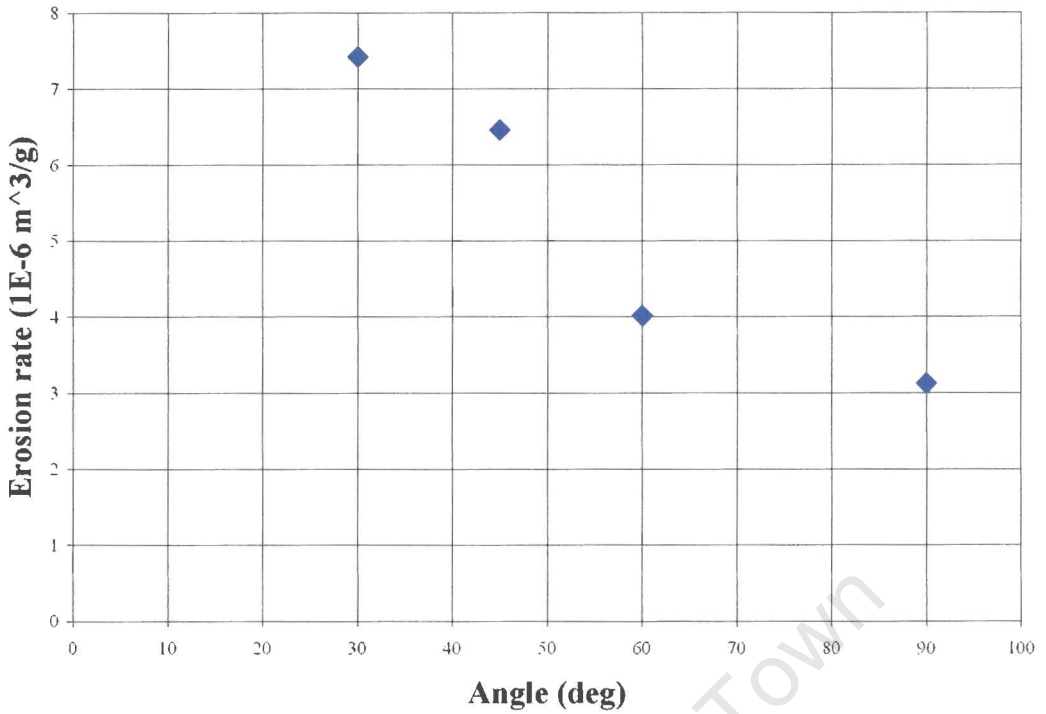

Figure 4.39 The erosion rate *vs.* angle of impingement for high performance epoxy.

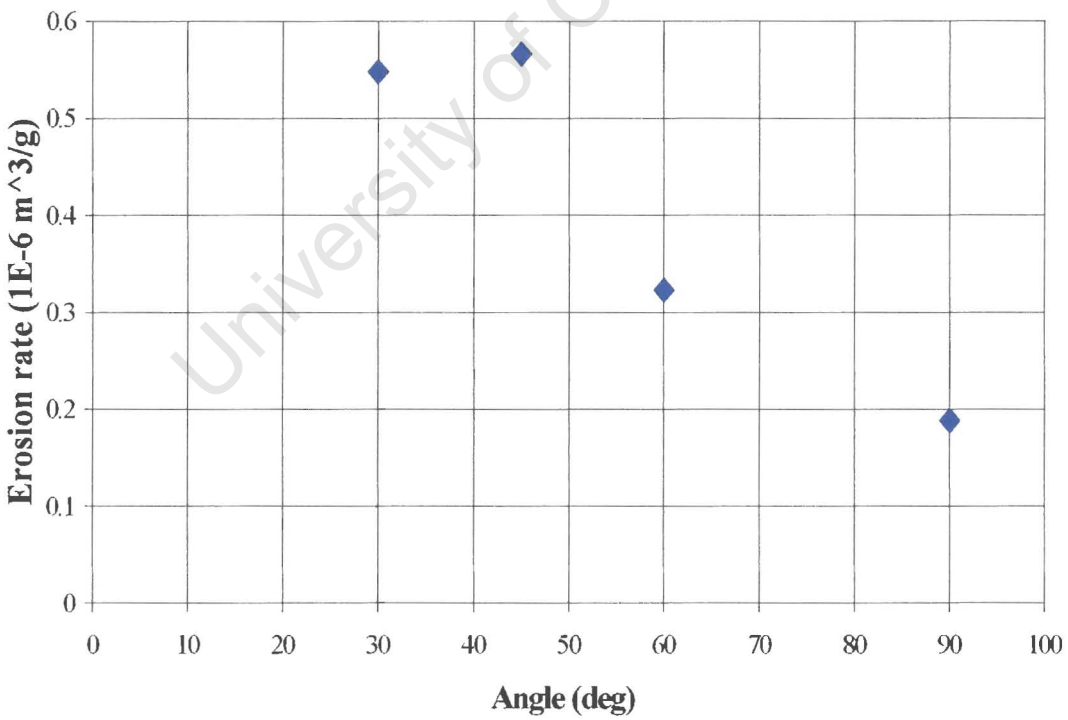

Figure 4.40 The erosion rate *vs.* angle of impingement for urethane gelcoat.

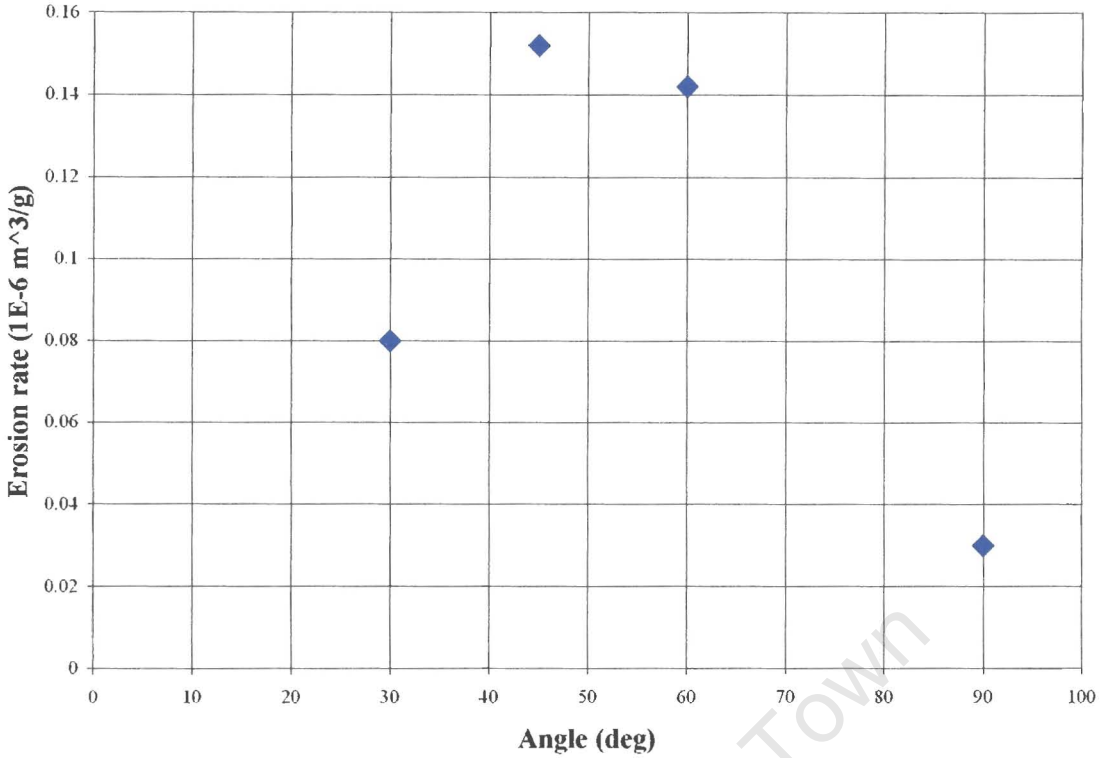

Figure 4.41 The erosion rate *vs.* angle of impingement for 3M polyurethane.

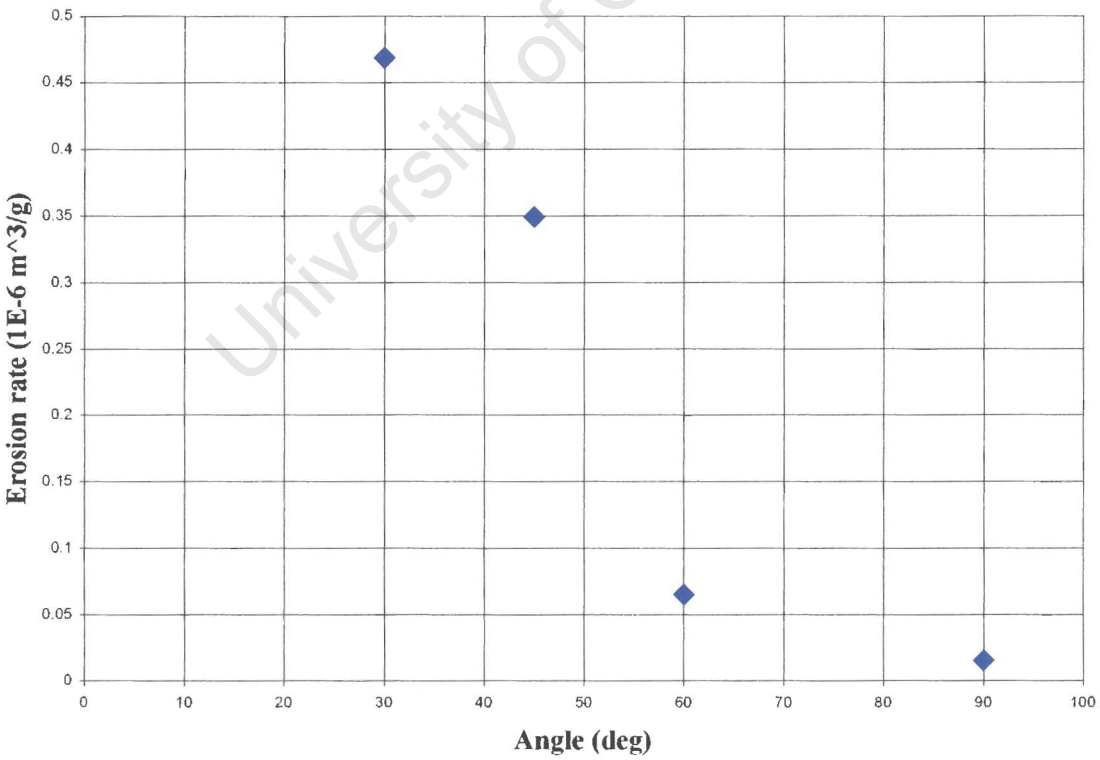

Figure 4.42 The erosion rate *vs.* angle of impingement for polyurethane T1.

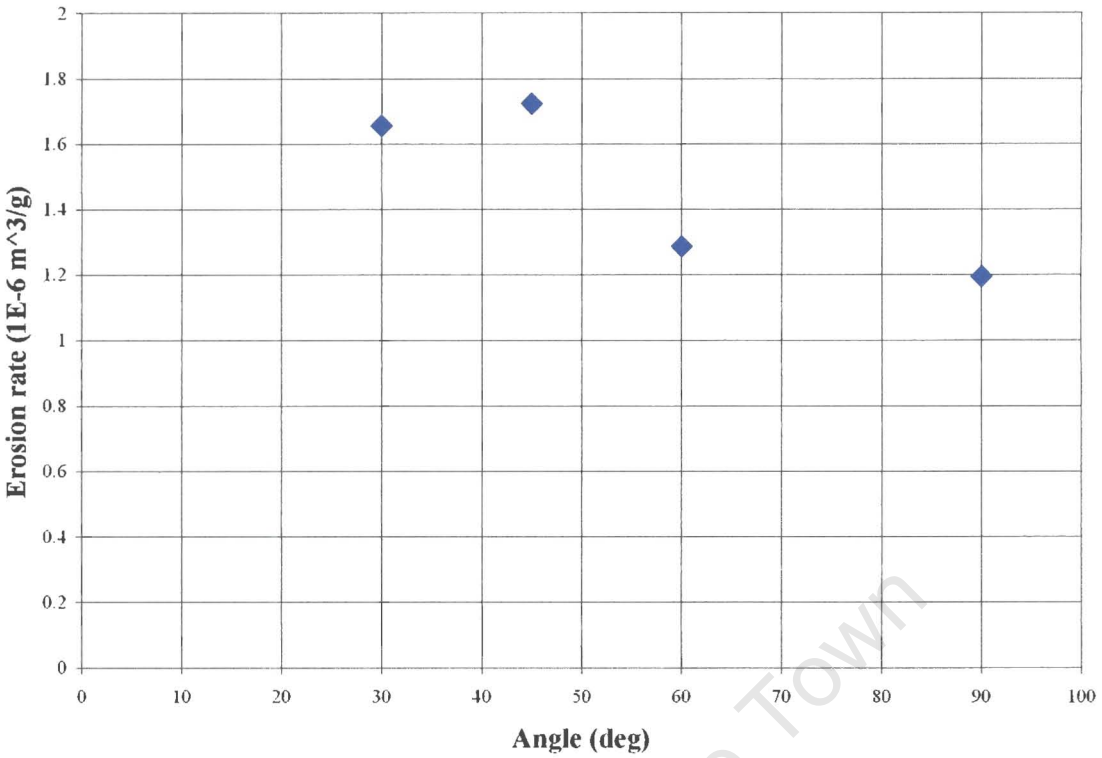

Figure 4.43 The erosion rate *vs.* angle of impingement for polyurethane T2.

The typical appearance of the eroded surfaces of the coatings are shown in Figures 4.44 to 4.46. The surface of the urethane gelcoat is relatively smooth and it appears that material is removed by a ductile ploughing mechanism by the rounded sand particles.

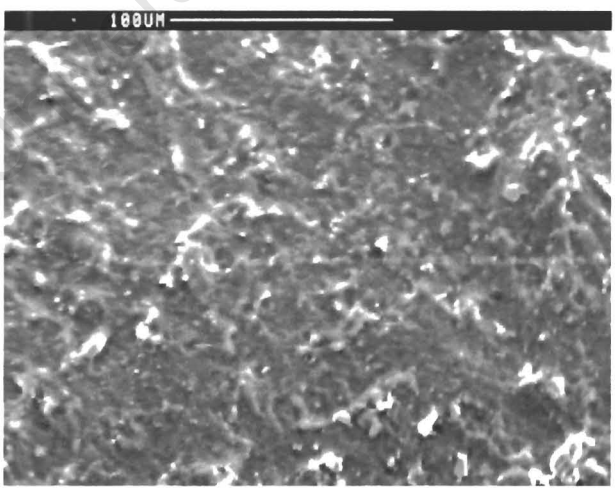

Figure 4.44 SEM micrograph of the eroded surface of the urethane gelcoat UR 3144, eroded at 30° impingement angle.

The mechanism of erosion for the 3M polyurethane tape appears to be through the initiation and intersection of fine cracks below the surface and removal of very fine flakes of material. The surface appeared smooth after erosion. The maximum erosion rate for the Tekochem T1 sample occurred at 30° impingement angles (Figure 4.42) and mode of erosion seemed to be through the detachment of small pieces of material at localised areas. For this material an incubation period of no or very low wear was observed. This initial low wear could be due to the embedment of some erodent particles which was observed in the SEM.

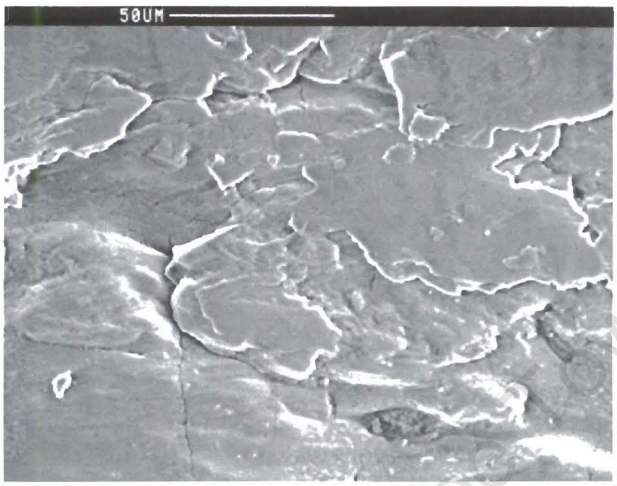

Figure 4.45 SEM micrograph of the eroded surface of the 3M polyurethane tape, eroded at 30° impingement angle.

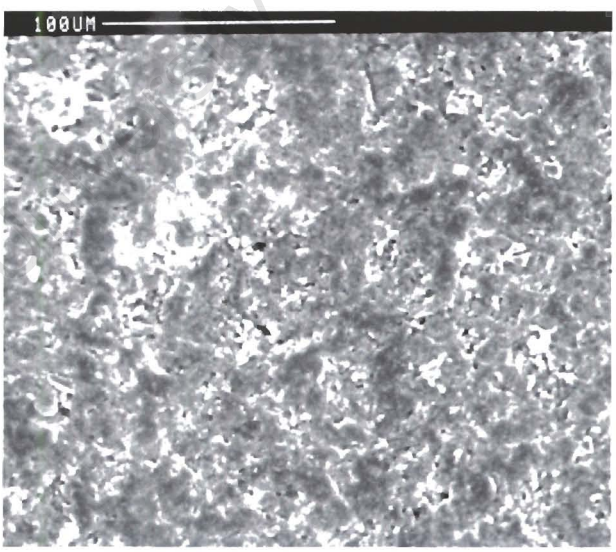

Figure 4.46 SEM micrograph of the eroded surface of the Tekochem T1 polyurethane sample, eroded at 30° impingement angle.

4.2.4 EROSION OF THE NICKEL COATING

The steady state erosion rates for nickel coated specimens are shown in Figure 4.47. The CFRP was first "activated" to allow a good bond between the composite and the metal coating. De Beers, UK, performed this process. The CFRP specimen was then electroplated with a nickel layer approximately 60 μm thick as shown in Figure 4.48. The maximum erosion angle occurs at 45° for the angles tested, which suggests a ductile mechanism of erosion[40]. The erosion rates of the nickel coating are lower than that for the titanium alloy tested (see Figure 5.6). However, the bonding between the nickel layer and the CFRP deteriorate during the erosion process. The nickel coating then de-laminates from the substrate. This observation suggests that the coating is not well suited for the application of protection a compressor blade against severe erosion, unless a thicker coating can be applied and the adhesion improved.

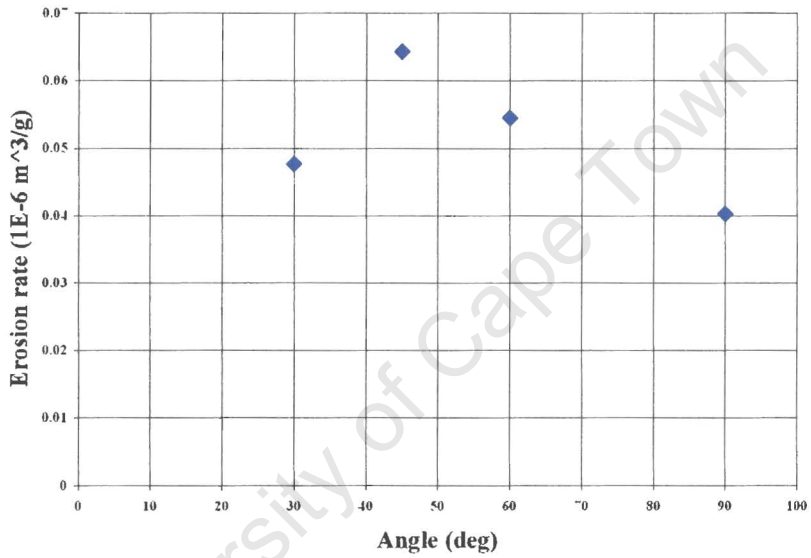

Figure 4.47 The erosion rate *vs.* angle of impingement for the nickel coating.

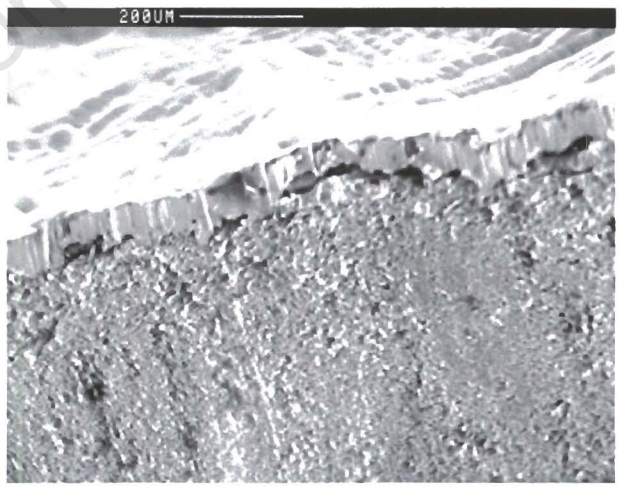

Figure 4.48 SEM micrograph showing the Ni coating bonded on the CFRP surface.

4.3 FLEXURAL BENDING TEST RESULTS

Three point bending tests were carried on three different laminate materials, *viz.* carbon, Kevlar® and carbon/Kevlar® hybrid, as specified in section 3.2.1. The stresses *vs.* deflection curves are shown for these composites in Figures 4.49 to 4.51. For each of these composite materials, four bending tests were performed to ensure accuracy and the averages of the strength values are tabulated in Table 4.11.

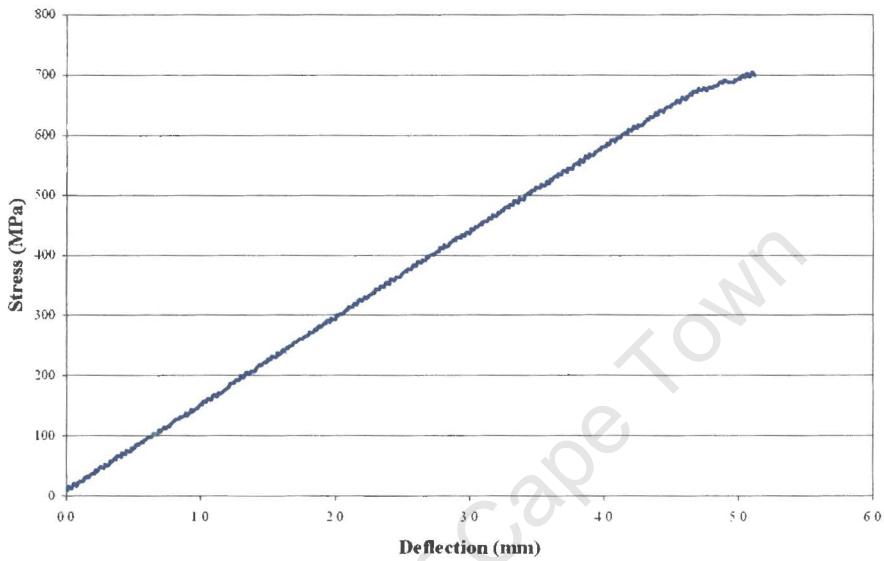

Figure 4.49 Stress *vs.* deflection in bending for CFRP.

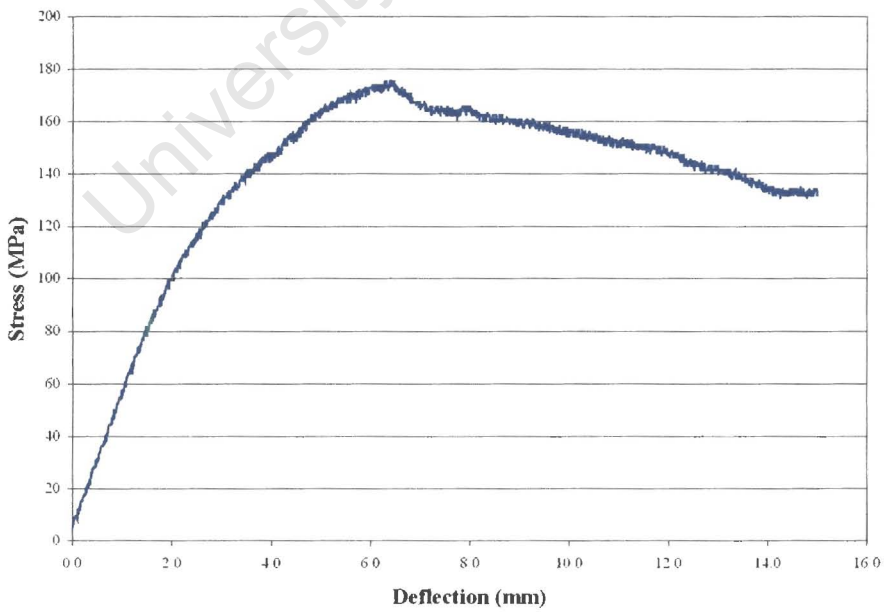

Figure 4.50 Stress *vs.* deflection in bending for KFRP.

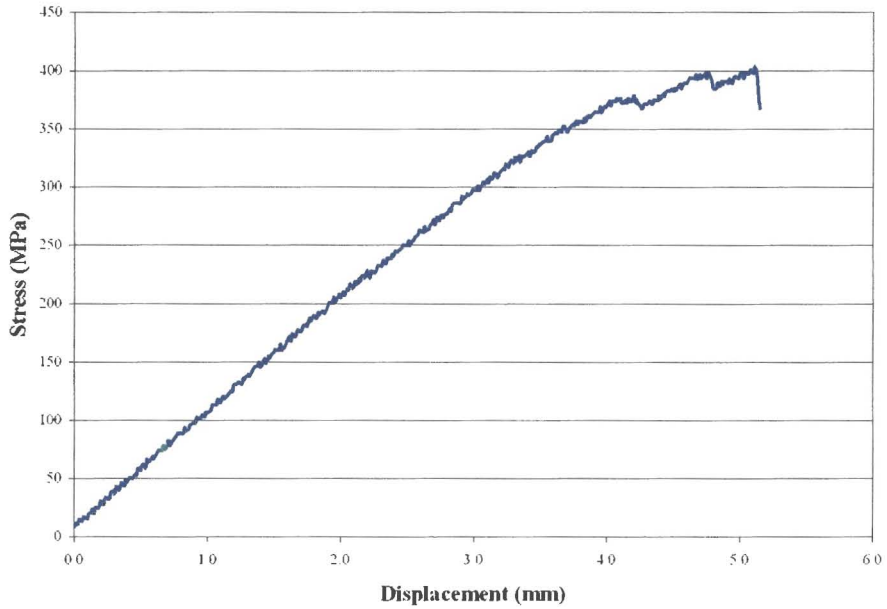

Figure 4.51 Stress *vs.* deflection in bending for the carbon / Kevlar® hybrid.

The CFRP laminate is far superior in bending strength to that of the KFRP laminate. The hybrid laminates have bending strength values that lies approximately half of the sum of the CFRP and KFRP bending strength values. This conforms well to the rule of mixtures for composite materials. The KFRP laminate shows a ductile behaviour whilst the CFRP failed at a low strain indicating a brittle behaviour. The bending moduli are obtained from the equation 3.2 in section 3.3 and are shown in Table 4.11.

Table 4.11 Bending properties of the tested laminates.

Fibre composite	Bending strength (MPa)	Bending modulus (GPa)
CFRP	707	50.4
KFRP	191	14.5
Carbon/Kevlar® hybrid	394	33.5

4.4 IMPACT TEST RESULTS

The results of the low velocity impact tests are presented in Figures 4.52 to 4.55 showing graphs of force *vs.* deflection and energy *vs.* deflection. These graphs are selected to illustrate the damage caused by the impact event at different velocities and to determine the impact properties of the laminates tested. Figures 4.52 and 4.54 compares the impact behaviour of the CFRP at different impact energies whilst Figures 4.53 and 4.55 compares the impact behaviour of different composites at the same impact energy. Only selected data is presented below, and the data for all other impact tests can be found in Appendix E.

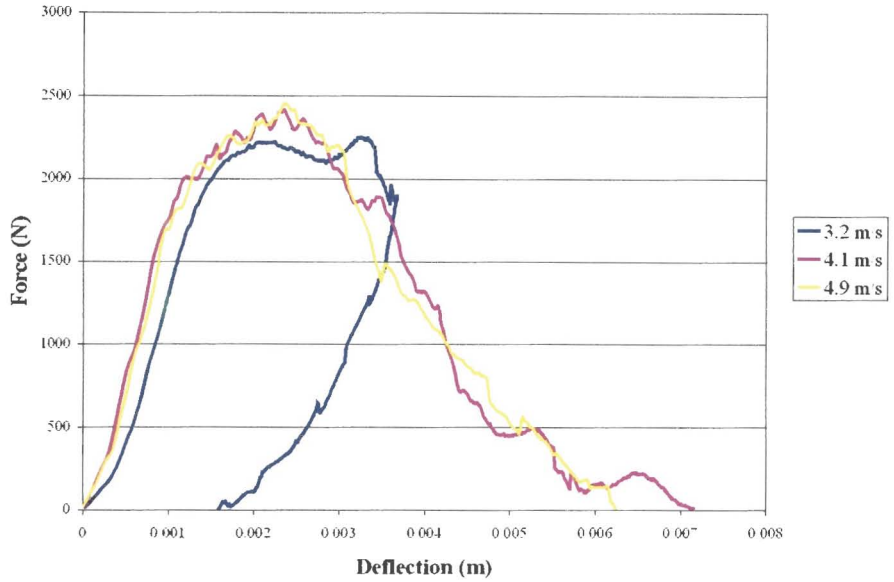

Figure 4.52 Force *vs.* deflection curves for the CFRP laminate at different impact velocities.

In Figure 4.52 it can be seen that at the impact velocity of 4.1 and 4.9 m/s the impacter penetrates the laminate. The deflection curve shows that for 3.2 m/s the curve reverts back.

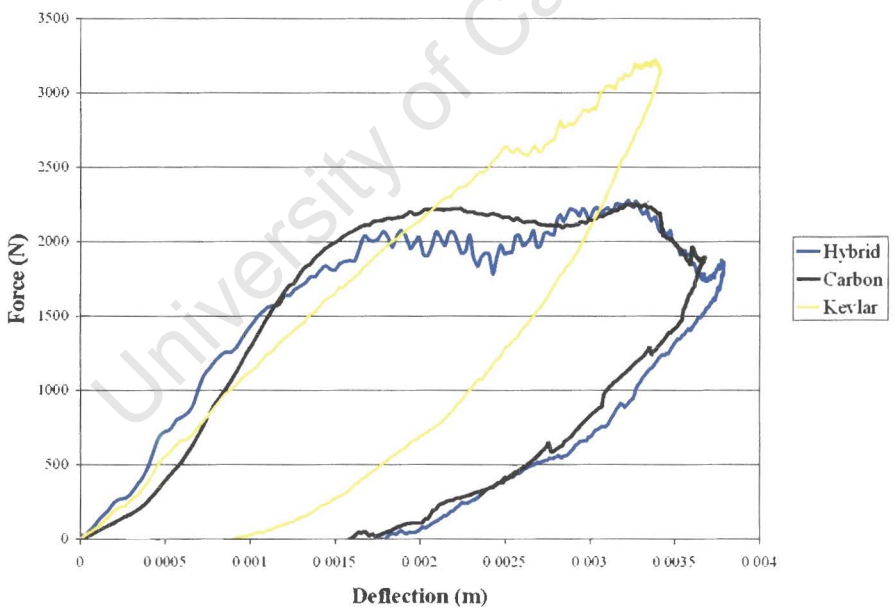

Figure 4.53 Force *vs.* deflection curves for carbon, Kevlar® and carbon/Kevlar® hybrid at 3.29 m/s impact velocity.

The graphs in Figure 4.53 show the impact events for a laminate of CFRP, KFRP and a hybrid of these. From these graphs, it is evident that the CFRP laminate is stiffer than the KFRP laminate. The relative stiffness of the carbon, Kevlar® and hybrid laminates can be determined from the slopes of the different graphs and are tabulated in Table 4.12.

It must be realised that these values can only be used for comparative assessment because the second moment of area of each specimen is different. The stiffness values in Table 4.12 are not modulus values since they are obtained from the gradient of force *vs.* displacement graphs. The CFRP laminate indicated severed impact damage and delamination compared to the KFRP laminate, which show a more ductile failure as indicated in Figures 4.54 and 4.55, respectively. The KFRP fractogram in Figure 4.53 shows that more energy is absorbed until a force of approximately 3.3 kN is reached. A microscopic examination suggest that the micro buckling fibre breaking mechanism in the KFRP laminate accounts for the increased amount of energy absorbed. The hybrid shows a behaviour in between that of the CFRP and the KFRP. This was also evident from the surface damage examination by photomacrography in Figure 4.56.

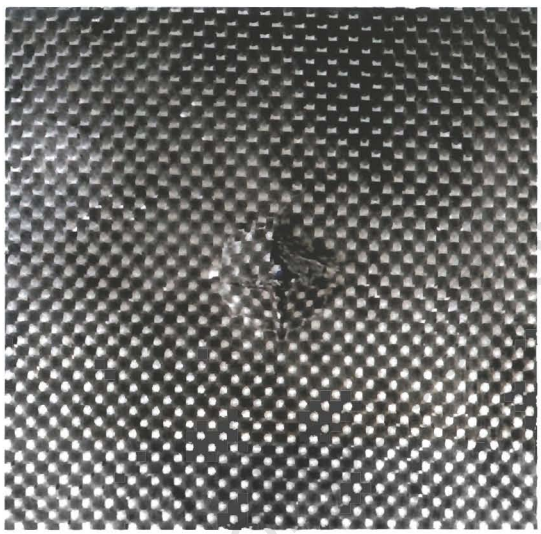

Figure 4.54 Severe surface damage on the bottom surface of the CFRP impacted specimen at approximately 6 J.

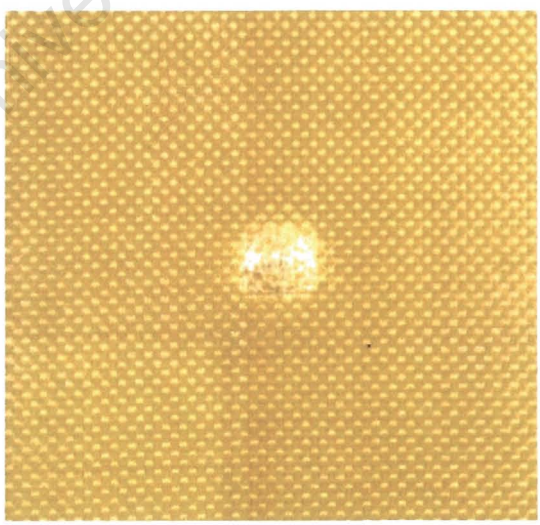

Figure 4.55 Ductile surface damage on the bottom surface of the KFRP impacted specimen at approximately 6 J.

Figure 4.56 Mixed ductile /brittle surface damage on the bottom surface of the carbon / Kevlar® hybrid impacted specimen at approximately 6 J.

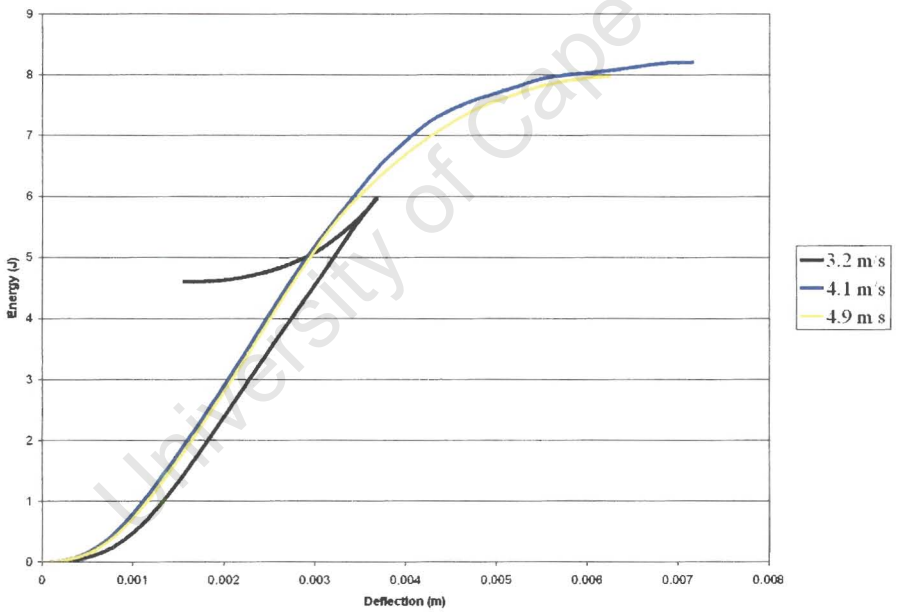

Figure 4.57 Energy *vs.* deflection curves for carbon laminate at different impact velocities.

The energy deflection curve for CFRP in Figure 4.57 shows that some of the elastic energy is returned to the impacter for the 3.2 m/s impact velocity. It is also evident that beyond approximately 8 J the carbon laminate cannot absorb more impact energy.

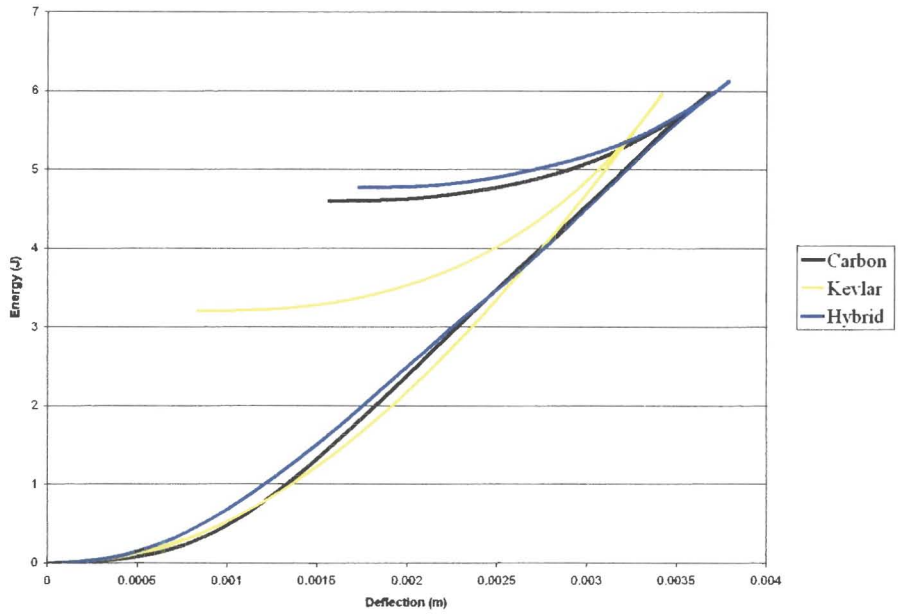

Figure 4.58 Energy *vs.* deflection curves for carbon, Kevlar® and carbon/Kevlar® hybrid laminates at an impact velocity of 3.3 m/s.

From the Figure 4.58 it is evident that the KFRP specimen can absorb more elastic energy which is returned to the impacter. The CFRP and the hybrid display similar impact behaviour. The information from the impact data for the laminates is summarised in Table 4.12. From the impact information given in Table 4.12 it is clear that the KFRP has a superior impact absorbing capability compared to that of the CFRP.

Table 4.12 Impact properties of the laminates investigated.

Fibre	Ultimate impact energy (J)	Rate of energy absorption (J/m)	Ultimate impact force (N)	"Stiffness" (10^4 N/m)
Carbon	8.21	2214	2371	209
Kevlar®	17.37	3296	3386	111
Hybrid Carbon/Kevlar®	10.34	2159	2404	146

4.5 FINITE ELEMENT IMPACT RESULTS

The low velocity impact was modelled using a quarter model with the same dimensions as the impact specimens tested in section 4.4. The boundary conditions was modelled according to the testing performed. The impacter was modelled as a hemispherical rigid surface with the same dimensions used in the experimental testing. A velocity of 3.0 m/s was used to model the plate impact event. The material used in the model was a carbon fibre in the cross-ply configuration. The FE code used was ABAQUS and the plate was

modelled using continuum 8 noded brick elements. The mesh generated can be seen in Figures 4.59 and 4.60.

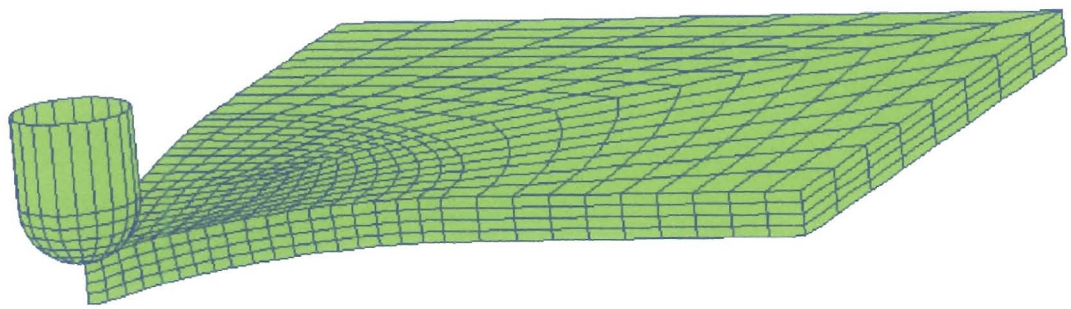

Figure 4.59 The quarter model FE mesh of a carbon/epoxy plate with the impacter.

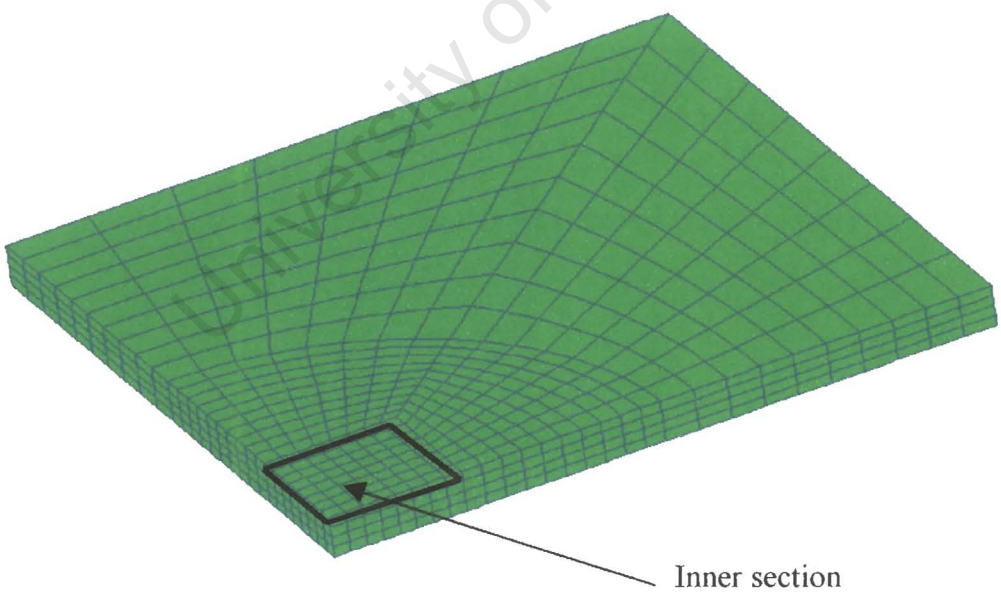

Figure 4.60 The quarter model FE mesh of the carbon/epoxy plate.

The highest stresses occur close to the vicinity of the impacter. The following stress plots have been taken from the '*inner section*' of the plate shown in Figure 4.60. Figure 4.61 shows localised intra-laminar compressive stresses at the point of impact and tensile stresses on the bottom side of the plate. The inter-laminar stress plot in Figure 4.62 shows high localised compressive stresses at the top surface which will cause localised damage on the plate.

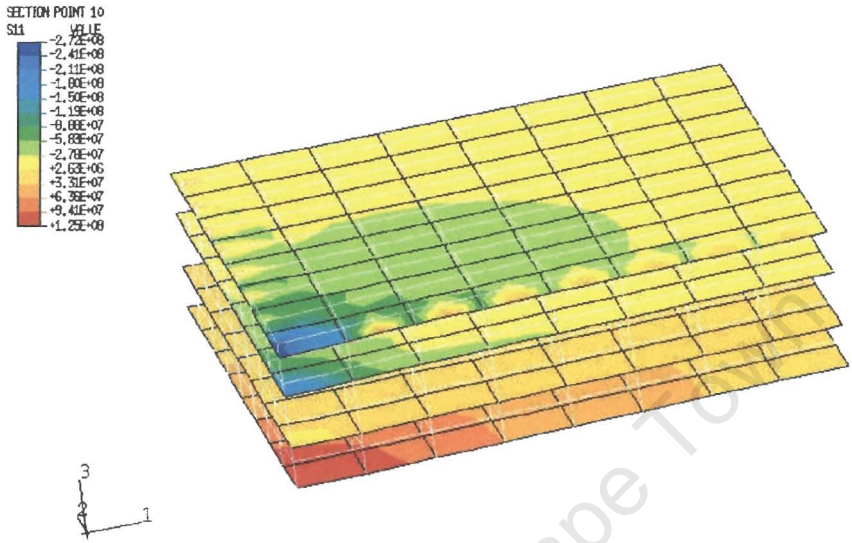

Figure 4.61 Intra-laminar stresses along the fibre direction.

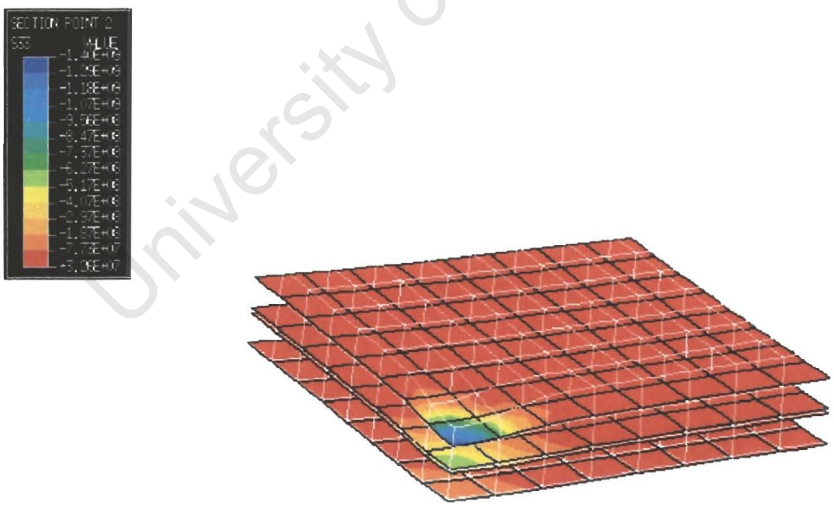

Figure 4.62 Inter-laminar stresses through the plate.

CHAPTER 5

DISCUSSION

The carbon fibre reinforced polymer (CFRP) composite compressor blade that could potentially replace the currently used titanium alloy Ti-6Al-4V blade, operates in a complex environment and hence both the properties of the blade itself and the operating conditions had to be considered. The following discussion systematically describes the most important factors that were considered. In some cases it was deemed necessary to make certain assumptions although simplifications were not found to have a significant impact on the overall conclusions reached.

5.1 FINITE ELEMENT ANALYSIS

5.1.1 THE FE MODELS

The FE model used for modelling the behaviour of the compressor blades utilises solid brick elements. The use of continuum tetrahedral elements for composite structures is not supported. In addition, the base of the compressor blade is relatively thick which makes plate or shell elements less suitable to accurately model the blade. Assumptions have been made in the boundary conditions, regarding the drag and pressure load for the blade. These loads, however, do not make a significant contribution in comparison to the large centrifugal load and is therefore a minor source of error. An additional simplification that has been made is a compromise in the geometry of the model compared to the actual blade. The fillet at the root of the blade has been slightly reduced which will yield some discrepancies. Three FE models are studied with respect to deflections, stresses and vibrations. These three models are:

- the currently used titanium blade,
- a composite blade *lay-up 1*, where 70 % of the fibres are in the radial direction and the remaining 30 % of the fibres are in a +/- 45° direction to the radial direction, and
- a composite blade *lay-up 2*, which has a cross-ply configuration $(0°/90°)_s$.

5.1.2 DEFLECTIONS OF THE TITANIUM COMPRESSOR BLADE

The significant deflection that occurs for the compressor blade during operation of the turbine is the untwisting of the blade, resulting from the centrifugal load and the geometry of the compressor blade. In addition, there is also a bending behaviour associated with the high centrifugal load. The greatest deflection occurs towards the top of the leading edge. The elongation due to the centrifugal load in the radial direction was found to be considerably less.

5.1.3 DEFLECTIONS OF THE COMPOSITE COMPRESSOR BLADES

The composite material models investigated show different behaviour due to the difference in lay-up configuration. Lay-up 1 (see section 4.1) which has fibres in the +/- 45° direction, displaces the least of the FE models. A comparison of the deflections the titanium blade and the composite blade (lay-up 1) in the 2 direction is shown in Figure 5.1.

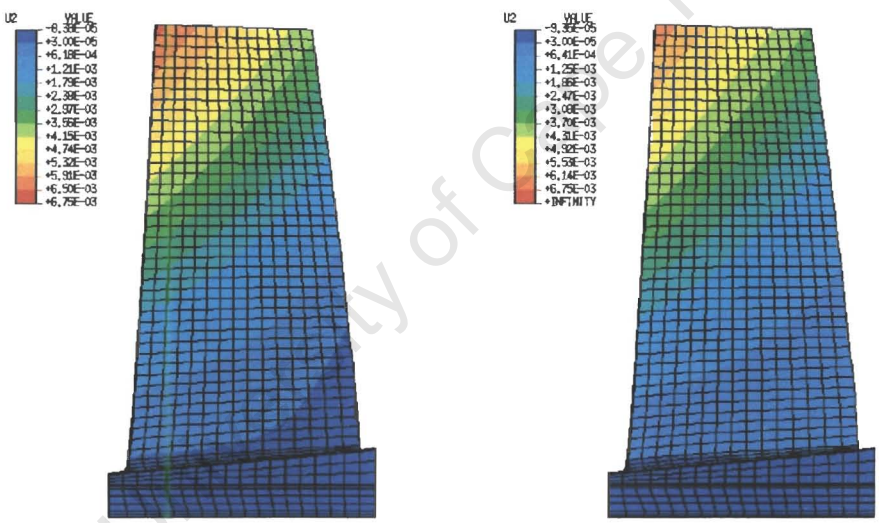

Figure 5.1 FEA comparison of deflections in the 2 direction (into the page) for the titanium alloy left, and CFRP composite (lay-up 2) to the right. Note: The two displacement plots are plotted on the same scale. The 'infinity legend' belonging to the composite blade in Figure 5.1 means that no deflections reach this value.

The FE results suggest that the +/- 45° direction plies give the blade a higher torsional rigidity, resulting in less untwisting of the blade during the operation of the turbine. It is also noted that the lack of +/- 45° plies in lay-up 2 results in larger deflections, which again can be explained by a lower torsional rigidity compared with that of lay-up 1. Furthermore, it is found that the displacement in the radial direction of the composite

with lay-up 1 is less than that of the composite with lay-up 2. The smaller deflection in this direction can be explained by to the higher concentration of fibres in the radial direction of lay-up 1.

It is found that by using a fibre composite material it is possible to control the untwisting behaviour by using different materials and different fibre orientations. At the moment the turbine unit has to run at a specific speed for optimum performance. Any deviation from this optimum speed results in a considerable reduction of efficiency. It would be an advantage if the compressor blades could twist according to the aerodynamic load required. The turbine could in that case run efficiently over a wider operating range, which cannot be achieved using isotropic titanium blades. It is suggested that by optimising the fibre lay-up in the compressor blade, it could be possible to tailor the aerodynamic performance of the blade at different speeds.

5.1.4 STRESSES IN THE TITANIUM BLADE

The material used in the current compressor blades is the titanium alloy Ti-6Al-4V. The material specification for the titanium alloy used in the gas turbine states that the 0.2 % *proof stress* and the *tensile strength* must not be less than 862 MPa and 931 MPa, respectively (see Table 4.1). Proof stress is often quoted instead of yield stress for characterising materials that show continuous yielding and not a distinct yield point[82]. To compare the proof stress value stated in the material specification to the induced stresses in the blade during operation, a von Mises stress plot is created. The von Mises criterion is probably the most accurate way to predict failure in the titanium alloy. The von Mises elastic failure theory is widely regarded as the most reliable basis for design, particularly when dealing with ductile materials[38]. The highest von Mises 'stresses' occurring in the titanium blade in the FE prediction is approximately 795 MPa. This value is very close the proof stress of 862 MPa stated in the material specification. The calculated factor of safety is thus approximately 1.08. The highest stresses in the blade occur in the area of the leading edge in the blade root. To compare the tensile strength specified for the material, it is more appropriate to compare maximum principal stresses. The FE model shows that the maximum principal stress is found to be 783 MPa. By comparing the corresponding tensile strength to this value, the factor of safety is found to be approximately 1.19. The above calculated safety factors suggest that the titanium compressor blades currently used are close to their design limit criteria.

5.1.5 STRESSES IN THE COMPOSITE BLADE

The FE analysis the fibre composite (CFRP) blade is considerably more complex. The composite blade consists of a multi-layered structure and each layer needs to be examined in order to ensure structural reliability. The approach in this section is to use the maximum stress failure theory. The use of Tsai-Hill and Tsai-Wu failure theories

would perhaps have been more appropriate to use but these theories are unfortunately not supported for layered continuum (solid) elements in ABAQUS*. Thus, the approach in this section is to consider the intra-laminar stresses normal *(longitudinal and transverse)* to the fibre direction and the shear stresses acting on a lamina. These stresses can then be compared to the corresponding strengths of the fibre composite material to predict whether failure will occur.

The results show that the most critical stresses are found in the root section of the leading edge of the blade, in the outer plies on the pressure side. These results were shown in all Figures in section 4.1.6. The stresses experienced on the suction side of the compressor blade are less critical (see Appendix C). The stresses on plies that are located closer to the centre of the blade profile experience relatively low stresses (see Table 4.3 and Appendix C). For example, the highest stress along the fibres in the 7^{th} ply is approximately 288 MPa. The maximum tensile stress along the fibre direction that is found in the blade at any point is approximately 400 MPa in magnitude. The corresponding longitudinal strength of the lamina (see Table 4.2) is stated to be 1300 MPa. This indicates that the maximum longitudinal stress to the fibres in the blade is approximately 30 % of the corresponding strength.

Chamis and Lynch reported similar results in their investigation of high-speed composite compressor blades[15]. The transverse tensile stresses in the outermost ply indicate stress values exceeding the corresponding strength. It is noted that there exists a stress concentration in the root of the blade where the FE model predicts failure (see Figure 4.17). The geometry of the 'real' blade used in the compressor has a smoother transition at this section. This is not obtained in the CAD/FE model, which accounts for the stress raising effect. The simplification that was made in the root section was necessary to avoid distorted elements. However, to ensure structural reliability of the composite compressor blades it is suggested that care must be taken so that the geometry of the blade in this area does not give rise to stress concentration effects. Figure 5.2 shows the incorporation of a fillet in the base section that reduces the stresses found here.

Apart from this stress concentration, FE stress values do not exceed the corresponding transverse strength. The FE stress values are close to 20 MPa, which is approximately 50 % of the transverse tensile strength of the lamina. The transverse compressive stresses are relatively low and, since the compressive strength in the transverse direction is considerable higher than the transverse tensile strength, it is suggested that this aspect is not critical. The shear stress calculated indicate a maximum value of 47 MPa, which is approximately 76 % of the corresponding shear strength of the lamina. This maximum value is also found at the stress concentration at the base section of the blade, which is considerably higher than for any other location in the blade.

When the second outermost layer is investigated the stresses are reduced for all the considered stress parameters. The stress concentration at the base section of the blade still predicts failure for the tensile stresses in the transverse direction to the fibre but the stress level is reduced compared to the first ply investigated. It was also decided to

* See ABAQUS v5.8 manuals.

investigate the possibility of using a cross-ply configuration of fibre lay-up in the compressor blade. The motivation being that the impact resistance would be greater if a woven cloth was used. The results for this model show that the maximum stress along the fibre direction increase by approximately 40 % in magnitude but is still about 44 % that of the corresponding strength for the lamina. The reason for the higher stresses along the fibre direction in the cross ply (lay-up 2) is the reduced amount of fibres in the radial direction, which carry the majority of the centrifugal load.

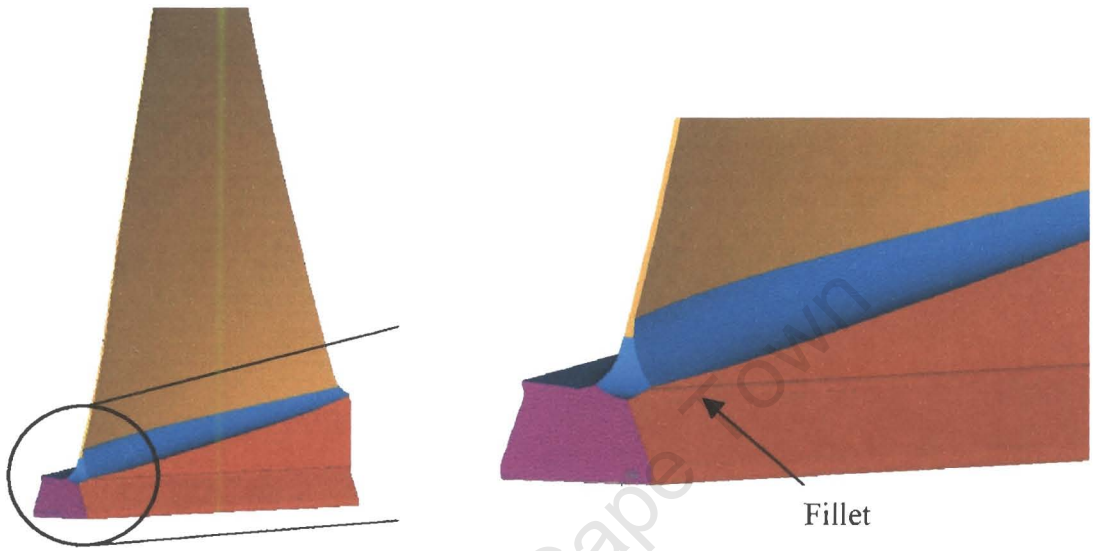

Figure 5.2 Stress concentrations in the compressor blade can be reduced by incorporating a fillet.

The transverse tensile stresses occurring in the outer plies in this lay-up is close to failure at the stress concentration point in the blade root section. Apart from the stress raising effect at this particular section, relatively low stresses are encountered with respect to the corresponding strength. The maximum shear stresses in the blade are found to be approximately 70 % of the corresponding composite strength. The cross-ply (lay-up 2) configuration is modelled using unidirectional fabric data. The material properties of a woven cloth will be slightly worse than that of a unidirectional cloth with the same configuration due to the lower efficiency of the cloth. Since the FE stress values encountered are relatively low in comparison to the corresponding strength, it is suggested that a woven cloth could sustain the induced loading in the blade.

This study has not considered inter-laminar properties for the composite blade FE models. The inter-laminar material properties are not available for the fibre composite materials used in this study. However, the inter-laminar strain occurring in the CFRP blade, lay-up 1 for the outermost ply indicates a maximum strain of approximately 0.0086 which occur at the base section of the CFRP blade (see Appendix G).

5.1.6 VIBRATION ANALYSIS

The harmonic excitations were supplied by ABB STAL and compared to the blade model frequencies to ensure that no excitation occurs during the design speed of the turbine. A comparison is made between ABB STAL's calculations for the titanium blade frequencies for the first two vibrational modes at 10 000 rpm and calculations done in this study. These values are compared in Table 5.1 for verification purposes and it can be seen that the results are found to be in good agreement.

Table 5.1 Verification for the first two titanium blade frequency modes at the design speed 10 000 rpm.

Mode	ABB STAL (Hz)	FE (this study) (Hz)	Correlation (%)
1	369.9	340	98
2	902.8	896	99

The fundamental blade frequencies and mode shapes (see Appendix D) are calculated for the titanium blade and the two composite blades. It is observed that the composite blades experience higher frequencies than that of titanium except for one vibrational mode where the CFRP blade with the cross ply lay up has a lower blade frequency than the titanium blade as shown in Figure 5.3. The composite blade with 70 % of the fibres in the radial direction (lay-up 1) is found to have the highest blade frequencies for all the vibrational modes. This is due to the lower density of the carbon fibre composite compared to the titanium alloy, in combination with the high stiffness of the carbon fibres. An examination of the blade mode shapes (see Appendix D) suggests that the first two modes are predominantly bending and torsion, respectively. The remaining motions are however complex and hard to characterise but it is apparent that the blades undergo large deflections in all the vibrational modes.

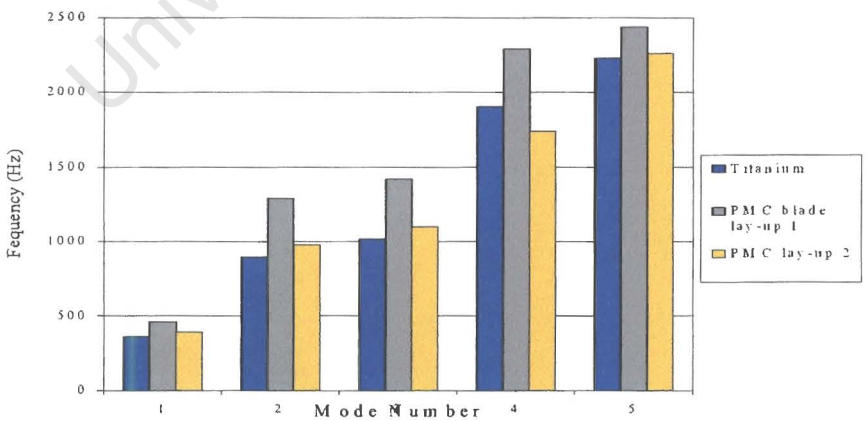

Figure 5.3 Fundamental blade frequencies at 10 000 rpm for titanium and composite blades.

5.2 EROSION

5.2.1 THE EROSION CONDITIONS

To simulate the erosive environment the compressor blades might experience it was decided to use silica sand as the erodent material. Silica sand is readily available and is likely to be more aggressive than the erosive operating environment found when the gas turbine is operating.

5.2.2 THE EROSION OF THE TITANIUM ALLOY, TI-6AL-4V

The erosion performance of the titanium alloy used in the compressor blade show a ductile behaviour[40]. The erosion resistance of the titanium alloy is relatively high compared to most of the materials investigated in this study. The aim was to find a coating that had a comparable resistance to that of the titanium alloy.

5.2.3 THE EROSION OF FIBRE REINFORCED COMPOSITE MATERIALS

The composite materials investigated are carbon- and Kevlar® fibres in an epoxy matrix. The CFRP tested was a plain cross-ply weave and a unidirectional configuration. The unidirectional CFRP was studied with the erodent particles impinging the target perpendicular to the fibre direction. This will simulate the most likely erosive situation in the compressor blade. The erosion results for the CFRP indicates a dominating brittle behaviour with maximum erosion rate at high impact angles. The matrix is removed first, exposing the graphite fibres which are then easily fractured and removed. The brittle nature of the fibres dominates the erosion mechanism for CFRP. Similar results were reported by Mathias *et al.*[45] The erosion rate was found to be constant throughout the tests. Scanning electron microscopy (SEM) performed on the eroded carbon fibre composite specimens show that the fibres break in a brittle manner. In the case of the plain weave carbon fibre it is noted that the damaged area forms ridges and valleys due to the nature of the woven carbon fibre plies. It is found that where more matrix rich areas are encountered, the damage to the fibres is less severe.

The erosion results of the KFRP indicate a different mechanism of material removal. The erosion rate *vs.* angle for the KFRP show a more ductile behaviour compared to the CFRP. The maximum erosion rate for the KFRP occurs at a lower angle and the erosion resistance is greater than that for the carbon fibre composites. The same observations were made by Pool *et al.*[44] The SEM inspection of the eroded Kevlar specimen reveal, that the fibres break in a ductile manner with the fibres undergoing large deformations

before failure, hence absorbing more energy during particle impingement. A comparison of the erosion rate *vs.* impingement angle for the fibre composites tested are shown in Figure 5.4.

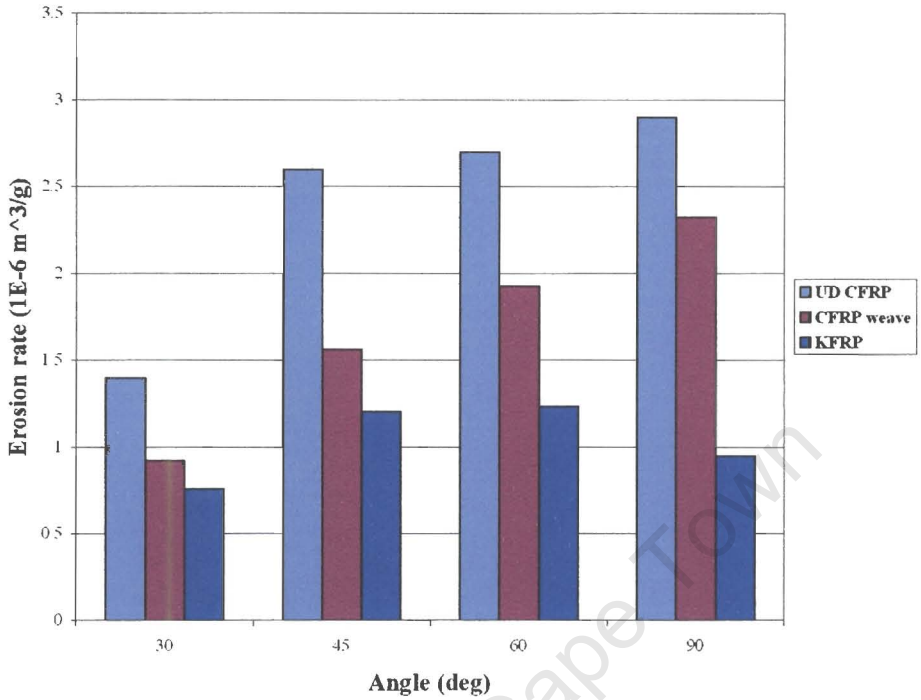

Figure 5.4 Erosion rate *vs.* impingement angle comparison for CFRP and KFRP composites.

From Figure 5.4 it is clear that the Kevlar® fibre reinforced composite exhibit the lowest erosion rate compared to the carbon fibre reinforced composites. The lower erosion rate of the woven carbon composite compared to the unidirectional CFRP is suggested to originate from the enhanced bonding interaction in the woven cloth. Zahavi *et al.* also reported that better adhesion between the matrix and fibres lead to lower erosion rates[46]. It is noted that all of the investigated fibre composites have erosion rates of an order of magnitude higher than that of the titanium alloy.

5.2.4 THE EROSION OF POLYMER COATINGS

Epoxy and polyurethane coatings were considered in an attempt to protect the fibre reinforced composite that would be used in the compressor blade. The aim is to find a coating that has sufficient erosion resistance to protect the blade from general dust and sand particles that might enter the compressor during operation. The erosion for the various polymeric coatings are summarised in Figure 5.5. The performances of the selected coatings show a wide variation in erosion performance. Differences of several

orders of magnitude for some angles are noted for the coatings. The comparison also shows that all the coatings have generally higher erosion rates for shallow angles of impact than that for perpendicular impact angles, which indicates a ductile erosion behaviour. This was verified by examining the damage modes of the eroded specimens in the SEM. The mechanisms of erosion observed for the polyurethane coatings show ductile ploughing at low angles while at higher angles the formation of fragments that are gradually removed from the surface. The high erosion resistance of some of the polyurethane coatings at high angles can be explained in terms of the high rebound resilience of these elastomers.

The softer coatings *viz.* the 3M polyurethane tape and the Tekochem polyurethane T1 sample showed the highest erosion resistance as shown in Figure 5.5. Li and Hutchings reported that the higher erosion resistance of softer materials can be accounted for by visco-elastic effects[50]. It is also suggested that when a hard particle strikes the surface the strains developed are insufficient to cause damage and erosion results from local accumulation of strain by many impacts. Micro-cracks were observed in the 3M polyurethane coating which eventually intersect and lead to fragments of material being removed. The erosion rates at 90° are lower for some of the coatings compared to that of the titanium. The bonding between the fibre composite and the polymeric coatings tested show no signs of delamination.

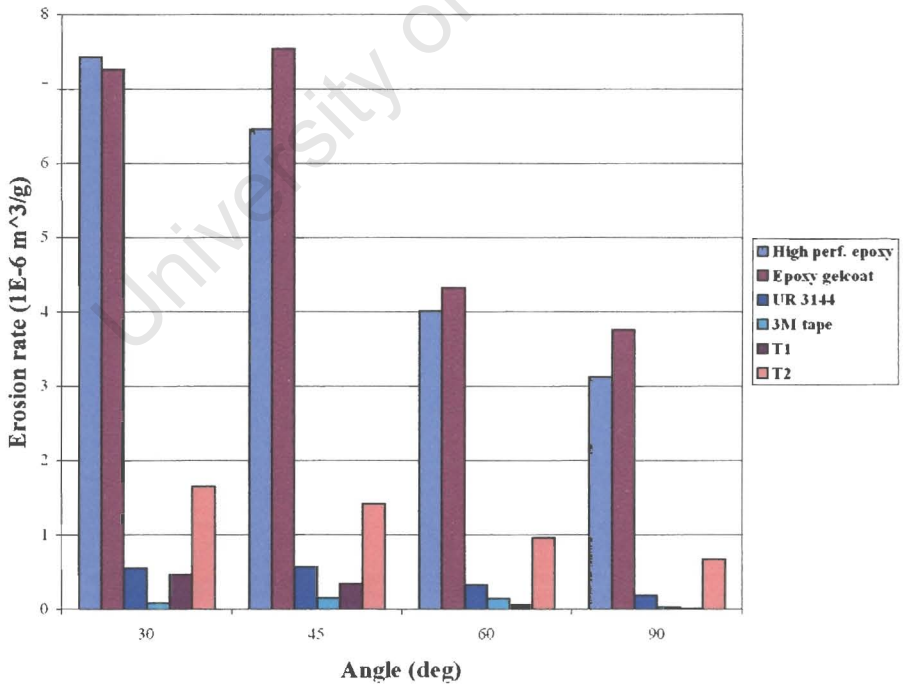

Figure 5.5 Erosion rate *vs.* impingement angle comparison for polymeric coatings.

5.2.5 THE EROSION OF A NICKEL COATING

A nickel coating of about 70 μm (confirmed by EDS) was applied to a CFRP laminate and subjected to erosion. The nickel coating has a higher erosion *resistance* for all the angles tested compared to that of the titanium as shown in Figure 5.6. The SEM study of the coating shows ductile behaviour with the formation of micro-cracks and the gradual removal of material. It is furthermore observed that the bonding between the CFRP and the coating is problematic. The high centrifugal forces that are present are likely to cause the nickel coating to detach from the composite after a moderate amount of erosion exposure.

5.2.6 EROSION COMPARISONS

The most promising coatings are compared to the titanium alloy in Figure 5.6. The nickel coating has the highest erosion resistance but for reasons discussed earlier it is not well suited for the compressor blade application. The 3M polyurethane tape might also suffer from de-lamination when exposed to high rotational speeds for a prolonged amount of time. This tape is usually replaced on helicopter blades after a month interval when rain and dusty environments are present. The most promising coating tested when all the factors are considered is the soft elastomeric Tekochem polyurethane T1 coating. It is easy to apply on the fibre composite and the polyurethane coating can be sprayed on or applied in the moulding process of the CFRP blade. The advantage of re-applying the coating easily in the event of it being eroded, is also an important factor to consider and this gives the polyurethane coating an advantage compared to a metal coating.

The erosion rates of the polyurethane coatings tested have better erosion rates than that of the titanium alloy for the higher impact angles. However, at shallow impact angles the titanium alloy has a considerably better erosion resistance. The leading edge of the compressor blade is very thin due to the transonic nature of the blade. It is suggested that the blade should be fitted with a protective shield of titanium to prevent the blade from severe erosion and foreign impact damage. During operation it is likely that erodent particles will strike the blade at shallow angles close to the leading edge. The shield can be bonded onto the composite blade leading edge with an adhesive. This technique has been widely used and is well documented with respect to the materials to be bond-jointed and adhesives[68].

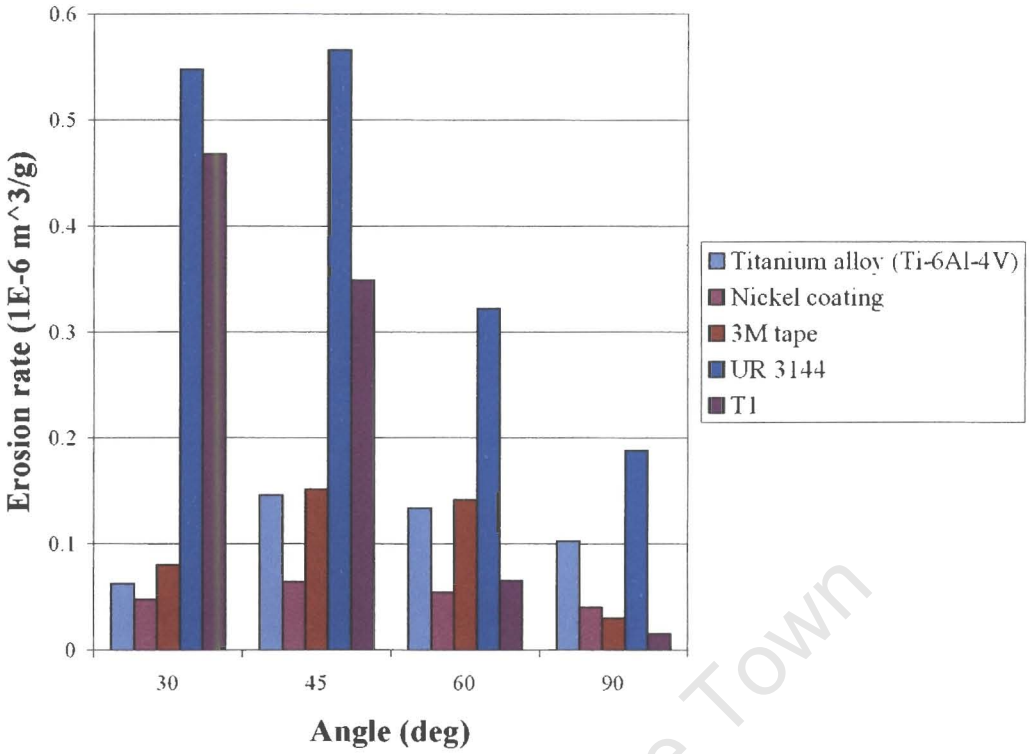

Figure 5.6 Erosion rate *vs.* impingement angle comparison for potential coatings.

5.3 FLEXURAL BENDING PROPERTIES OF FIBRE REINFORCED POLYMERS

During operation, the composite compressor blades do not only untwist but also exhibit bending due to the load and geometry of the blade. It is therefore suggested that the bending properties of the composite play a role in determining a suitable material for the composite compressor blade. The bending test results show that the bending strength of Kevlar® composite is low compared to the bending strength of carbon. The low bending strength of the KFRP is due to the low compressive strength of the Kevlar® fibres. The bending tests show that the carbon reaches a critical point where it suddenly breaks. All the CFRP bending specimens broke in a brittle manner. The KFRP show a far more progressive failure mode and a large portion of the fibres are not broken but rather deformed to allow the bending failure to occur. The hybrid composite shows a combination of the brittle nature of the carbon and the more ductile behaviour of the Kevlar®. The bending strength and modulus are however considerably lower than that of the carbon composite. The addition of Kevlar® in the compressor blade will have a positive effect in that it will prevent sudden catastrophic failure but the lower stiffness will make the blade deflect more.

5.4 IMPACT PROPERITES OF FIBRE COMPOSITE MATERIALS

To investigate the impact properties of the fibre reinforced composites, a low velocity impact rig was used due to the unavailability of a high-speed impact apparatus. It must be realised that the low impact velocity tests cannot accurately determine the impact events occurring on the compressor blade during operation since low *vs.* high speed impact have different mechanisms of energy absorption present. The approach in this section is to study general impact properties for the different composites and conduct a comparative study on impact energy absorption properties for various composites. The study shows the superior impact properties of the KFRP composite compared to the CFRP. Kevlar® have a higher capacity for energy absorption than carbon. The hybrid composite shows higher values of ultimate impact energy and force. It is interesting to note however, that the rate of energy absorption in the hybrid composite is the lowest of the materials tested. This suggests that the stiffer carbon fibres in the hybrid absorb most of the energy in the elastic region, which will result in a low energy absorption rate due the smaller amount of carbon fibres present. From the impact *vs.* displacement curves for carbon at an impact velocity of 4.1 and 4.9 m/s, the following stages of impact deformation can be identified: linear load deflection, onset of fracture (matrix cracking), fibre breakage, the maximum load and the friction force exerted by the specimen when the impactor travels through the specimen.

5.5 FINITE ELEMENT IMPACT INVESTIGATION

The purpose of this section is to investigate the possibility of failure prediction in an impact event, using a FEA approach. The intention being to initially verify the low velocity impact event on the composite plates and then use the model to predict high velocity impact. The results show high localised compressive stresses at the impact area and high tensile stresses at the bottom of the plate, which conforms well compared to the experimental results. From the FE results it is possible to identify areas where failure will occur but the FE analysis cannot however, give a failure prediction beyond the elastic region. In addition, a distinction with respect to de-lamination, matrix cracking or fibre failure is also beyond the capabilities of the finite element code used. To predict an accurate failure model of the composite plate, extensive work would be needed to write an additional program that could be incorporated to classify the type of failure, shape and geometry of the plate after the impact event. It was decided that the modelling of high-speed impact on the composite blade using the software available is beyond the scope of this study.

5.6 MANUFACTURE OF A CFRP COMPRESSOR BLADE

An attempt was made to manufacture the carbon fibre reinforced polymer (CFRP) composite blade using resin transfer moulding (RTM). The composite blade is shown in Figure 5.7 along with the currently used titanium alloy (Ti-6Al-4V) blade. The composite blade on the LHS has an aluminium backing on its leading edge. The first attempt, unfortunately, contain a high porosity which is deleterious for mechanical properties.

Figure 5.7 CFRP and titanium compressor blades.

CHAPTER 6

CONCLUSIONS

The principle objective of this study has been to investigate feasibility of using a fibre reinforced polymer (FRP) to replace the titanium alloy (Ti-6Al-4V) for use in turbine compressor blades. Based on the findings of this study, the following conclusions may be drawn:

7.1 The finite element analysis conducted show that deflections of the composite blade can be tailored by altering the lay-up configuration of the individual plies in the blade.

7.2 The stresses induced in the titanium alloy compressor blades are closed to the design limit criteria for this material.

7.3 The finite element analysis for the proposed composite blade generally shows low stresses in comparison to the corresponding strength for the composite material. It is noted that a stress concentration exists in the base section of the blade that predicts failure in some plies. If foreign impact damage (FOD) is of major concern, it is found that a woven composite could be used with respect to induced stresses in the blade.

7.4 The vibrational analysis indicates higher fundamental blade frequencies for the composite compressor blades. The calculated blade frequencies suggest that no excitation will occur for the blades during the design speed of the turbine.

7.5 The erosion resistance of the carbon- and the Kevlar® fibre reinforced composites is determined to be at least an order magnitude less than that of the titanium alloy.

7.6 The most suitable coating to protect the fibre composite compressor blade was found to be an elastomeric polyurethane coating. The polyurethane coating has comparable erosion resistance to that of the titanium alloy.

7.7 The flexural bending properties of the CFRP are superior to that of the KFRP. The failure mode in bending for the KFRP shows a progressive failure mechanism whilst the CFRP fail in a catastrophic brittle manner.

7.8 The impact resistance for the KFRP is greater than that of the CFRP for low velocity impact.

FUTURE WORK

The FE analysis should be extended to include an analysis of the inter-laminar stresses occurring in the PMC blade to make sure that delaminations do not arise. The next step in the process of replacing the titanium alloy blades with PMC compressor blades should involve experimental testing on a prototype to verify the FE analysis results found in this study. The prototype should be exposed to the expected operating conditions to ensure its mechanical reliability as well as erosion and impact related events. It is suggested that the elastomeric polyurethane coatings should be applied onto these prototypes and their integrity tested at the extreme operating conditions. If impact events of relatively large objects are likely to be problematic, it is suggested that Kevlar® is explored in more detail to enhance the impact resistance of the fibre composite blade.

References:

[1] Cohen, H., Rogers, G. F. C., and Saravanamuttoo H. I. H., Gas Turbine Theory, 4th edn., Addison Wesley Longman Ltd., T.J. Press, 1996.

[2] Sayers, A. T., Hydraulic and Compressible Flow Turbomachines, British Library Cataloguing in Publication Data, 1990.

[3] URL, http://www.airforce-technology.com/contractors/engines/volvo/index.html

[4] URL, http://www.abb.se/stal/product/indexpro.html

[5] Benvenuti, E., and Bianchi, D., Small Gas Turbines, Matching Market Needs, PEi, pp 39-43, Oct. 1999.

[6] Isles, J., Distributed Generation, Microturbines: The Natural Choice?, PEi, pp 55-57, Oct. 1999.

[7] Frost, T. H., Anderson, A. and Agnew, B., A Hybrid Gas Turbine Cycle (Brayton / Ericsson): An Alternative to Conventional Combined Gas and Steam Turbine Power Plant, Proc. Instn. Mech. Engrs. Part A, Vol. 211, pp 121-130, 1997.

[8] Gyarmathy, G., Innovation and Tradition in Steam Turbine Engineering, Proc. Instn. Mech. Engrs. Part A, Vol. 204 (A4), p 217, 1990.

[9] Çengel, Y. A. and Boles M. A., Thermodynamics, An Engineering Approach, McGraw-Hill, Inc. 1994.

[10] URL, http://www.abb.se/stal/product/indexpro.html

[11] Moore, M. J., NO_x Emission Control in Gas Turbines for Combined Cycle Gas Turbine Plant, Proc. Instn. Mech. Engrs. Part A, Vol. 211, pp 43-52, 1997.

[12] Cumpsty, N. A., Compressor Aerodynamics, Longman Scientific & Technical, Longman Group, UK Ltd. 1989.

[13] Kedward, K. T., Large Composite Fan Blade Development for Modern Aeroengines, in Press.

[14] URL, http://www.hsrclients.com/clients/ge90/

[15] Chamis, C. C., and Lynch, J. E., High-Tip-Speed Fiber Composite Compressor Blades, Vibration and Strength Analysis (NASA), NASA Technical Memorandum, NASA TM X-71589, 2nd Conference on Fibrous Composites in Flight Vehicle Design, Dayton , Ohio, May, 1974.

[16] Frischbier, J., Sikorski, S., and Peter, O., Fatigue Life and Bird Strike Resistance of a Composite Fan Blade for Advanced Ducted Engines, Proc. of the 4th European Propulsion Forum pp 149-156, Bath, 1993.

[17] Kedward, K. T., The Application of CFRP to Aero Engine Components, Int. Conf. on Carbon Fibres, Their Composites and Applications, The Plastics Inst., London, 1971.

[18] Frischbier, J. and Sikorski, S., All-Composite Fan Blade for Advanced Ducted Engines, 10th International Symposium on Air Breathing Engines (ISOABE), Vol. 2, UK, pp 780-787, Sept., 1991.

[19] Schulze, D. K., Hennecke, J. and Sikorski, S., Entwicklung einer Verdichterleitschaufel aus kohlefaserverstärktem Kunststoff (CFK), MTU Focus, München, pp 17-22, 1995.

[20] Tilly, G. P., Erosion Caused by Airborne Particles, Wear, Vol. 14, pp 63-79, 1969.

[21] Lessard, L.B., Nemes, J. A., and Lizotte, P.L., Utilization of FEA in the Design of Composite Bicycle Frames, Composites, Vol. 26, No. 1, pp 72-74, 1995.

[22] Stenberg, R., Carbon Fibre Composite on the Viggen Aircraft, Composite Structures Vol. 10, pp 75-81, 1988.

[23] Finegan, I. C., and Gibson, R. F., Recent Research on Enhancement of Damping in Polymer Composites, Composites Structures, Vol. 44, pp 89-98, 1999.

[24] Burnett, D. S., Finite Element Analysis, From Concepts to Applications, Addison-Wesley Publishing Company, Amsterdam, 1987.

[25] Balden, V., Finite Elements – AMU 502z Course Notes, Centre for Research in Computational & Applied Mathematics (CERECAM), University of Cape Town, 1999.

[26] Moser, K., and Schmid, A., Composite Structures - Modelling, Finite Element Analysis and Evaluation, Composite Structures Vol. 11, pp 33-56, 1989.

[27] Cook, R. D., Malkus, D. S., and Plesha, M. E., Concepts and Applications of Finite Element Analysis, 3rd edn., Wiley & Sons, 1989.

[28] Wood, J., Finite Element Analysis of Composite Structures, Composite Structures, Vol. 29, pp 219-230, 1994.

[29] Rizzo, A. R., Estimating Errors In FE Analyses, Mechanical Engineering, pp 61-63, May, 1991.

[30] Noor, A. K., Peters, J. M., Error Indicators and Accuracy Improvement of Finite Element Solutions, Eng. Comput., Vol. 5, pp 39-49, March, 1988.

[31] Lawry, M. H., I-DEAS Master Series™, Mechanical CAE/CAD/CAM Software Student Guide, Structural Dynamics Research Corporation, 1997.

[32] Hibbit, Karlsson & Sorensen, ABAQUS ® Inc., Version 5.8, 1998.

[33] Sussman, T., and Bathe, K. J., Studies of Finite Element Procedures - On Mesh Selection, Computers & Structures, Vol. 21, No. 1 / 2, pp 257-264, 1985.
[34] Ireman, T., Three-dimensional Stress Analysis of Bolted Single-Lap Composite Joints, Composite Structures, Vol. 43, pp 195-216, 1998.
[35] Hull, D., An introduction to Composite Materials, Cambridge University Press, Great Britain, 1981.
[36] Kaw, A. K., Mechanics of Composite Materials, CRC Press, 1997.
[37] Tsai, S. W., and Hahn, T. H., An Introduction to Composite Materials, Technomic Publishing Company, Inc., 1980.
[38] Hearn, E. J., Mechanics of Materials, Pergamon Press, 1985.
[39] Lansdown, A. R., and Price, A. L., Materials to Resist Wear, A Guide to their Selection and Use, Pergamon Press, Oxford, Publ., 1986.
[40] Hutchings, I. M., Tribology: Friction and Wear of Engineering Materials, Hodder & Stoughton, British Library Cataloguing in Publication Data, London, 1992.
[41] Tilly, G. P., Erosion Caused by Impact of Solid Particles, Materials Science and Technology, Vol. 13, 1979.
[42] Levy, A. V., The Platelet Mechanism of Erosion of Ductile Metals, Wear, Vol. 108, pp 1-21, 1986.
[43] Lawn, B. R. and Swain, M. V., J. Mat. Sci. Vol. 10, pp 113-122, 1975.
[44] Pool, K. V., Dharan, C. K. H. and Finnie, I., Erosive Wear of Composite Materials, Wear, Vol. 107, pp 1-12, 1986.
[45] Mathias, P. J., Wu, W., Goretta, K. C., Routbort, J. L., Groppi, D. P., and Karasek, K. R., Solid Particle Erosion of a Graphite-Fiber-Reinforced Bismaleimide Polymer Composite, Wear, Vol. 135, pp 161-169, 1989.
[46] Zahavi, J., Solid Particle Erosion of Reinforced Composite Materials, Wear, Vol. 71, 179-190, 1981.
[47] Wilson, S. and Ball, A., Wear Resistance of an Aluminium Matrix Composite, Proc. Conf. On Tribology of Composite Materials, Oak Ridge, TN, pp 103-112, 1990.
[48] Zahavi, J., Solid Particle Erosion of Polymeric Coatings, Wear, Vol.71, pp 191-210, 1981.
[49] Wood, R. J. K., The Sand Erosion Performance of Coatings, Materials and Design, Vol. 20, 1999.
[50] Li, J. and Hutchings, I. M., Resistance of Cast Polyurethane Elastomers to Solid Particle Erosion, Wear of Materials, ASME, New York, 1989.
[51] Tilly, G. P. and Sage, W., The Interaction of Particle and Material Behaviour in Erosion Processes, Wear, Vol. 16, pp 447-465, 1970.
[52] Tilly, G. P., A Two Stage Mechanism of Ductile Erosion, Wear, Vol. 23, pp 87-96, 1973.
[53] Liebhard, M. and Levy, A., The Effect of Erodent Particle Characteristics on the Erosion of Metals, Wear, Vol. 151, 1991, pp 381-390.
[54] Finnie, I., Wolak, J. and Kabil, Y., Erosion of Metals by Solid Particles, J Mat. Sci., Vol. 2, pp 682-700, 1967.
[55] Feng, Z., The Erosion of Materials, PhD Thesis, University of Cape Town, 1999.
[56] Tilly, G. P., Sand Erosion of Metals and Plastics: A Brief Review, Wear, Vol. 14, pp 241-248, 1969.
[57] Bahadur, S. and Badruddin, R., Erodent Particle Characterization and the Effect of Particle Size and Shape on Erosion, The International Conference on Wear of Materials, Denver, Colorado, pp 143-152, 1989.
[58] Srinivasan, S. and Scattergood, R. O., Effect of Erodent Hardness on Erosion of Brittle Materials, Wear, Vol. 128, pp 139-152, 1988.
[59] Feng, Z. and Ball, A., Overview of Erosive Wear, Proceedings of the 8th International Conference on Tribology, Aarhus, Denmark, NORDTRIB, 1998.
[60] Uuemous, H. and Kleis, I., A Critical Analysis of Erosion Problems Which Have Been Little Studied, Wear, Vol. 31 pp 359-371, 1975.
[61] Misra, A. and Finnie, I., On the Size Effect in Abrasive and Erosive Wear, Wear, Vol. 65, pp 359-373, 1981.
[62] Sundararajan, G. and Roy, M., Solid Particle Erosion Behaviour of Metallic Materials at Room and Elevated Temperatures, Tribology Int. Vol. 30, pp 339-359, 1997.
[63] Wilson, S. and Ball, A., Performance of Metal Matrix Composites in Various Tribological Conditions, Advances in Composite Tribology, Composite Materials Series, K Friedrich (ed.), Vol. 8, 1993.
[64] Mittelman, A. and Roman, I., Tensile Properties of Real Unidirectional Kevlar/Epoxy Composites, Composites, No. 1, Vol. 21, pp 63-69, Jan., 1990.
[65] Edwards, K. L., An Overview of the Technology of Fibre-Reinforced Plastics for Design Purposes, Materials and Design, Vol. 19, pp 1-10, 1998.
[66] Cantwell, W. J. and Morton, J., The Impact Resistance of Composite Materials-a Review Composites, Vol. 22, No. 5, pp 347-360, Sept., 1991.

[67] Harris, B., Engineering Composite Materials, The Institute of Metals, London, 1986.
[68] ASM International Engineered Materials Handbook, Vol. 1, Composites, USA, 1987.
[69] Drzal, L. T. and Madhukar, M., Fibre-Matrix Adhesion and its Relationship to Composite Mechanical Properties, J. Mat. Sci., Vol. 28, pp 569-610, 1993.
[70] Franz, T., "Fundamentals of Anisotropic Material Behaviour of Laminated Composites", Centre for Computational and Applied Mathematics (CERECAM) AMU 508Z course notes, University of Cape Town, 1999.
[71] Carmel, P., A Laboratory Simulation of Low Velocity Projectile Impact on Thin Plates, MSc Thesis, University of Cape Town, 1999.
[72] Sun, C. T. and Rechak, S., Effect of Adhesive Layers on Impact Damage in Composite Laminates, Composite Materials: Testing and Design (8th Conference), USA, 1988.
[73] Foreman, A. D., Optimizing the Damage Tolerance of Carbon-Fibre Composites Using Hollow Fibre Layers, Seminar on *Foreign Object Impact and Energy Absorbing Structure*, UK, pp 65-73, 1998.
[74] Siow, Y. P. and Shim, V. P. W., Experimental Study of Low Velocity Impact In Woven Fiber Composites, J. Composite Materials, Vol. 32, 1998.
[75] Abrate, S., Impact on Composite Structures, Cambridge Universiy Press, UK, 1998.
[76] Ruiz, C. and Martindale, I., Containment of High-Energy Fragments in Aeroengines, Seminar on *Foreign Object Impact and Energy Absorbing Structure*, UK, pp 75-86, 1998.
[77] Lakshminarayana, H. V., Boukhili, R. and Gauvin, R., Finite Element Simulation of Impact Tests of Laminated Composites Plates, Composite Structures, Vol. 28, pp 47-59, 1994.
[78] Al-Bastaki, N. M. S., Design of Fibre Reinforced Composite Structures Subjected to High Strain Rates Using Finite Element Analysis, Applied Composite Materials, Vol. 5, pp 223-236, 1998.
[80] Ruff, A. W., and Ives, L. K., Measurement of Solid Particle Velocity in Erosive Wear, Wear, Vol. 35, pp 195-199, 1975.
[81] American Society for Testing and Materials, Annual Book of ASTM Standards, Vol. 8.01 D790M-92, Easton, 1998.
[82] Ashby, M. F., and Jones, D. R. H., Engineering Materials 1, An Introduction to their Properties and Applications, Int. Series on Mat. Sci. and Tech., Vol. 34, Pergamon Press, 1991.

Publication Record

- Composite turbine compressor blade, JA Branehög, K Marcus and A Ball , Proc. of 2nd International Conference on Composites at Lake Louise, Lake Louise, Canada 1999

- On composite turbine compressor blades, JA Branehög, K Marcus and A Ball, ECCM 9: Composites - From Fundamentals to exploitation, Brighton, United Kingdom 2000, in press

- Finite element analysis of composite turbine blades, JA Branehög, K Marcus, Sacam 2000, International Conference on Applied Mechanics, Durban, South Africa 2000

- An investigation of composite compressor blades, JA Branehög, K Marcus and A Ball, 3rd International Conference on Composite Science and Technology, Durban, South Africa 2000

- An investigation of the erosive behaviour of fibre-reinforced composite materials, JA Branehög, K Marcus and A Ball, Microscopy Society of Southern Africa, 38th Annual Conference 1999, Bloemfontein, South Africa

- An investigation of composite compressor blades, JA Branehög, and K Marcus, Composite Structures, ICCST/3, 2000, in press

AN INVESTIGATION OF EROSIVE BEHAVIOUR OF FIBRE-REINFORCED COMPOSITE MATERIALS

J. Branehög, K. Marcus and A. Ball
Department of Materials Engineering, University of Cape Town

The use of carbon- and Kevlar fibre reinforced composite materials has found a wide range of advanced applications where a high specific strength is required[1]. These composite materials have many other advantages over traditional materials such as steel and aluminium, but there are disadvantages that need to be considered when using composite fibre materials in engineering applications.

This paper is concerned with the erosive behaviour of carbon and Kevlar fibre based composites to be used for turbine compressor blades. The turbine blades operate in an aggressive environment which include dust and ice particles, that get ingested into the turbine, and cause erosive wear on the blades. The composite materials were blasted with silica particles of approximately 180μm in size at 400 km/h. The mechanisms and erosion resistance was then determined as a function of material properties.

The carbon and Kevlar fibre reinforced composite materials consist of an epoxy resin matrix with multiple layers of fibres. The fibres are either arranged in a unidirectional configuration or as a woven cloth. The fibres are saturated in the epoxy matrix and vacuum laminated to avoid a high void content in the composite.

The qualification of the erosion damage was determined using a Cambridge S200 SEM operating at 15kV. The eroded specimens were collected and cleaned in an ultrasonic bath. The specimens were then fixed on aluminium stubs and coated to ensure electrical conductivity.

Figure 1 shows a carbon composite that was eroded by approximately 30 grams of silica particles. From Fig.1 it can be observed that the damaged area forms ridges and valleys due to the nature of the woven carbon fibre plies. The epoxy matrix is easily eroded by the silica particles. SEM analysis of the eroded composite also shows that the fibres break in a brittle manner, and where more matrix rich areas are encountered, the damage to the fibres is less severe.

The extremely high resolution of the near field scanning optical microscope (SNOM) allowed us to determine the depth profile of the damaged areas. The SNOM image in Fig. 2 also gave the profile of the broken fibres that protrude from the epoxy matrix.

Ms. S Marais at the Polymer Institute, University of Stellenbosch, kindly performed the SNOM analysis.

Reference

1. Stachowiak, G.W. (1993) In: K. Friedrich, ed. Advances in Composite Tribology, Composite Materials Series, 8, Amsterdam, Elsevier, 510.

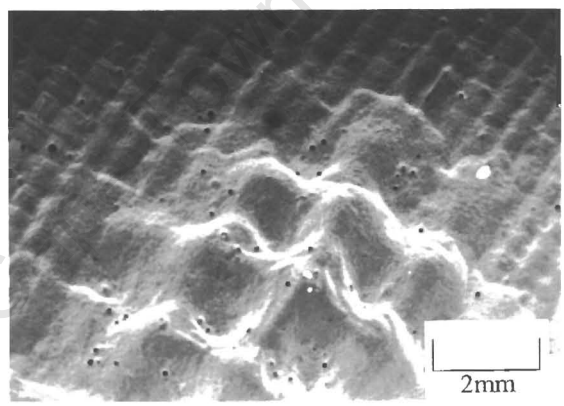

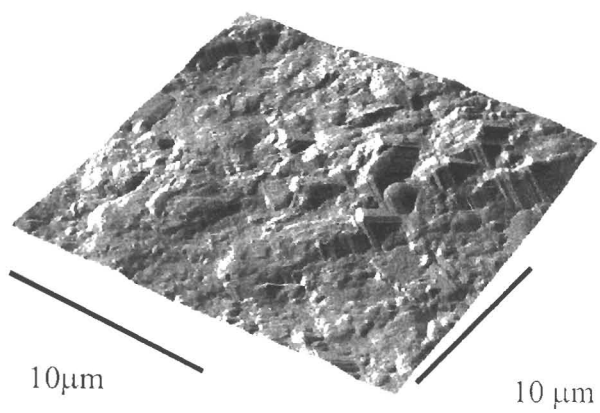

Figure 1. SEM micrograph showing a typical eroded area in a carbon fibre composite.
Figure 2. SNOM image of the eroded area and damage mode.

APPENDIX A

Fortran Code for Calculation of Composite Plies

Subroutine1

```
CROSSP(COORD,NORMAL)
!.....................................................................
!    Purpose: To calculate crossproduct of two vectors and add it to
!          array NORMAL
!.....................................................................
!
     implicit   NONE


     real       COORD(3,3),     &
                NORMAL(3),      &
                VECT1(3),       &
                VECT2(3)
!
     VECT2 = COORD(1,1:3) - COORD(2,1:3)
     VECT1 = COORD(3,1:3) - COORD(2,1:3)
!
     NORMAL(1) = VECT1(2)*VECT2(3) - VECT1(3)*VECT2(2)
     NORMAL(2) = VECT1(3)*VECT2(1) - VECT1(1)*VECT2(3)
     NORMAL(3) = VECT1(1)*VECT2(2) - VECT1(2)*VECT2(1)
!
     return
     end
```

subroutine 2

```
SHARK(KREEF,HEIGHT,ERROR)
!.....................................................................
!    Purpose: Calculate heights of nodes
!.....................................................................
!
     implicit     NONE
     integer      I,ERROR
!
     real       KREEF(8,3),                    &
                          HEIGHT, MAG,VECT3(3),LCOORD(3,3),  &
                          NORMAL(3),DHEIGHT,ZERO
     parameter (ZERO=0.)
!
     ERROR = 0
          HEIGHT = 0.
1000  format(t3,'Node A',3e10.3,3x,3e10.3,/,E12.3)
2000  format(t3,'Node B',3e10.3,3x,3e10.3,/,E12.3)
3000  format(t3,'Node C',3e10.3,3x,3e10.3,/,E12.3)
4000  format(t3,'Node D',3e10.3,3x,3e10.3,/,E12.3)
!.....................................................................
!NODE A
!.....................................................................
!
```

```
        LCOORD(1,1:3)=KREEF(4,1:3)
        LCOORD(2,1:3)=KREEF(1,1:3)
        LCOORD(3,1:3)=KREEF(2,1:3)
!
        call CROSSP(LCOORD,NORMAL)
!
        MAG=sqrt(NORMAL(1)**2+NORMAL(2)**2+NORMAL(3)**2)
!
        NORMAL=NORMAL/MAG
!
        VECT3=KREEF(5,1:3)-KREEF(1,1:3)
        DHEIGHT = 0.
        do I = 1, 3
          DHEIGHT = DHEIGHT+NORMAL(I)*VECT3(I)
        end do
   if (DHEIGHT.le.ZERO) then
     ERROR = ERROR + 1
   end if
   HEIGHT = HEIGHT + DHEIGHT
!      write(6,1000)NORMAL,VECT3,DHEIGHT
!
!
```

Repeated for the corner nodes in the element!

```
        NORMAL=NORMAL/MAG
!
        VECT3=KREEF(8,1:3)-KREEF(4,1:3)
        DHEIGHT = 0.
        do I = 1, 3
          DHEIGHT = DHEIGHT+NORMAL(I)*VECT3(I)
        end do
   if (DHEIGHT.le.ZERO) then
     ERROR = ERROR + 1
   end if
   HEIGHT = HEIGHT + DHEIGHT
!      write(6,4000)NORMAL,VECT3,DHEIGHT
!
        HEIGHT=HEIGHT/4.
!
        return
        end


program JOHAN
!.....
!    Purpose: Calculate nr of layers needed in the compressor blade
!
!    To output element sets according to element thickness.
!    Limitations: Can handle up to thicknesses of maximum of 999 layers per element.
!.....
!
```

```
      implicit      NONE

      character(80)  BUFFER
      character(12)  FILEIN,FILEOUT

      integer    NPNT (10000),          &
                 ELPNT(10000),          &
                 NMAX,                  &
                 ELMAX,                 &
                 ELEMENT(10000,8),      &
                 I,J,K,L,DUMMY,         &
                                T(100), THICK(100,1000),  &
                                ERROR
!
      integer    FLAG,SYS,COUNT
      real       COORD (10000,3),     &
                 TOL,                 &
                 DIST,                &
                          MAG,        &
                 CRAYFISH(8,3),       &
                 THICKNESS,NLAYER,ZERO
!
      parameter  (ZERO=0.D0)
!
!      write(6,1000,advance='NO')
!      read(5,*) FILEIN
!      write(6,1010,advance='NO')
!      read(5,*) FILEOUT
1000  format(t3,'Input file  ')
1010  format(t3,'Output file ')
!
      FILEIN = 'skovel1.inp'
!     FILEIN = 'trial.inp'
      FILEOUT ='test.txt'

      NPNT      = 0
      ELPNT     = 0
      ELEMENT   = 0
      COUNT     = 0
          T     = 0
          THICK     = 0
!
      COORD     = ZERO
!
      open (unit=10,file = FILEIN, status='OLD' )
      open (unit=13,file = FILEOUT,status='UNKNOWN')
!
      I = 0
      J = 0
      K = 0
      L = 0
```

```
!
    write (6,1100)
1100  format (/,t3,'Reading input file')
!
    DO WHILE (.not.EOF(10))                    ! check for EOF
      BUFFER = ""
      READ (10, '(A80)') BUFFER
!      write(6,*)BUFFER
      if (BUFFER(1:1) == "*") then
        if     (BUFFER(2:2)  == "**") then     ! comment
!
        else if (BUFFER(2:5)  == "NODE") then
          FLAG = 1
        else if (BUFFER(2:18) == "ELEMENT,TYPE=C3D8") then
          FLAG = 2
            else
          FLAG = 0
        end if
      else
        if (FLAG == 1) then
          I = I + 1
          read (BUFFER,*) NPNT(I),(COORD(NPNT(I),K),K=1,3)
!                                write(6,*)'reading node', I
        else if (FLAG == 2) then
          J = J + 1
          read (BUFFER,*) ELPNT(J),(ELEMENT(ELPNT(J),K),K=1,8)
!           READ (10, *)
!           READ (10, *)
!           write(6,*)BUFFER
!           write(6,*)'reading element', J
        end if
      end if
    end do
!
!
    close (10,status='KEEP')
    NMAX  = I
    ELMAX = J
!     write(13,*)'nmax=',NMAX,' ELMAX=',ELMAX
!
    write (6,1200)
1200  format (/,t3,'Calculating element thicknesses')
!
    do I = 1, ELMAX
      do J = 1, 8
        do K = 1, 3
          CRAYFISH(J,K) = COORD(ELEMENT(ELPNT(I),J),K)
        end do
      end do
      call SHARK (CRAYFISH,THICKNESS,ERROR)
          if (ERROR.ne.0) then
```

```
        write(6,1300) ERROR, ELPNT(I)
1300      format(t3,'WARNING: negative or zero height at ',i5,  &
              ' points in element',i5)
          end if
              if (THICKNESS.le. ZERO) then
                stop 'ERROR - negative or zero element thickness'
              end if

          NLAYER=int(THICKNESS/0.14478+0.5)
!       write(13,*)'element', ELPNT(I),' layer',NLAYER
!
      T(NLAYER) = T(NLAYER) + 1
              THICK(NLAYER,T(NLAYER)) = ELPNT(I)
!
    end do
!
    write (6,1400)
1400  format (/,t3,'Outputting to file')
!
2100  format(\,i8,',')
2200  format(\,i8)
2300  format(t1,'*ELSET, ELSET=THICK',I1)
2400  format(t1,'*ELSET, ELSET=THICK',I2)
2500  format(t1,'*ELSET, ELSET=THICK',I3)
!
    do I = 1, 99
          if (T(I).ge.1) then
                if (I.le.9) then
                  write (13,2300) I
                else if (I.le.99) then
                  write (13,2400) I
        else
                  write (13,2500) I
                    end if
                  if (int(T(I)/8).gt.1) then
                    do J = 1, int(T(I)/8)
                      do K = (J-1)*8+1, (J-1)*8+8
                        if (K==T(I)) then
                              write(13,2200) THICK(I,K)
                            else
                              write(13,2100) THICK(I,K)
            end if
          end do
                        write (13,*)
                      end do
              if (K-1.ne.T(I)) then
                        do L = K, T(I)
                          if (L==T(I)) then
                              write(13,2200) THICK(I,L)
                            else
                              write(13,2100) THICK(I,L)
```

```
            end if
          end do
                        write (13,*)
                      end if
                    else
                      do L = 1, T(I)
                        if (L==T(I)) then
                              write(13,2200) THICK(I,L)
                            else
                              write(13,2100) THICK(I,L)
            end if
          end do
                      write (13,*)
                    end if
      end if
        end do
!
    end program
```

APPENDIX B

ABAQUS INPUT DECKS FOR COMPOSITE COMPRESSOR BLADES

LAY-UP 1. 70% O DEG / 30% +/- 45 DEG

```
*HEADING
ABB carbon fibre composite turbine compressor blade
*NODE, SYSTEM=R
1,0.45935328,-0.033598009,0.001907673
2,0.45945657,-0.033726159,0.000759638
3,0.45922915,-0.033443997,-0.00033360
4,0.45190356,-0.036383346,0.001907673
```

All the nodes …

```
5138,0.4722903,-0.047274188,0.202
5139,0.46886843,-0.054146348,0.202
*ELEMENT,TYPE=C3D8  ,ELSET=BLADE
  212,  247,  248,  264,  263,  423,  424,  440,  439
  213,  248,  249,  265,  264,  424,  425,  441,  440
  214,  249,  250,  266,  265,  425,  426,  442,  441
```

All the elements…

```
3496,  4385,  4386,  4402,  4401,  5121,  5122,  5138,  5137
3497,  4386,  4387,  4403,  4402,  5122,  5123,  5139,  5138
**-------------------------------------------------------------------
**-----------------------------------
*MATERIAL, NAME=ENGCON
*ELASTIC, TYPE=ENGINEERING CONSTANTS
10.E9, 141.E9, 11.E9,     0.0213, 0.3, 0.3,    5.1E9, 4.0E9
5.1E9,    24
**
*DENSITY
1580.5
**-------------------------------------------------------------------
*INCLUDE, INPUT=trial1.txt------Include all element sets with same thickness...
*ELSET, ELSET=THICK1
  1997,  2012,  2027,  2042,  2057,  2072,  2087,  2102,
  2117,  2132,  2147,  2672,  2687,  2702,  2717,  2732,
  2747,  2762,  2777,  2792,  2807,  2822,  3347,  3362,
  3377,  3392,  3407,  3422,  3437,  3452,  3467,  3482,3497
*ELSET, ELSET=THICK2
  1713,  1727,  1728,  1742,  1743,  1757,  1758,  1772,

…
**-------------------------------------------------------------------
**
*SOLID SECTION, ELSET=THICK1, COMPOSITE, STACK DIRECTION=3,
ORIENTATION=OWN
0.145E-3, 5, ENGCON, PL45
*SOLID SECTION, ELSET=THICK2, COMPOSITE, STACK DIRECTION=3,
ORIENTATION=OWN
```

0.145E-3, 5, ENGCON, PL45
0.145E-3, 5, ENGCON, PL0
**
*SOLID SECTION, ELSET=THICK3, COMPOSITE, STACK DIRECTION=3,
ORIENTATION=OWN
0.145E-3, 5, ENGCON, PL45
0.145E-3, 5, ENGCON, PL0
0.145E-3, 5, ENGCON, PL0

All the plies….

---

*SOLID SECTION, ELSET=THICK50, COMPOSITE, STACK DIRECTION=3,
ORIENTATION=OWN
0.145E-3, 5, ENGCON, PL45
0.145E-3, 5, ENGCON, PL-45
0.145E-3, 5, ENGCON, PL0
0.145E-3, 5, ENGCON, PL0
0.145E-3, 5, ENGCON, PL0
0.145E-3, 5, ENGCON, PL0
0.145E-3, 5, ENGCON, PL0
0.145E-3, 5, ENGCON, PL45
0.145E-3, 5, ENGCON, PL-45
0.145E-3, 5, ENGCON, PL0
0.145E-3, 5, ENGCON, PL0
0.145E-3, 5, ENGCON, PL0
0.145E-3, 5, ENGCON, PL0
0.145E-3, 5, ENGCON, PL0
0.145E-3, 5, ENGCON, PL45
0.145E-3, 5, ENGCON, PL-45
0.145E-3, 5, ENGCON, PL0
0.145E-3, 5, ENGCON, PL0
0.145E-3, 5, ENGCON, PL0…

**ORIENTATION OF LAYERS
**
*ORIENTATION, NAME=OWN, DEFINITION=OFFSET TO NODES
2,4
3, 0.
*ORIENTATION, NAME=PL0, DEFINITION=OFFSET TO NODES
2,4
3, 0.
*ORIENTATION, NAME=PL90, DEFINITION=OFFSET TO NODES
2,4
3, 90
*ORIENTATION, NAME=PL45, DEFINITION=OFFSET TO NODES
2,4
3, 45
*ORIENTATION, NAME=PL-45, DEFINITION=OFFSET TO NODES
2,4
3,-45

```
**----------------------------------------------
**APPLY BOUNDARY CONDITIONS, LOCK BOTH SIDES + FRONT
**----------------------------------------------
*NSET, NSET=LEFTSIDE, GENERATE
276,  290,  1
292,  306,  1
308,  322,  1
324,  338,  1
1895,  1901,  2
1,     4,  3
7,    12,  5
15,    18,  3
20,    21,  1
24,    25,  1
28,    29,  1
*NSET, NSET=RIGHTSIDE, GENERATE
1702,  1878,  11
1701,  1877,  11
1700,  1876,  11
1699,  1875,  11
1090,  1092,  1
1085,  1088,  1
1094,  1096,  1
**----------------------------------------------
**NODE SET FOR FRONT BOUNDARY----------------------
**----------------------------------------------
**NSET, NSET=FRONT, GENERATE
**184,  194,  1
**----------------------------------------------
**TRANSFORM, NSET=LEFTSIDE
**1.0,  0.0,  0.0,     0.0,  0.5,  0.866
**----------------------------------------------
**TRANSFORM, NSET=RIGHTSIDE
**1.0,  0.0,  0.0,     0.0,  -0.5,  0.866
**----------------------------------------------
*BOUNDARY
LEFTSIDE,  1,  3,  0.
RIGHTSIDE,  1,  3,  0.
**----------------------------------------------
**
**----------------STEP 1  blade frequencies (egenfrekvenser) vid 0 rpm-------------
*STEP,NLGEOM
*FREQUENCY
6,2000
**BOUNDARY,OP=NEW
**BS000001,    1,3,      .00000E+00
*RESTART, WRITE
*NODE PRINT, FREQUENCY=0
*EL PRINT,FREQUENCY=0
*END STEP
**----------------------------------------------------------
```

```
**----------STEP 2 loading at 10000 rpm----------
**------------------------------------------------------------
*STEP,AMPLITUDE=RAMP,INC=20,NLGEOM=YES
*STATIC
0.25, 1.0, 1.0e-06
**------------------------------------------------
*CLOAD,OP=NEW
**axiell gaskraft
2574,    1,-4.4374E+02
**tangentiell gaskraft
2574,    2, 4.7377E+02
**------------------------------------------------
** NODE CHECK ORIGINAL MODEL
**------------------------------------------------
**CENTRIFUGAL LOADING 10000 RPM
**------------------------------------------------
*DLOAD
BLADE, CENTRIF, 1.1E6, -5.1647E-3,  -1.5E-2,   -0.216499,    1., 0., 0.
**------------------------------------------------
*RESTART,WRITE,FREQUENCY=100,OVERLAY
**
*NODE PRINT, FREQUENCY=0
*EL PRINT,FREQUENCY=0
sp3
**
*PRINT, CONTACT=YES
*END STEP
**------------------------------------------------
**----------step 3 blade frequencies (egenfrekvenser) vid 10 000 rpm----------
*STEP,NLGEOM
*FREQUENCY
6,2000
*restart, write
*NODE PRINT, FREQUENCY=0
*EL PRINT,FREQUENCY=0
*END STEP
```

LAY-UP 2 70% O DEG / 30% +/- 45 DEG

```
*HEADING
ABB carbon fibre XPLY compressor blade
*NODE, SYSTEM=R
1,0.45935328,-0.033598009,0.001907673
2,0.45945657,-0.033726159,0.000759638
3,0.45922915,-0.033443997,-0.00033360
4,0.45190356,-0.036383346,0.001907673
```

All the nodes …

```
5138,0.4722903,-0.047274188,0.202
5139,0.46886843,-0.054146348,0.202
*ELEMENT,TYPE=C3D8  ,ELSET=BLADE
  212,  247,  248,  264,  263,  423,  424,  440,  439
  213,  248,  249,  265,  264,  424,  425,  441,  440
  214,  249,  250,  266,  265,  425,  426,  442,  441
```

All the elements…

```
3496,  4385,  4386,  4402,  4401,  5121,  5122,  5138,  5137
  3497,  4386,  4387,  4403,  4402,  5122,  5123,  5139,  5138
**-------------------------------------------------------------------
**-----------------------------------
*MATERIAL, NAME=ENGCON
*MATERIAL, NAME=ENGCON
*ELASTIC, TYPE=ENGINEERING CONSTANTS
10.E9, 141.E9, 11.E9,     0.0213, 0.3, 0.3,    5.1E9, 4.0E9
5.1E9,    24
**
*DENSITY
1580.5
**
**
**-------------------------------------------------------------------
*INCLUDE, INPUT=trial1.txt-----Include all element sets with same thickness...

*ELSET, ELSET=THICK1
  1997,  2012,  2027,  2042,  2057,  2072,  2087,  2102,
  2117,  2132,  2147,  2672,  2687,  2702,  2717,  2732,
  2747,  2762,  2777,  2792,  2807,  2822,  3347,  3362,
  3377,  3392,  3407,  3422,  3437,  3452,  3467,  3482,3497
*ELSET, ELSET=THICK2
  1713,  1727,  1728,  1742,  1743,  1757,  1758,  1772,

*SOLID SECTION, ELSET=THICK1, COMPOSITE, STACK DIRECTION=3,
ORIENTATION=OWN
0.145E-3, 5, ENGCON, PL0
```

```
*SOLID SECTION, ELSET=THICK2, COMPOSITE, STACK DIRECTION=3,
ORIENTATION=OWN
0.145E-3, 5, ENGCON, PL0
0.145E-3, 5, ENGCON, PL90
**
*SOLID SECTION, ELSET=THICK3, COMPOSITE, STACK DIRECTION=3,
ORIENTATION=OWN
0.145E-3, 5, ENGCON, PL0
0.145E-3, 5, ENGCON, PL90
0.145E-3, 5, ENGCON, PL0
**
*SOLID SECTION, ELSET=THICK4, COMPOSITE, STACK DIRECTION=3,
ORIENTATION=OWN
0.145E-3, 5, ENGCON, PL0
0.145E-3, 5, ENGCON, PL90
0.145E-3, 5, ENGCON, PL0
0.145E-3, 5, ENGCON, PL90
```

All the plies….

```
*SOLID SECTION, ELSET=THICK50, COMPOSITE, STACK DIRECTION=3,
ORIENTATION=OWN
0.145E-3, 5, ENGCON, PL0
0.145E-3, 5, ENGCON, PL90
0.145E-3, 5, ENGCON, PL0
0.145E-3, 5, ENGCON, PL90
0.145E-3, 5, ENGCON, PL0
0.145E-3, 5, ENGCON, PL90
0.145E-3, 5, ENGCON, PL0
0.145E-3, 5, ENGCON, PL90
0.145E-3, 5, ENGCON, PL0
0.145E-3, 5, ENGCON, PL90
0.145E-3, 5, ENGCON, PL0
0.145E-3, 5, ENGCON, PL90
0.145E-3, 5, ENGCON, PL0
0.145E-3, 5, ENGCON, PL90
0.145E-3, 5, ENGCON, PL0
0.145E-3, 5, ENGCON, PL90
0.145E-3, 5, ENGCON, PL0
0.145E-3, 5, ENGCON, PL90
0.145E-3, 5, ENGCON, PL0
0.145E-3, 5, ENGCON, PL90
0.145E-3, 5, ENGCON, PL0
0.145E-3, 5, ENGCON, PL90
0.145E-3, 5, ENGCON, PL0
0.145E-3, 5, ENGCON, PL90
0.145E-3, 5, ENGCON, PL0
0.145E-3, 5, ENGCON, PL90
0.145E-3, 5, ENGCON, PL0
0.145E-3, 5, ENGCON, PL90…
```

```
**----------------------------------
**ORIENTATION OF LAYERS
**
*ORIENTATION, NAME=OWN, DEFINITION=OFFSET TO NODES
2,4
3, 0.
*ORIENTATION, NAME=PL0, DEFINITION=OFFSET TO NODES
2,4
3, 0.
*ORIENTATION, NAME=PL90, DEFINITION=OFFSET TO NODES
2,4
3, 90
**----------------------------------------------
**APPLY BOUNDARY CONDITIONS, LOCK BOTH SIDES + FRONT
**----------------------------------------------
*NSET, NSET=LEFTSIDE, GENERATE
276,  290,  1
292,  306,  1
308,  322,  1
324,  338,  1
1895,  1901,  2
1,     4,  3
7,    12,  5
15,    18,  3
20,    21,  1
24,    25,  1
28,    29,  1
*NSET, NSET=RIGHTSIDE, GENERATE
1702,  1878,  1
1701,  1877,  1
1700,  1876,  1
1699,  1875,  1
1090,  1092,  1
1085,  1088,  1
1094,  1096,  1
**----------------------------------------------
**NODE SET FOR FRONT BOUNDARY----------------------
**----------------------------------------------
*NSET, NSET=FRONT, GENERATE
184,  194,  1
**----------------------------------------------
*TRANSFORM, NSET=LEFTSIDE
1.0,  0.0,  0.0,     0.0,  0.866,  0.5
**----------------------------------------------
*TRANSFORM, NSET=RIGHTSIDE
1.0,  0.0,  0.0,     0.0,  -0.866,  0.5
**----------------------------------------------
*BOUNDARY
LEFTSIDE,  2,  2,  0.
RIGHTSIDE,  2,  2,  0.
```

```
FRONT, 1,  1,  0.
**----------------------------------------------------------
*STEP,AMPLITUDE=RAMP,INC=20,NLGEOM=YES
*STATIC
0.25, 1.0, 1.0e-06
**----------------------------------------------------------
*CLOAD,OP=NEW
**axiell gaskraft
2574,    1,-4.4374E+02
**tangentiell gaskraft
2574,    2, 4.7377E+02
**----------------------------------------------------------
**NODE CHECK ORIGINAL MODEL
**----------------------------------------------------------
**CENTRIFUGAL LOADING 10000 RPM
**----------------------------------------------------------
*DLOAD
BLADE, CENTRIF, 1.1E6, -5.1647E-3,  -1.5E-2,   -0.216499,    1., 0., 0.
**----------------------------------------------------------
*RESTART,WRITE,FREQUENCY=100,OVERLAY
**
*NODE PRINT, FREQUENCY=0
*EL PRINT,FREQUENCY=0
**
*PRINT, CONTACT=YES
*END STEP
```

APPENDIX C

FE Stress Analysis Plots for Composite Compressor Blade

The stresses towards the centre of the profile are less than at the surface. This appendix verifies this behaviour showing plies close to the centre of the PMC blade lay up 1. Figure C1 to C3 shows the stresses on the PMC blade lay-up 1 for plies close to the centre profile.

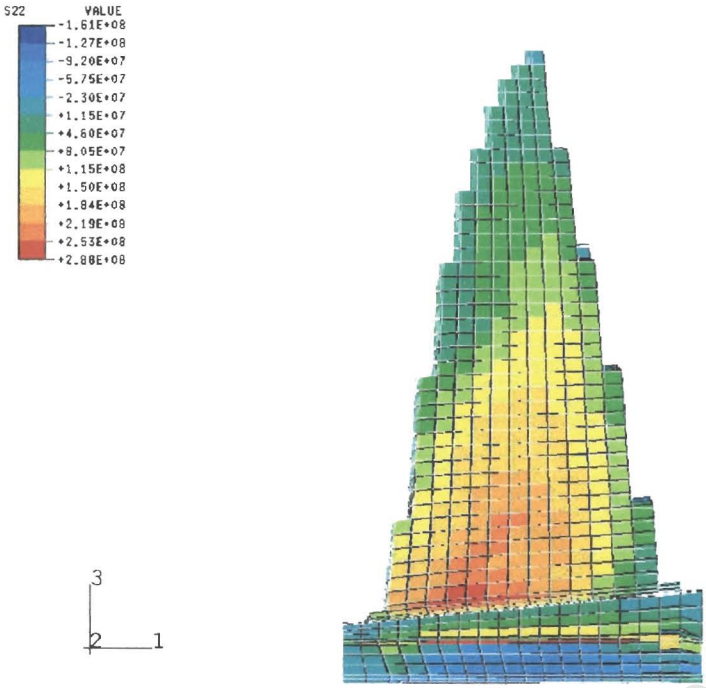

Figure C1 Stresses parallel to the fibre direction in the 7th ply.

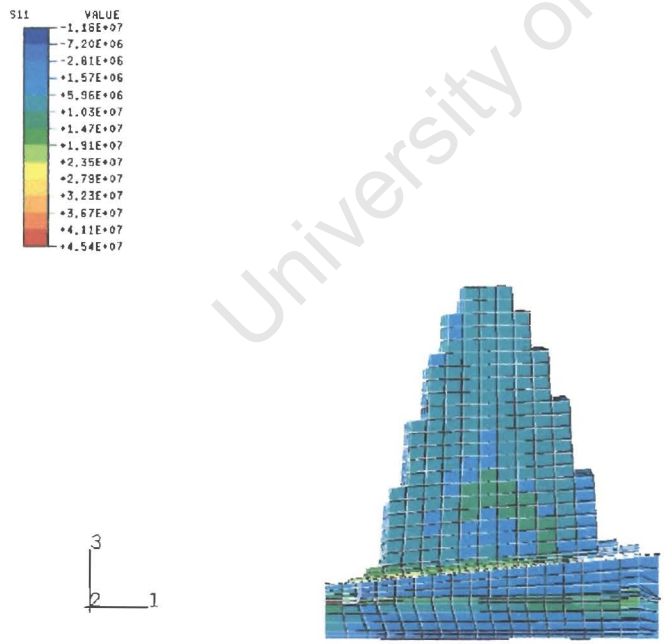

Figure C2 Stresses transverse to the fibre direction in the 25th ply.

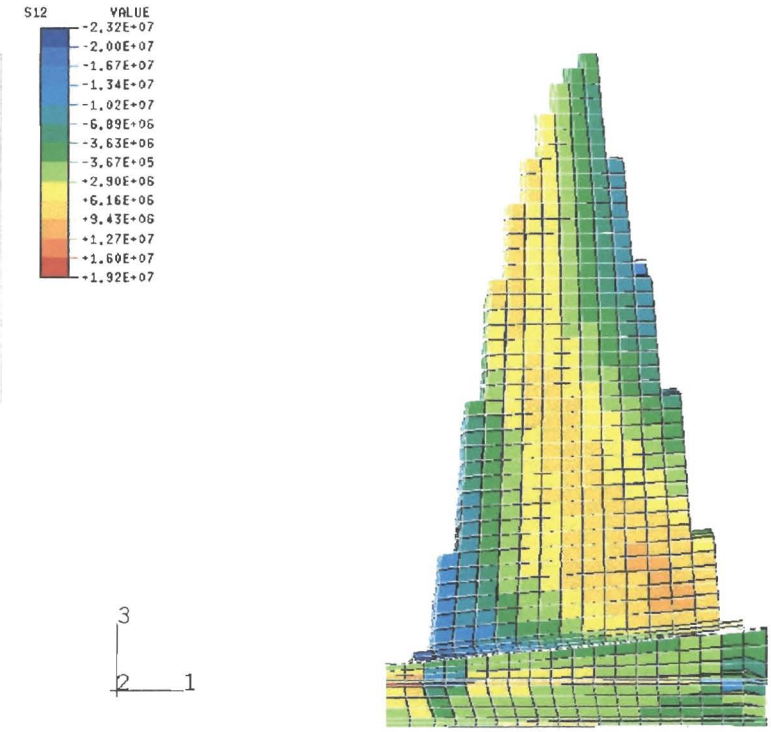

Figure C3 Shear stresses in the 7th ply.

Figure C4 to C6 show the ply stresses occurring on the ***suction*** side of the PMC blade.

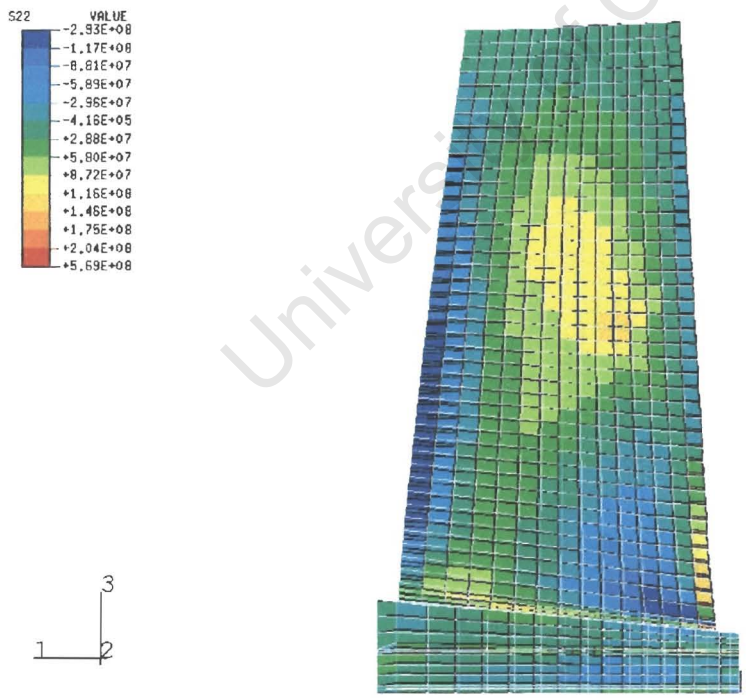

Figure C4 Stresses parallel to the fibre direction in the outermost ply on the suction side of the PMC compressor blade.

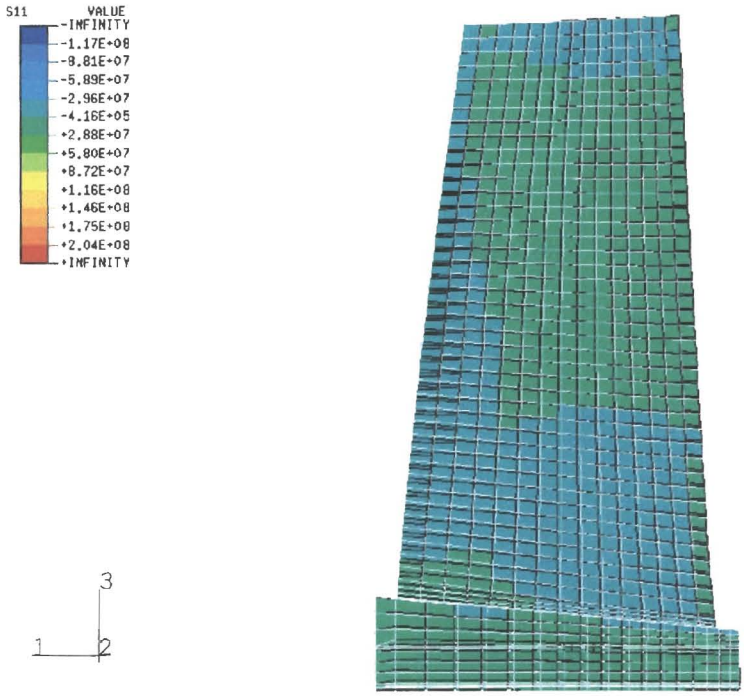

Figure C5 Stresses transverse to the fibre direction in the outermost ply on the <u>suction</u> side of the PMC compressor blade.

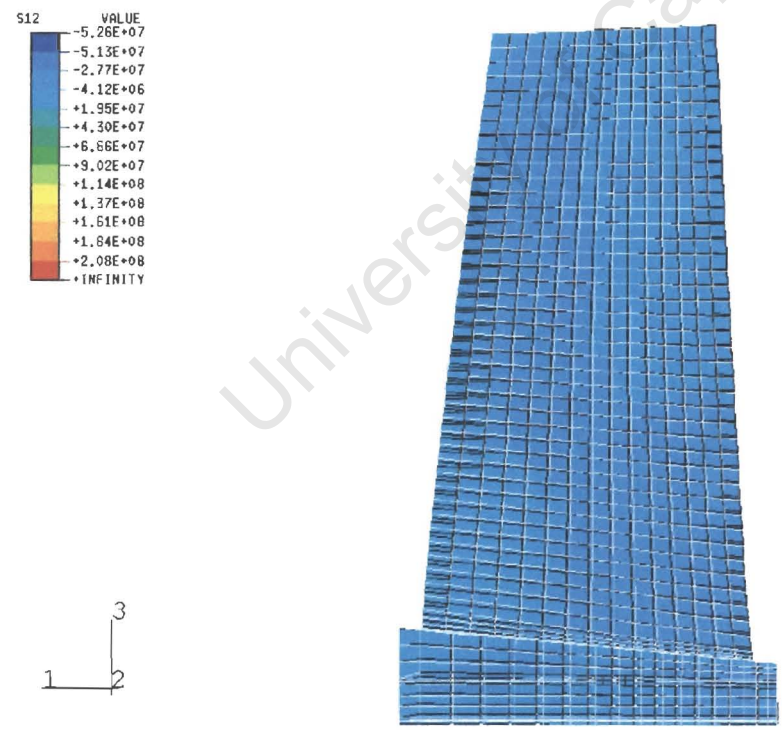

Figure C6 Shear stresses in the outermost ply on the <u>suction</u> side of the PMC compressor blade.

APPENDIX D

Mode Shapes for Titanium, PMC Lay-up 1 and PMC Lay-up 2 Compressor blades.

The first five mode shapes are shown for zero rotational speed for all the compressor blade models considered.

Figures D1 to D5 show the mode shapes of the titanium alloy.

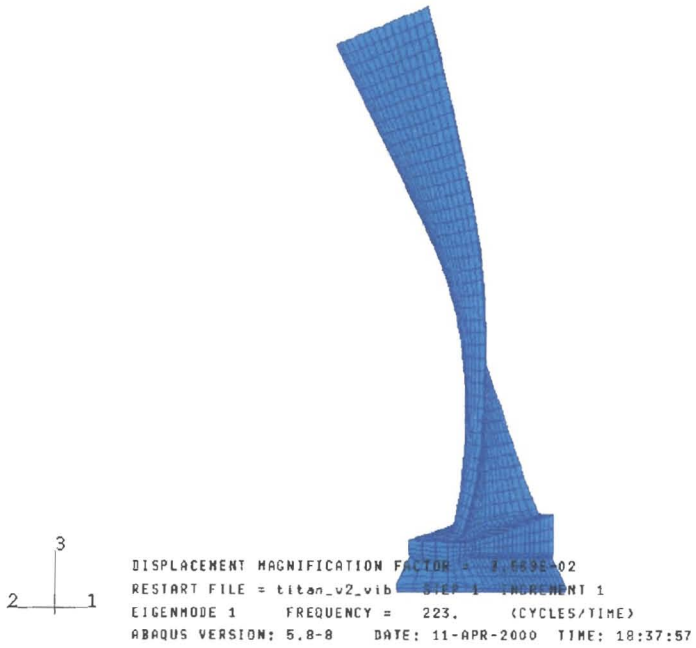

Figure D1 Mode no. 1 for the titanium alloy blade.

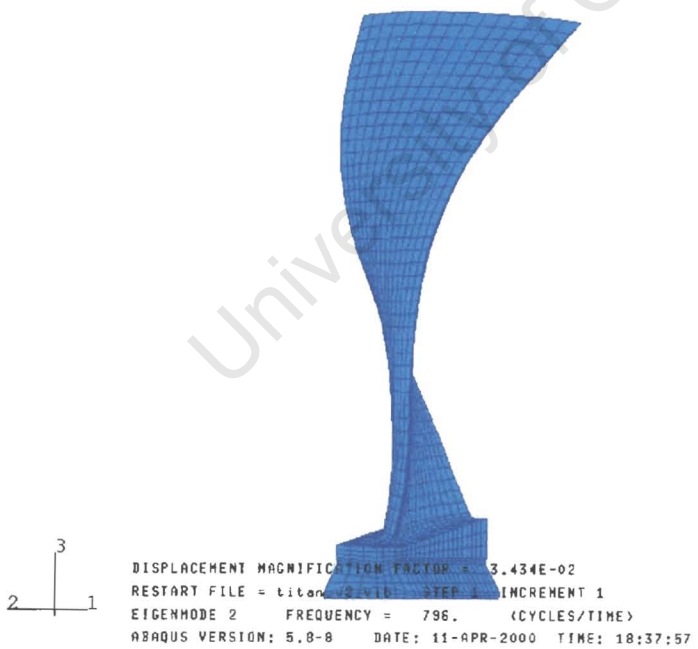

Figure D2 Mode no. 2 for the titanium alloy blade.

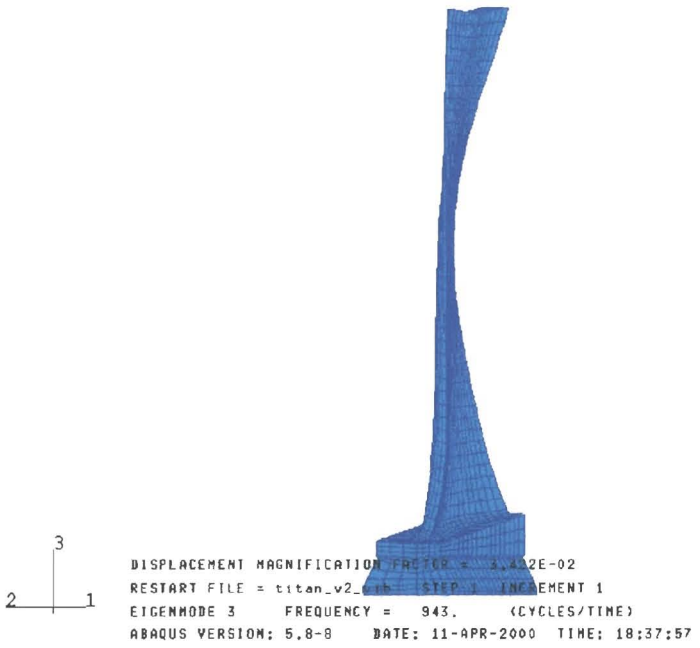

Figure D3 Mode no. 3 for the titanium alloy blade.

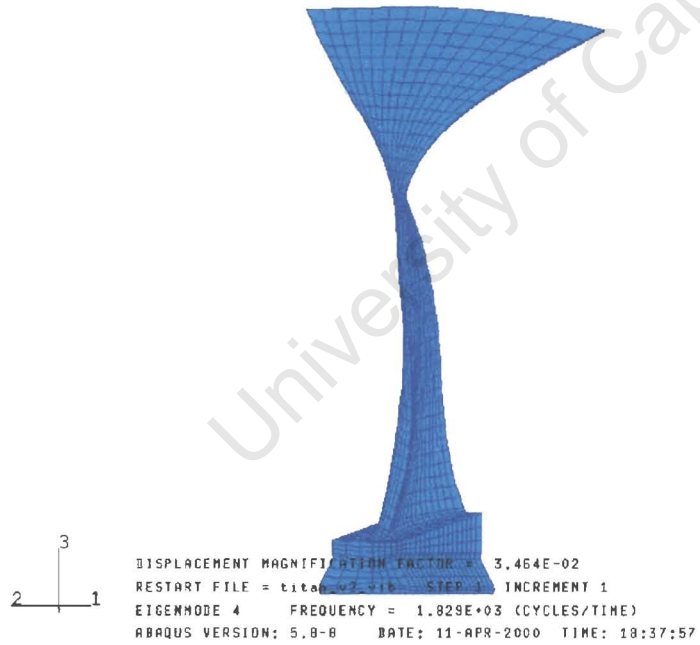

Figure D4 Mode no. 4 for the titanium alloy blade.

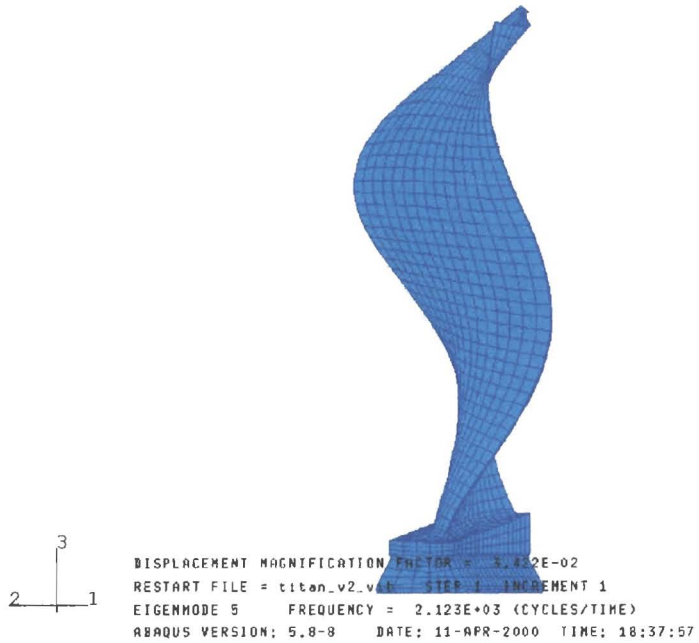

Figure D5 Mode no. 5 for the titanium alloy blade.

Figures D6 to D10 show the mode shapes of the PMC blade lay-up 1.

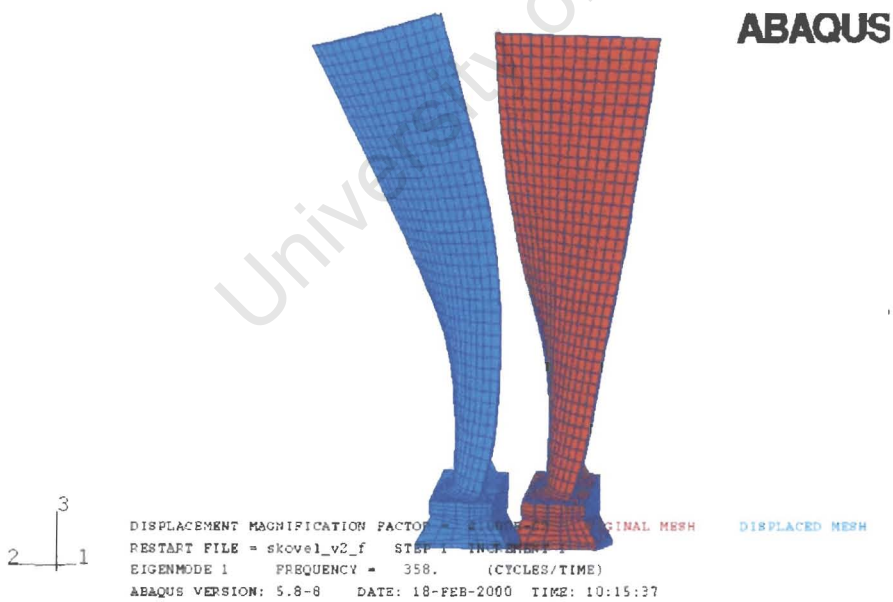

Figure D6 Mode no. 1 for the PMC blade lay-up 1. (The red shape to the right shows the blade for no excitation)

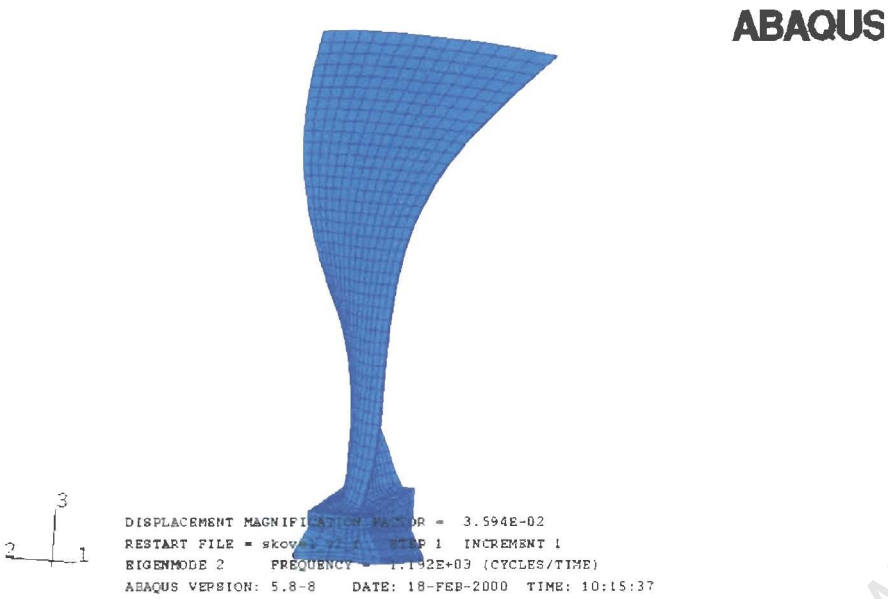

Figure D7 Mode no. 2 for the PMC blade lay-up 1.

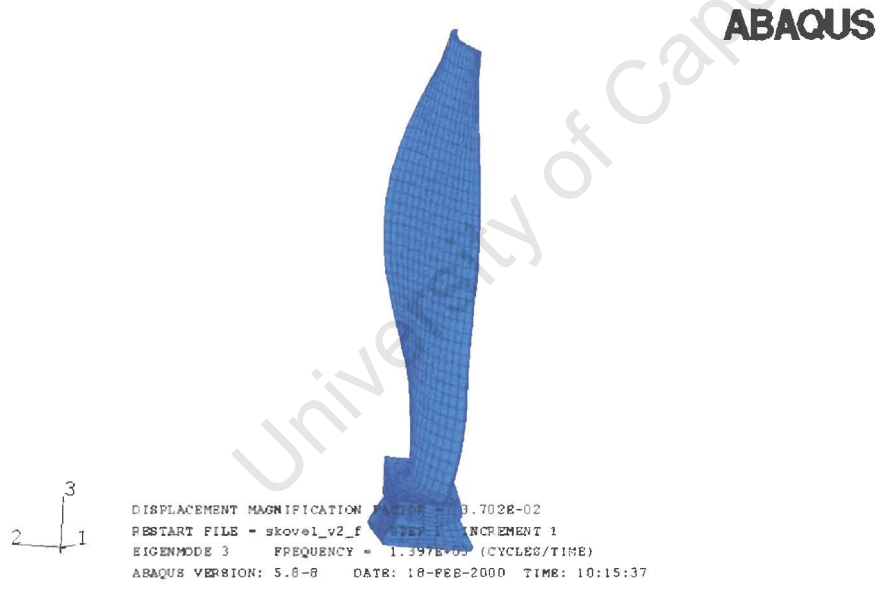

Figure D8 Mode no. 3 for the PMC blade lay-up 1.

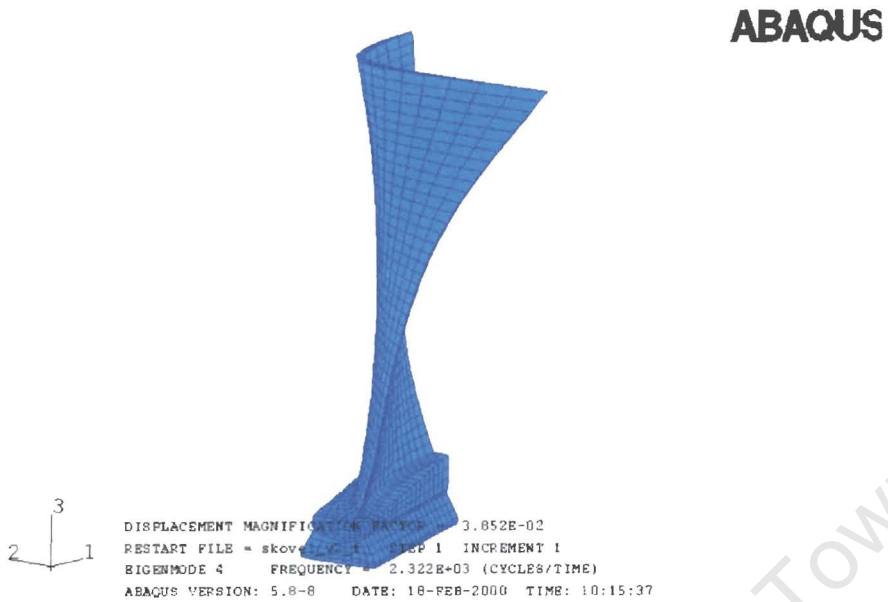

Figure D9 Mode no. 4 for the PMC blade lay-up 1.

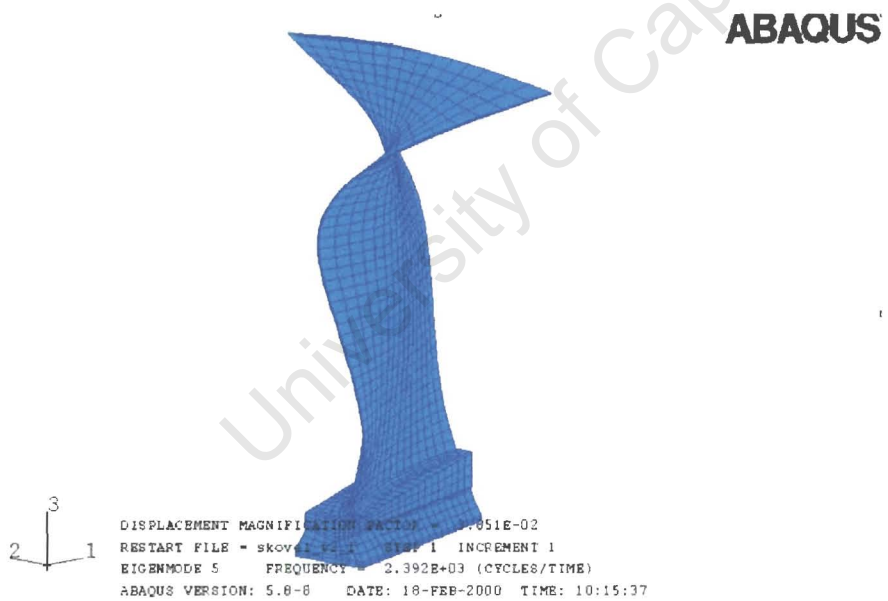

Figure D10 Mode no. 5 for the PMC blade lay-up 1.

Figures D11 to D15 show the mode shapes of the PMC blade lay-up 2.

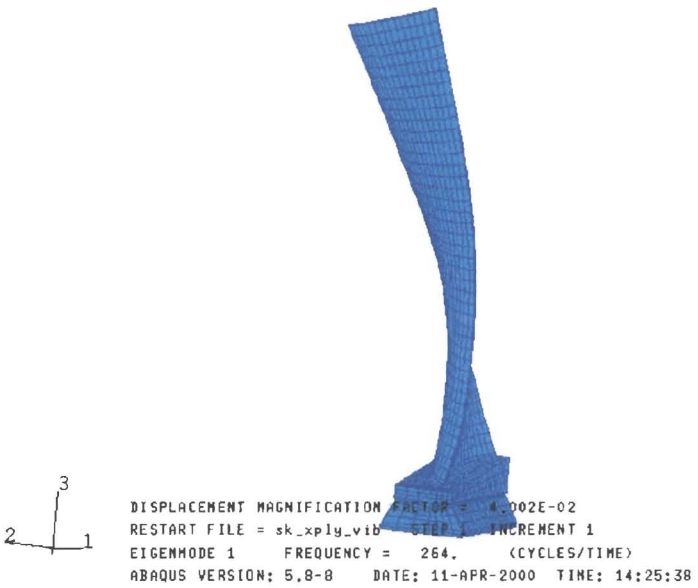

Figure D11 Mode no. 1 for the PMC blade lay-up 2.

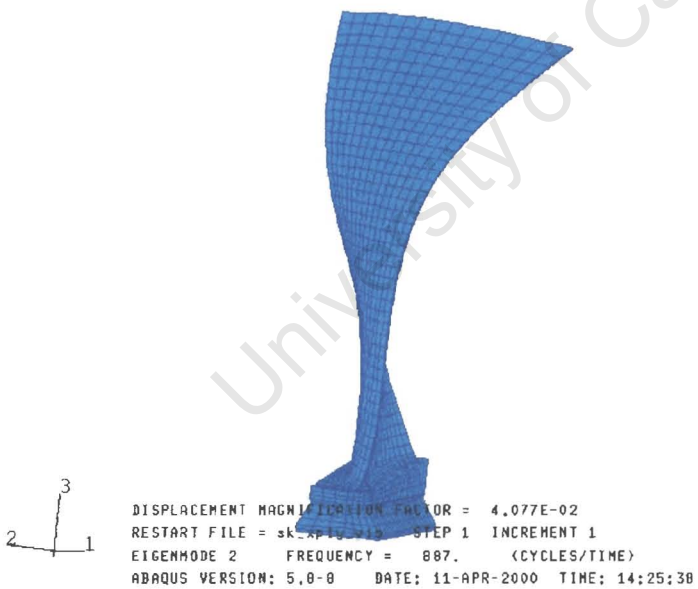

Figure D12 Mode no. 2 for the PMC blade lay-up 2.

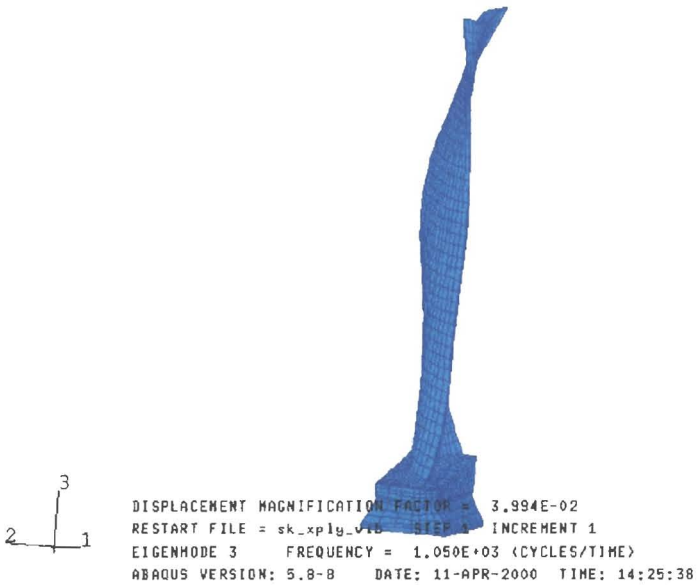

Figure D13 Mode no. 3 for the PMC blade lay-up 2.

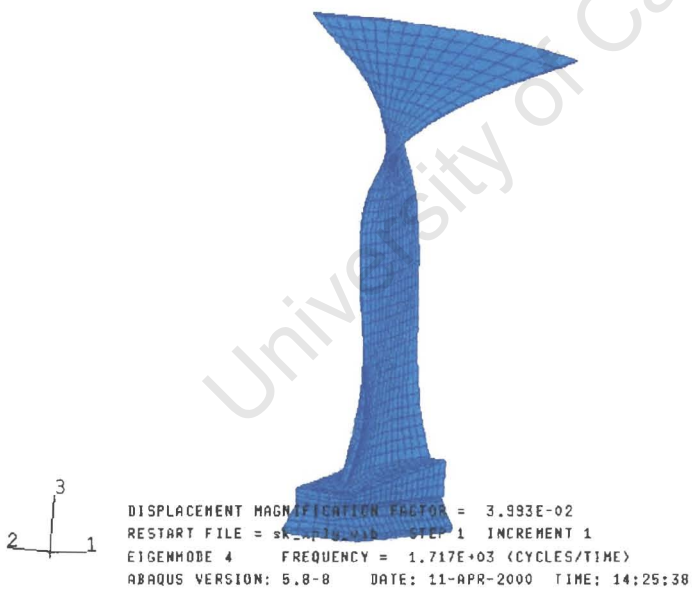

Figure D14 Mode no. 4 for the PMC blade lay-up 2.

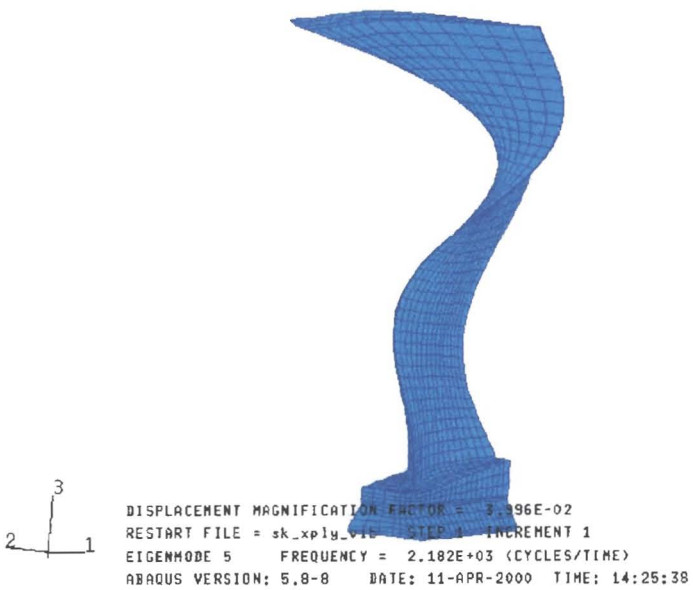

Figure D15 Mode no. 5 for the PMC blade lay-up 2.

APPENDIX E

Impact Data

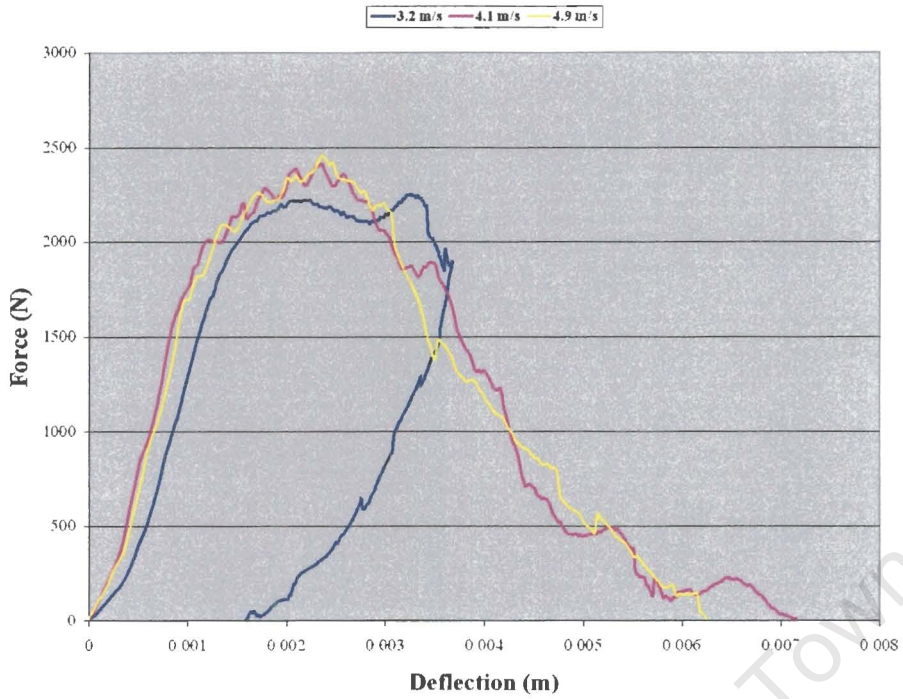

Figure E1 Force vs. deflection for carbon laminate at different impact velocities.

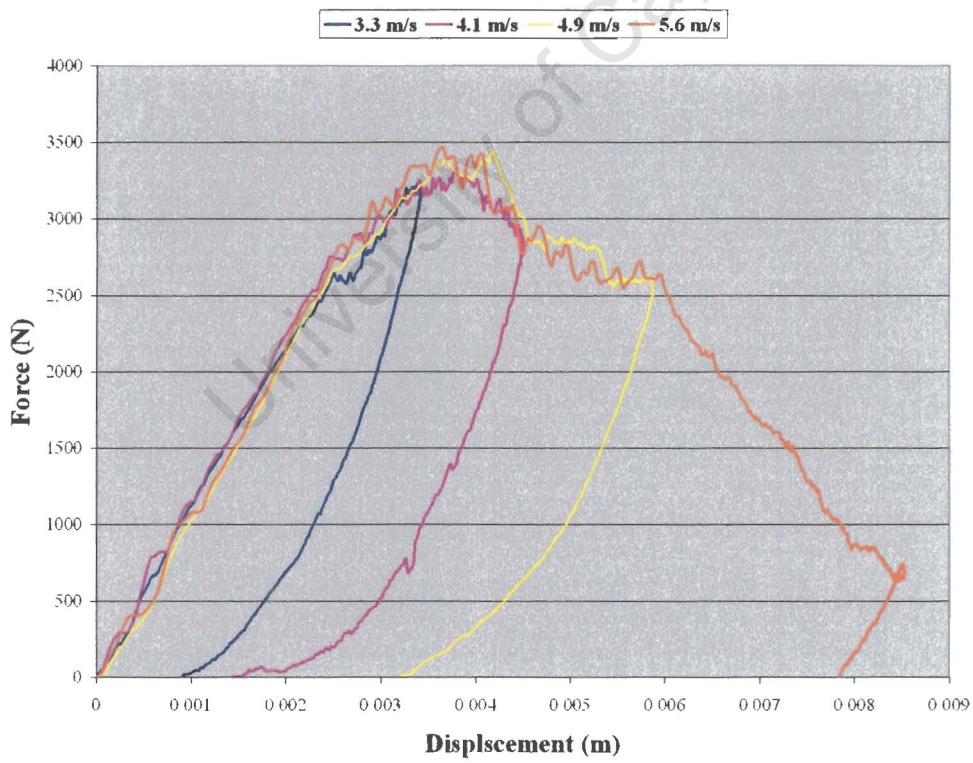

Figure E2 Force vs. deflection for Kevlar laminate at different impact velocities.

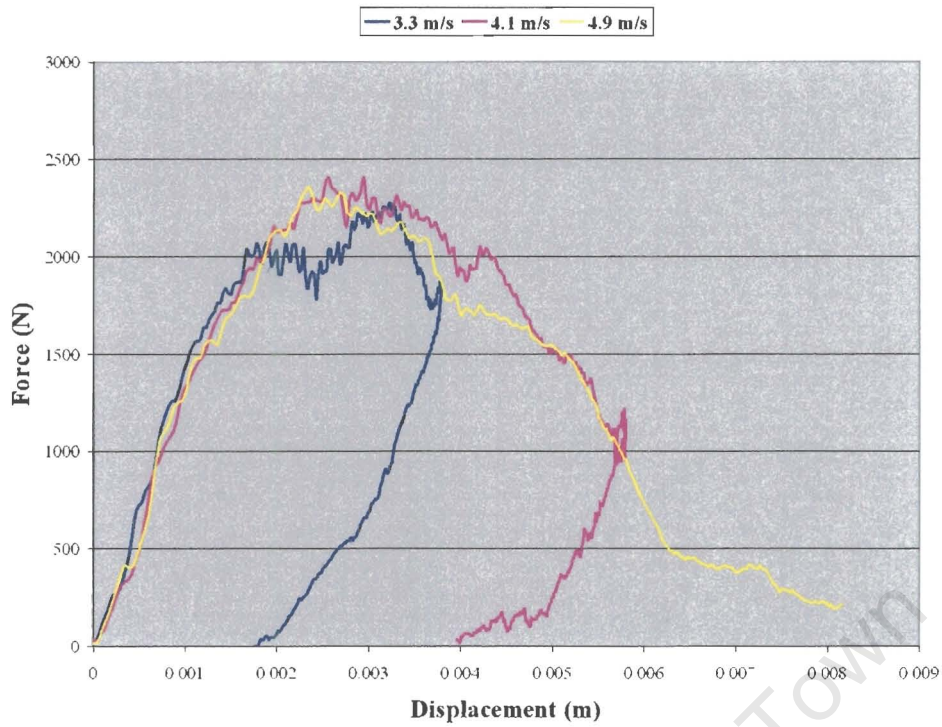

Figure E3 Force vs. deflection for carbon/Kevlar hybrid laminate at different impact velocities.

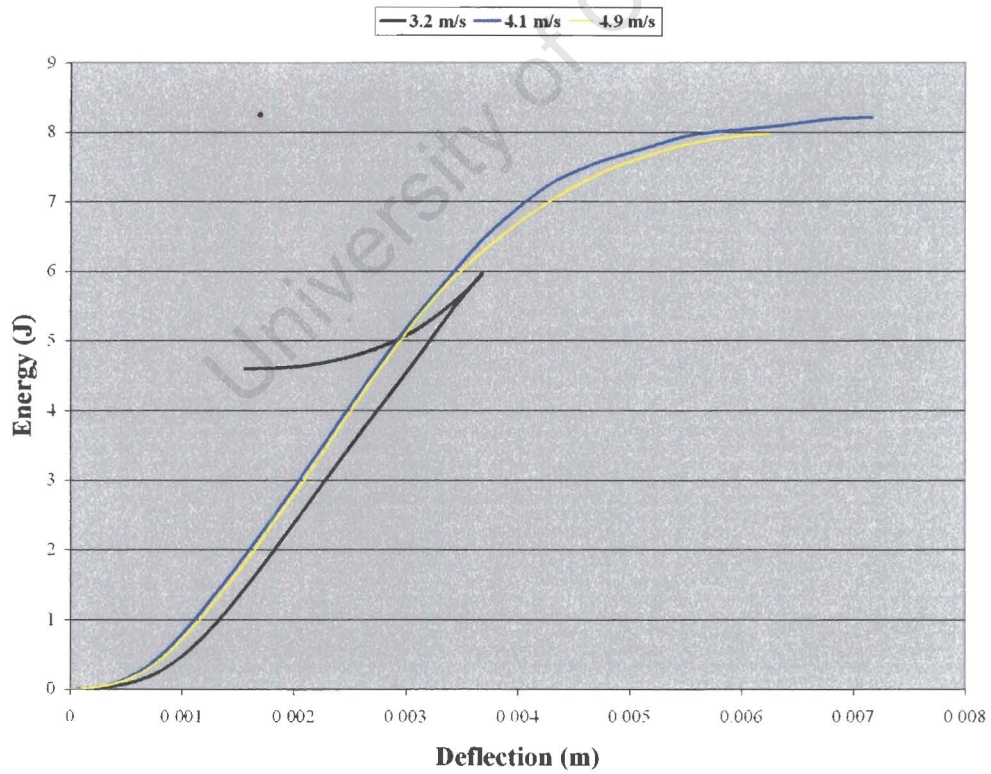

Figure E4 Energy vs. deflection for carbon laminate at different impact velocities.

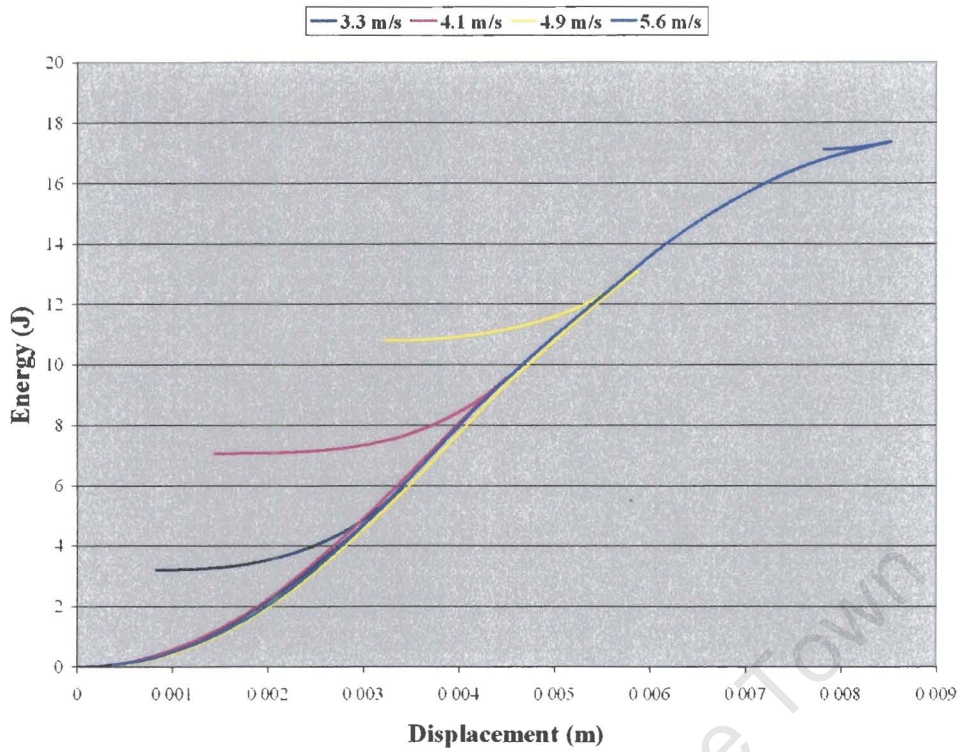

Figure E5 Energy vs. deflection for Kevlar laminate at different impact velocities.

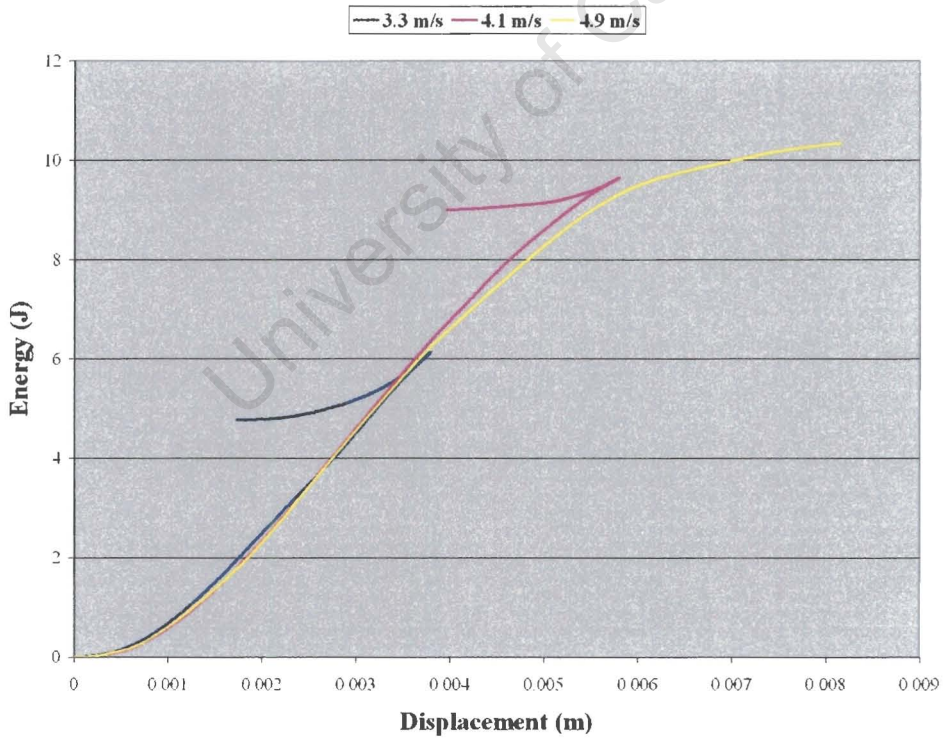

Figure E6 Energy vs. deflection for carbon/Kevlar hybrid laminate at different impact velocities.

	Erosion volume rate (1E-6 m^3)/g			
	Angle (deg)			
Material	**30**	**45**	**60**	**90**
Titanium, Ti-6Al-4V	0.0625	0.1461	0.1337	0.1028
Carbon UD	1.4	2.6	2.7	2.9
Carbon crossply	0.923	1.562	1.926	2.325
Kevlar	0.7566	1.2034	1.2327	0.947
PU coating, UR 3144	0.5479	0.5662	0.3226	0.1884
T1	0.4684	0.349	0.0653	0.0157
T2	1.6559	1.421	0.956	0.6754
3M	0.08	0.152	0.142	0.03
High perf. Epoxy	7.425	6.458	4.012	3.124
Nickel coating	0.0477	0.0643	0.0545	0.0403

APPENDIX F

Erosion Data

APPENDIX G

Interlaminar strain in the CFRP blade, lay-up 1

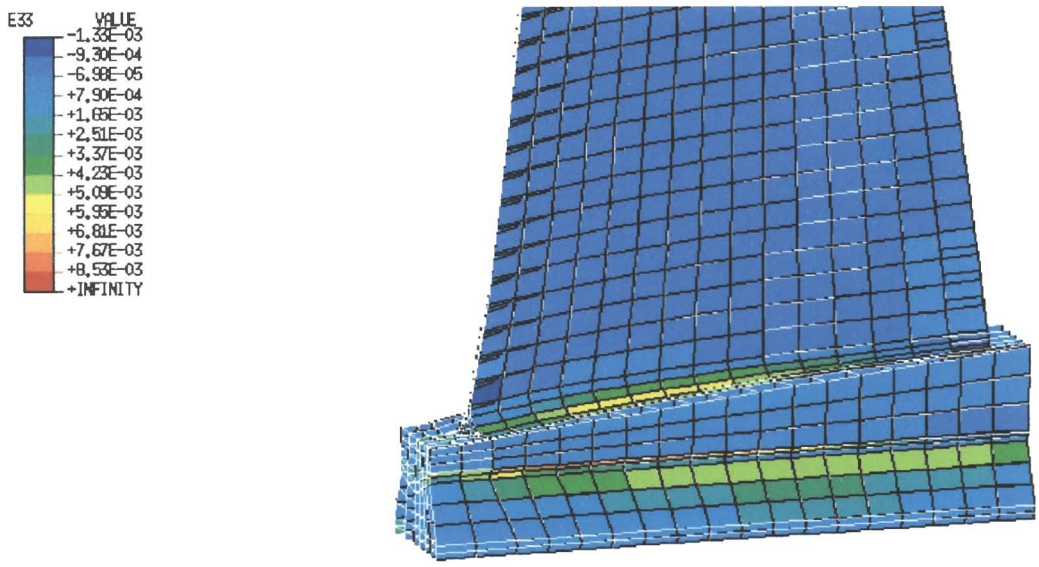

Figure G1 Interlaminar strain for the outermost layer on the pressure side of the CFRP blade, lay-up 1.

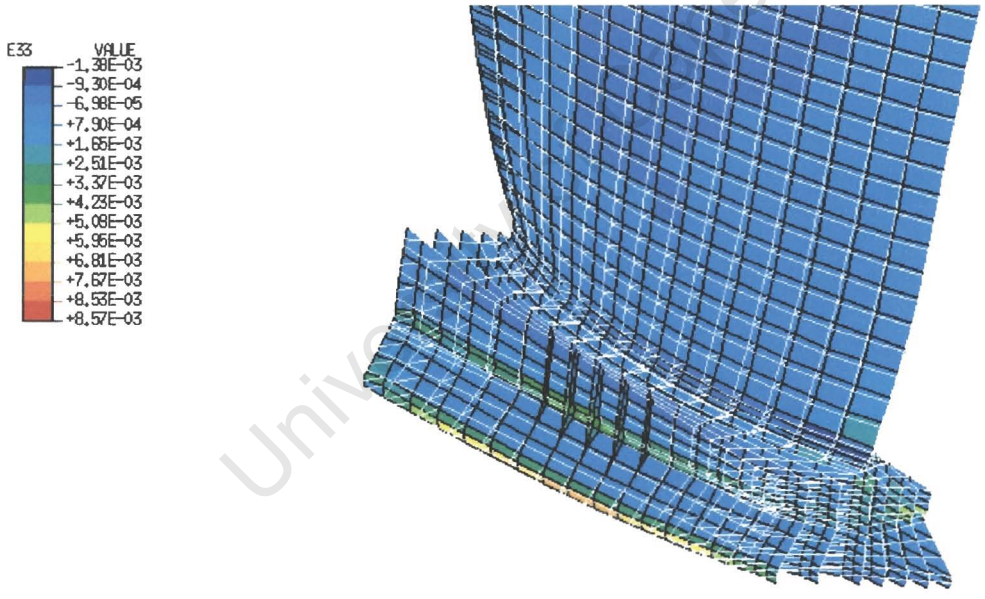

Figure G2 Interlaminar strain for the outermost layer on the suction side of the CFRP blade, lay-up 1.